

QSAR/QSPR AND MECHANISTIC STUDIES OF ELECTRON DONORS IN  
ZIEGLER-NATTA CATALYZED PROPYLENE POLYMERIZATION

Miss Manussada Ratanasak



จุฬาลงกรณ์มหาวิทยาลัย

CHULALONGKORN UNIVERSITY

บทคัดย่อและแฟ้มข้อมูลฉบับเต็มของวิทยานิพนธ์ตั้งแต่ปีการศึกษา 2554 ที่ให้บริการในคลังปัญญาจุฬาฯ (CUIR)  
เป็นแฟ้มข้อมูลของนิสิตเจ้าของวิทยานิพนธ์ ที่ส่งผ่านทางบัณฑิตวิทยาลัย

The abstract and full text of theses from the academic year 2011 in Chulalongkorn University Intellectual Repository (CUIR)  
are the thesis authors' files submitted through the University Graduate School.

A Dissertation Submitted in Partial Fulfillment of the Requirements  
for the Degree of Doctor of Philosophy Program in Nanoscience and Technology  
(Interdisciplinary Program)  
Graduate School  
Chulalongkorn University  
Academic Year 2014

Copyright of Chulalongkorn University

การศึกษาทาง QSAR/QSPR และทางกลไกของสารให้อิเล็กตรอนในปฏิกิริยาพอลิเมอร์ไรเซชัน  
ของโพรพิลีนที่เร่งปฏิกิริยาด้วยซีเกลอร์-แมนททา



วิทยานิพนธ์นี้เป็นส่วนหนึ่งของการศึกษาตามหลักสูตรปริญญาวิทยาศาสตรดุษฎีบัณฑิต  
สาขาวิชาวิทยาศาสตร์นาโนและเทคโนโลยี (สหสาขาวิชา)  
บัณฑิตวิทยาลัย จุฬาลงกรณ์มหาวิทยาลัย  
ปีการศึกษา 2557  
ลิขสิทธิ์ของจุฬาลงกรณ์มหาวิทยาลัย

Thesis Title	QSAR/QSPR AND MECHANISTIC STUDIES OF ELECTRON DONORS IN ZIEGLER-NATTA CATALYZED PROPYLENE POLYMERIZATION
By	Miss Manussada Ratanasak
Field of Study	Nanoscience and Technology
Thesis Advisor	Associate Professor Vudhichai Parasuk, Ph.D.

---

Accepted by the Graduate School, Chulalongkorn University in Partial Fulfillment of the Requirements for the Doctoral Degree

.....Dean of the Graduate School  
(Associate Professor Sunait Chutintaranond, Ph.D.)

THESIS COMMITTEE

.....Chairman  
(Assistant Professor Sukkaneste Tungasmita, Ph.D.)

.....Thesis Advisor  
(Associate Professor Vudhichai Parasuk, Ph.D.)

.....Examiner  
(Ratthapol Rangkupan, Ph.D.)

.....Examiner  
(Thanyada Rungrotmongkol, Ph.D.)

.....Examiner  
(Rungroj Chanajaree, Dr.rer.nat.)

.....Examiner  
(Duangamol Tungasmita, Ph.D.)

.....External Examiner  
(Oraphan Saengsawang, Dr.rer.nat.)

มนัสดา รัตนศักดิ์ : การศึกษาทาง QSAR/QSPR และทางกลไกของสารให้อิเล็กตรอนในปฏิกิริยาพอลิเมอไรเซชันของโพรพิลีนที่เร่งปฏิกิริยาด้วยซีเกลอร์-นัททา (QSAR/QSPR AND MECHANISTIC STUDIES OF ELECTRON DONORS IN ZIEGLER-NATTA CATALYZED PROPYLENE POLYMERIZATION) อ.ที่ปรึกษาวิทยานิพนธ์หลัก: รศ.ดร. วุฒิชัย พาราสุข, 114 หน้า.

สารให้อิเล็กตรอนถูกเติมเข้าไปในตัวเร่งซีเกลอร์-นัททาในปฏิกิริยาการเกิดพอลิเมอไรเซชันของโพรพิลีนเพื่อเพิ่มผลผลิตและค่าไอโซแทคติกของพอลิเมอไรเซชัน การพัฒนาสารให้อิเล็กตรอนตัวใหม่จึงเป็นเป้าหมายที่สำคัญของการออกแบบตัวเร่งปฏิกิริยาในปฏิกิริยาการเกิดพอลิเมอไรเซชันของโพรพิลีน งานวิจัยนี้ศึกษาความสัมพันธ์ระหว่างแอกทิวิตี/สมบัติของสารกับโครงสร้างของสารให้อิเล็กตรอน 3 กลุ่ม โดยเทคนิคควิเอสเออาร์/ควิเอสพีอาร์ แบบจำลองควิเอสเออาร์ทั้งหมดสามแบบของพทาเลข 1,3-ไดออีเทอร์ และมาโลเนท ให้ค่าการทำนายผลที่ดี ( $R^2 \geq 0.93$ ,  $R^2_{CV} \geq 0.84$ ) แต่อย่างไรก็ตามประโยชน์ที่ได้รับจากแบบจำลองนี้จำกัด เนื่องจากจำนวนของสารในชุดข้อมูลสร้างแบบจำลองมีน้อย การศึกษาครั้งนี้พบว่าพลังงานการดูดซับของสารให้อิเล็กตรอนไปยังพื้นผิวตัวเร่งปฏิกิริยามีความสัมพันธ์เชิงเส้นตรงกับค่าแอกทิวิตีที่ได้จากการทดลอง ดังนั้นแบบจำลองควิเอสพีอาร์สำหรับพลังงานการดูดซับจึงได้ถูกสร้างขึ้นสำหรับชุดข้อมูลของ 24 สารที่มาจาก 3 กลุ่มที่แตกต่างกัน แบบจำลองควิเอสพีอาร์ให้ค่าสหสัมพันธ์ที่สูง ( $R^2 = 0.84$ ,  $R^2_{CV} = 0.83$ ,  $R^2_{predict} = 0.77$ ) ระหว่างค่าพลังงานดูดซับกับสามตัวแปรที่สำคัญ เมื่อเปรียบเทียบระหว่างสารให้อิเล็กตรอนทั้ง 3 กลุ่ม พบว่ามาโลเนทเป็นสารที่มีศักยภาพมากที่สุด ท้ายที่สุดแล้ว บทบาทของสารให้อิเล็กตรอนมาโลเนทได้ถูกนำมาศึกษาด้วยการคำนวณดีเอฟที การคำนวณการดูดซับของสารมาโลเนทบนพื้นผิวแมกนีเซียมคลอไรด์ชนิด 110 แสดงให้เห็นว่ามาโลเนทชอบจับแบบคีเลตมากกว่าแบบโมโน แบบบริดจ์ และแบบชิป จากการศึกษาทางกลไกเราสามารถสรุปว่าบทบาทของมาโลเนทคือเป็นตัวกำหนด สเตอริโอซึ่งเกิดจากความเกะกะระหว่างโพรพิลีนและมาโลเนท นอกจากนี้เรายังพบว่าสารมาโลเนททำให้โครงสร้างทรานซิสต์สเตอริโอโดยการส่งผ่านอิเล็กตรอนไปยังไทเทเนียมทำให้ค่าพลังงานการกระตุ้นลดลงเป็นผลให้ตัวเร่งทำงานได้ดีขึ้น สรุปได้ว่าแบบจำลองควิเอสพีอาร์และการศึกษาทางกลไกให้ผลที่สอดคล้องกัน

สาขาวิชา วิทยาศาสตร์นาโนและเทคโนโลยี

ปีการศึกษา 2557

ลายมือชื่อนิสิต .....

ลายมือชื่อ อ.ที่ปรึกษาหลัก .....

# # 5487856020 : MAJOR NANOSCIENCE AND TECHNOLOGY

KEYWORDS: QSAR / QSPR / ELECTRON DONOR / MECHANISTIC STUDIES / POLYPROPYLENE

MANUSSADA RATANASAK: QSAR/QSPR AND MECHANISTIC STUDIES OF ELECTRON DONORS IN ZIEGLER-NATTA CATALYZED PROPYLENE POLYMERIZATION. ADVISOR: ASSOC. PROF. VUDHICHAJ PARASUK, Ph.D., 114 pp.

Electron donors are added to Ziegler-Natta catalyzed propylene polymerization to enhance the productivity and isotacticity of polymer products. The development of new electron donors becomes the key target in designing new generation catalysts for propylene polymerization. In this research, relationships between the activity/property and structures of 3 groups of electron donor were investigated by QSAR/QSPR approaches. All three QSAR models of phthalates, 1,3-diethers and malonates showed good predictive ability ( $R^2 \geq 0.93$ ,  $R^2_{CV} \geq 0.84$ ). However, the usage of obtained QSAR models is limited owing to the small size of the training set. This study founded that adsorption energies of electron donors to catalyst surface are linearly related to experimental activities. Hence, the QSPR for adsorption energies was performed for a set of 24 compounds from 3 different groups. The QSPR model shows high correlation ( $R^2 = 0.84$ ,  $R^2_{CV} = 0.83$ ,  $R^2_{predict} = 0.77$ ) between adsorption energies and three dominant descriptors. Among three groups of electron donor, malonate compounds are the most potent. Finally, the roles of malonate donors were investigated by DFT calculations. Adsorption calculations of a malonate compound on the  $MgCl_2(110)$  surface revealed that the chelate mode was preferred over mono, bridge, and zip modes. From mechanistic study, we can conclude that the role of malonate donors is to give stereoselectivity which elucidated by the steric hindrance between the propylene and the malonate donor. In addition, we found that the malonate donor also stabilized the transition state structure by transferring electrons to Ti resulting in the reduction of the activation energy and hence the catalyst becomes more active. In conclusion, the results from QSPR model and mechanistic studied are in good agreement.

Field of Study: Nanoscience and  
Technology

Student's Signature.....  
Advisor's Signature.....

Academic Year: 2014

## ACKNOWLEDGEMENTS

This thesis would not have been accomplished without contributions from many persons who helped me to overcome extensive hindrances and difficulties during my past three years of study. Truly, I cannot acknowledge the names of all individuals who either directly or indirectly give me helps. I would like to apologize to them whom I failed to mention.

First of all, I wish to express my deepest appreciation and grateful thank to my thesis advisor, Associate Professor Dr.Vudhichai Parasuk who gives a great opportunity to me study Ph.D. program in Nanoscience and Technology. Moreover, he kindly helped me and gave valuable advices throughout my period of study.

I also would like to thank the thesis committee, Assistant Professor Dr.Sukkaneste Tungasmita, Dr.Duangamol Tungasmita, Dr.Ratthapol Rangkupan, Dr.Thanyada Rungrotmongkol, Dr.Oraphan Saengsawang, and Dr.Rungroj Chanajaree for their kind attention, valuable construction, criticism and helpful suggestions.

I wish to express my infinite gratitude to my family, and my friends for their everlasting love and understandings. Special thanks to Dr. Malinee Promkatkaew for her encouragement and smile.

I would like to acknowledge the National Electronics and Computer Technology Center (NECTEC), the Computational Chemistry Chemical Unit Cell (CCUC), Chulalongkorn University for computer resources and other facilities.

Finally, I gratefully acknowledge the financial supports from the Center of Innovative Nanotechnology, Nanoscience and Technology program, Graduate School, Chulalongkorn University, The 90th anniversary of Chulalongkorn University, The National Research University Project of CHE and the Ratchadaphisek Somphot Endowment Fund (AM1078I, RES560530184-AM, WCU-031-AM-57) and IRPC Public Company Limited, Thailand.

## CONTENTS

	Page
THAI ABSTRACT .....	iv
ENGLISH ABSTRACT .....	v
ACKNOWLEDGEMENTS .....	vi
CONTENTS .....	vii
LIST OF TABLES .....	xi
LIST OF FIGURES .....	xiv
LIST OF ABBREVIATIONS .....	xvi
CHAPTER I INTRODUCTION .....	1
1.1 Literature Review of Roles of Electron Donors.....	2
1.1.1 Experimental Significance Studies .....	2
1.1.2 Theoretical Significance Studies.....	4
1.2 Research Objectives .....	7
1.3 Scope of This Dissertation.....	7
CHAPTER II THEORETICAL BACKGROUND.....	8
2.1 Background on Ziegler-Natta Catalyst and Electron Donors in Polypropylene.....	8
2.1.1 Ziegler-Natta Catalysts .....	8
2.1.2 Mechanism for Ziegler-Natta Polymerization.....	9
2.1.2.1 Cossee-Arlman Mechanism.....	9
2.1.2.2 Brookhart-Green Mechanism .....	10
2.1.3 Electron Donors.....	11
2.1.4 Polypropylene .....	13
2.1.4.1 Physical Properties of Polypropylene .....	13

	Page
2.1.4.2 Polypropylene in the World and in Thailand .....	13
2.1.4.3 Tacticity of Polypropylene.....	14
2.2 Background on Quantum Chemistry.....	16
2.2.1 Density Functional Theory .....	16
2.2.2 DFT Functionals.....	19
2.2.2.1 Local Density Approximations (LDA).....	20
2.2.2.2 Generalized Gradient Approximation (GGA) .....	21
2.2.2.3 Meta-GGA.....	22
2.2.2.4 Hybrid-GGA.....	22
2.2.2.5 Hybrid Meta-GGA.....	23
2.2.3 Dispersion Part in the Functionals.....	24
2.3 Background on Quantitative Structure-Activity/Property Relationship.....	25
2.3.1 Theory in QSAR/QSPR Statistics .....	25
2.3.1.1 Initial Data Analysis.....	25
2.3.1.2 Data Reduction.....	26
2.3.1.3 Model Building .....	27
2.3.2 Regression Analysis for QSAR/QSPR Study.....	27
2.3.2.1 Multiple Linear Regression.....	27
2.3.2.2 Partial Least Squares.....	28
2.3.2.3 Genetic Function Approximation.....	29
CHAPTER III STRUCTURE AND ACTIVITY DATA.....	31
3.1 Chemical Structure of Electron Donors.....	31
3.1.1 Data and Activity .....	31



	Page
CHAPTER IV QSAR.....	33
4.1 Three Types of Electron Donors Groups.....	33
4.2 Geometry Optimization Details.....	34
4.3 Molecular Descriptors for QSAR.....	34
4.4 Results and Discussions .....	35
4.4.1 QSAR model of Phthalate Group.....	35
4.4.2 QSAR model of 1,3-Diether Group .....	39
4.4.3 QSAR model of Malonate Group.....	42
4.5 QSAR Summary.....	45
CHAPTER V QSPR.....	46
5.1 QSPR Model Setup .....	47
5.2 Adsorption Energy Calculations .....	49
5.3 QSPR Procedure .....	49
5.4 Results and Discussion.....	50
5.4.1 Adsorption Energy of Electron Donor on Catalyst Surface .....	50
5.4.2 Adsorption Energy and Experimental Activity.....	52
5.4.3 QSPR Model on the Adsorption Energy.....	53
5.4.4 Validation of QSPR Model .....	58
5.4.5 Suggestions for Potent Electron Donors.....	59
5.5 QSPR Summary.....	60
CHAPTER VI Mechanistic Study.....	62
6.1 Introduction.....	62
6.2 Models and Computational Details .....	67

	Page
6.2.1 Four Adsorption Mode of Malonate Donor .....	67
6.2.2 Reaction Model Without Electron Donors .....	68
6.2.3 Reaction Model With Malonate Donor .....	68
6.3 Results and Discussion .....	69
6.3.1 Favorable Adsorption Mode of Malonate Donor .....	69
6.3.2 Ziegler-Natta Reaction Without Electron Donor .....	71
6.3.3 Influence of Malonate Donor on Ziegler-Natta Reaction .....	74
6.4 Mechanistic Study Summary .....	82
CHAPTER VII CONCLUSIONS .....	83
REFERENCES .....	85
APPENDIX-A .....	100
APPENDIX-B .....	111
VITA .....	114

## LIST OF TABLES

	Page
Table 1 Generations of ZN catalysts for the PP polymerization [16].	8
Table 2 Physical properties of polypropylene [24].	13
Table 3 Example of the correlation matrix for a group of four variables.	26
Table 4 Chemical structures of 29 internal electron donors with different substituents (R1, R2 and R3) [77-80].	31
Table 5 Relationship between the two dominant descriptors from the best QSAR model of the eight compounds in phthalate group and experimental activity.	36
Table 6 Predicted activity and residual values of the eight phthalate compounds by the best QSAR model.	37
Table 7 Relationship between the two descriptors from the best QSAR model of nine compounds in 1,3-diether group and experimental activity.	39
Table 8 Predicted activities and residual values of the nine 1,3-diether compounds by the best QSAR model.	40
Table 9 Relationship between the two descriptors from the best QSAR model of eight compounds in malonate group and experimental activity.	42
Table 10 Predicted log activities and residual values of the eight malonate compounds by the QSAR model.	43
Table 11 Calculated adsorption energy of electron donor on $TiCl_4/MgCl_2(110)$ surface ( $E_{ads}$ , kcal/mol) and their energy components of 29 electron donors in the phthalate (P1-P8), 1,3-diether (D1-D9) and malonate (M1-M12) groups.	51

Table 12	The best QSPR models on the adsorption energy ( $E_{\text{ads}}$ ) of 24 electron donors with one, two, three, four, five, and six descriptors shown with the square correlation coefficient ( $R^2$ ) and the square cross-validated value ( $R^2_{\text{CV}}$ ).....	53
Table 13	List of three dominant molecular properties of 24 electron donors as training set from the best QSPR model. ....	56
Table 14	The three dominant descriptors were calculated and predicted adsorption energy for five compounds in the test set from the best QSPR model.....	58
Table 15	Calculated adsorption energy ( $E_{\text{ads}}$ , kcal/mol) and their energy components of di- <i>n</i> -butyl-2-cyclopentyl malonate adsorbed on the pre-activated $\text{MgCl}_2$ (110) surface.....	69
Table 16	The main interatomic distances for the di- <i>n</i> -butyl-2-cyclopentyl malonate adsorbed on the pre-activated $\text{MgCl}_2$ (110) surface.....	70
Table 17	The $\pi$ -complex formation energy ( $\Delta E_{\pi}$ ), The energy difference between the transition state and the $\pi$ complex ( $\Delta E_{\text{TS}}$ ), and The energy difference between the product and the $\pi$ complex ( $\Delta E_{\text{product}}$ ), and the intrinsic activation energy ( $E_a$ ) when absence malonate donor.....	72
Table 18	The relative barriers of the insertion step of ZN catalyzed propylene polymerization in the absence of the electron donor together with values of TS imaginary frequencies.....	73
Table 19	The $\pi$ -complex formation energy ( $\Delta E_{\pi}$ ), The energy difference between the transition state and the $\pi$ complex ( $\Delta E_{\text{TS}}$ ), and The energy difference between the product and the $\pi$ complex ( $\Delta E_{\text{product}}$ ), and the intrinsic activation energy ( $E_a$ ) when presence malonate donor.....	75

Table 20	The relative barriers of the insertion step of ZN catalyzed propylene polymerization in the presence of the di- <i>n</i> -butyl 2-cyclopentyl malonate donor together with values of TS imaginary frequencies.....	76
Table 21	Comparison of transition state structure of the Ti active ZN catalyst when absence and presence of malonate donor and their charge transfer through the MgCl <sub>2</sub> (110) support. ....	81



## LIST OF FIGURES

	Page
Figure 1 The Cossee-Arlman mechanism for a heterogeneous Ziegler-Natta catalyst [18, 19].	10
Figure 2 The Brookhart-Green mechanism for a heterogeneous Ziegler-Natta catalyst [20].	11
Figure 3 Chemical formulas of the most common internal donor types.	12
Figure 4 Chemical formulas of the most common external donor types.	12
Figure 5 A pie chart presenting world polymer usage [26].	14
Figure 6 Three stereoisomers of polypropylene structures; isotactic, syndiotactic, atactic [29].	16
Figure 7 Plot of actual versus predicted activity values from the best QSAR model for the eight phthalate compounds with the GFA statistical method.	38
Figure 8 Plot of actual versus predicted activity values from the best QSAR model for nine 1,3-diether compounds with the GFA statistical method.	41
Figure 9 Plot of actual versus predicted activity values from the best QSAR model for the eight malonate compounds with the GFA statistical method.	44
Figure 10 The 3D-structure of $\text{TiCl}_4$ on $\text{MgCl}_2(110)$ surface used in this study. (The color codes are as follows: Ti (yellow), Cl (green), and Mg (blue)).	47
Figure 11 The adsorption $\text{TiCl}_4/\text{MgCl}_2(110)$ complex structure generated by aligning the electron donor (Hydrogen atoms of donor are not shown for clarity).	48
Figure 12 Plotting graph relationship between the adsorption energy ( $E_{\text{ads}}$ ) and the experimental PP activity for the three types of internal electron donor: malonate (halo-malooate), phthalate, and 1,3-diether.	52

Figure 13 Relationship between calculated and predicted values of adsorption energies for the 24 compounds as training set using the best QSPR model.....	55
Figure 14 The predicted versus the calculated $E_{ads}$ values for test set using the best QSPR model.....	59
Figure 15 Summary of structure for design new potent electron donors based on malonate template by our QSPR model.....	60
Figure 16 Four adsorption modes of the malonate donor on the $MgCl_2(110)$ surface (all hydrogens are not shown for purposes of clarity). ....	64
Figure 17 Four possible insertion modes of propylene monomer into a Ti- <i>i</i> Bu growing chain of polypropylene.....	65
Figure 18 The primary (1,2)- <i>re</i> insertion of propylene monomer to a Ti - (+)/(-) <i>i</i> Bu growing chain. ....	66
Figure 19 Relative energy profiles (kcal/mol) for PP primary and secondary (both <i>re</i> and <i>si</i> faces) insertion into Ti-C bond when absence malonate donor.....	74
Figure 20 Energy profiles (kcal/mol) for PP primary and secondary (both <i>re</i> and <i>si</i> faces) insertion into Ti-C bond when presence malonate donor.....	78
Figure 21 Steric effect of the chelate-coordinated malonate donor at the transition state on the primary (1,2)- <i>re</i> insertion: the repulsion between the propylene and the malonate donor. ....	79
Figure 22 Structures of the chelate-coordinated malonate donor at the transition states for a) the primary (1,2)- <i>si</i> ; b) the secondary (2,1)- <i>re</i> ; c) the secondary (2,1)- <i>si</i> insertion. ....	80

## LIST OF ABBREVIATIONS

ZN	=	Ziegler-Natta
PP	=	Polypropylene
AlEt <sub>3</sub>	=	Triethylaluminium
DEAC	=	Diethylaluminum chloride
AlR <sub>3</sub>	=	Alkyl aluminum
I.I.	=	Isotactic Index
MW	=	Molecular Weight
MWD	=	Molecular Weight Distribution
QSAR	=	Quantitative Structure-Activity Relationship
QSPR	=	Quantitative Structure-Property Relationship
IED	=	Internal Electron Donor
EED	=	External Electron Donor
GGA	=	Generalized gradient approximation
MLR	=	Multiple Linear Regression
PLS	=	Partial Least Squares
GFA	=	Genetic Function Approximation
R <sup>2</sup>	=	Squared correlation coefficient
R <sup>2</sup> <sub>CV</sub>	=	Squared cross-validated correlation coefficient
R <sup>2</sup> <sub>pred</sub>	=	Predictive squared correlation coefficients
E <sub>HOMO</sub>	=	Energy of the highest occupied molecular orbital
E <sub>LUMO</sub>	=	Energy of the lowest unoccupied molecular orbital
E <sub>ads</sub>	=	Adsorption energies
PBE	=	Perdew Burke Ernzerh
DNP	=	Double Numerical Polarization
ECP	=	Effective Core Potentials
Rog	=	Radius of gyration
BE	=	Force bond energy
Dipole	=	Dipole moment
<i>i</i> Bu	=	isobutyl <i>i</i> Bu



## CHAPTER I

### INTRODUCTION

One of the most important discoveries in the petrochemical industries in the last century is that of the Ziegler-Natta catalysts for the olefins polymerization. In 1953, Karl Ziegler discovered the catalyst based on titanium tetrachloride and diethylaluminium chloride as a co-catalyst for the polymerization of ethylene into high density polyethylene at room [1]. Then, in the spring of 1954, this catalyst was employed by Giulio Natta to polymerize propylene into crystalline polypropylene. Ziegler and Natta are both awarded the Nobel Prize for Chemistry 1963 in recognition of their work on the Ziegler-Natta catalyst [2].

Nowadays, heterogeneous Ziegler-Natta (ZN) catalysts remain the top priority in the olefin polymerization industries. They are particularly around 62 million tons/year of isotactic polypropylene (PP) and more than 57% of PP capacities were built in the Asia-Pacific region [3]. Most of the commercial catalysts used for PP manufacture are modifications of the original ZN system. The catalyst for the production of isotactic polypropylene with high activity and stereospecificity consists of the  $MgCl_2$ -supported  $TiCl_4$  catalyst in conjunction with triethylaluminum ( $AlEt_3$ ) co-catalyst and organic additives (Lewis bases) which are normally referred to as electron donors. Electron donors can be added either during the catalyst preparation (internal donor) or the propylene polymerization process (external donor) [4].

Ziegler-Natta catalysts have advantages of producing products with high molecular weight, high melting point and controllable morphology. However, the drawback when using ZN catalysts is the acclaimed isotactic PP is a mixture of different types of PP: short atactic chains are present even in most isotactic

commercial PP. Obtaining isotactic PP of varying molecular weight, while keeping isotacticity almost constant, is not possible [5].

## 1.1 Literature Review of Roles of Electron Donors

### 1.1.1 Experimental Significance Studies

Both internal and external electron donors are necessary in supported ZN catalysts for PP polymerization. It is widely accepted that the internal donor can be extracted by cocatalyst  $\text{AlEt}_3$  [6, 7].

In 1991, Sacchi et al. [6] proposed some equilibrium reactions, shown in Figure 2.1. They suggested that electron donors coordinating with active sites could be removed by  $\text{AlEt}_3$  but these reactions were reversible. If the internal donor in the active sites is removed, it is possible for the external donor to interact with the resulting active sites. This leads to a decreased stereoblock structure which mainly exists in the polypropylene fractions with low isotacticity [7].



( $\text{C}^*$ : Active site; IED : Internal Electron Donor; EED : External Electron Donor)

### Equilibrium between $\text{AlEt}_3$ and electron donors [6].

In 2008, Andoni and coworkers [8] have been prepared an active model for a ZN propylene polymerization catalyst by spin-coating of  $\text{MgCl}_2$ -donor- $n\text{EtOH}$  from the ethanol solution onto a flat silicon wafer. They were investigated the effects of

diether and ester as internal donors in the controlling the crystallite faces of  $\text{MgCl}_2$  by AFM and SEM analytical techniques. The results revealed that the presence of a diether leads to the formation of  $\text{MgCl}_2$  crystallites only  $120^\circ$  edge angles which confirmed a strong preference for the formation of a particular crystallite face. In contrast, the use of a monoester or diester as internal donor generates crystallites with  $120^\circ$  and  $90^\circ$  edge angles indicating the presence of both the (110) and the (104) edge surfaces of  $\text{MgCl}_2$ . From this experiment provides strong evidence that the formation of the  $\text{MgCl}_2$  crystallite face depend on the nature of the internal donor and the ability of the donor to steer with the  $\text{MgCl}_2$  surface during catalyst preparation.

*In 2011*, Zhang et al. [9] studied the effect of the electron donors on catalyst activity, isospecificity, molecular weight and molecular weight distribution of PP. The results revealed that the catalyst activity with different internal donors decreases in the following order: diether > phthalate  $\approx$  succinate. Moreover, they were also investigated the effect of the structures of external donors on catalyst activity, The conclusions from this work, more or the bulkiness of alkoxy groups leads to decrease the catalyst activity, the isotactic index value and molecular weight of obtained PP. For the linear alkyl groups do not deactivate the active centers of catalyst, while the molecular weight increased with the increasing the alkyl group size in external donor.

*In 2012*, Guo et al. [10] investigated the catalytic activity, isotacticity and melting temperature of PP by use six different catalytic systems. The results indicated that the catalytic activities and thermal properties of PP were improved by adding cyclohexylmethyl dimethoxysilane external donor when diethyl ester or diester was used as an internal donor. Moreover, when 1,1-biethoxymethyl pentane (diether donor) was used as internal donor and without adding external donor which

gave the highest % Ti content, the highest catalytic activity, and the excellent isotacticity PP.

### 1.1.2 Theoretical Significance Studies

Many theoretical studies were carried out to study the mechanism of the ZN catalyst for PP polymerization. However, the mechanism underlying the role of the donor in PP polymerization has not yet been well understood. Some interesting research that relate to this research were revealed below.

*In 2007*, Correa et al. [11] investigated the interaction between the internal donors (1,3-diethers, alkoxysilanes, phthalates, succinates) and the  $\text{MgCl}_2(110)$  surfaces using the BP86 functional in the TURBOMOLE package. The results indicated that donors can be separated into two classes. Only the chelate coordination mode (the two O atoms of donor coordinate to the same Mg atom) is allowed for donors with a short spacer between the coordinating O atoms (alkoxysilanes and 1,3-diethers), whereas donors with a longer spacer (succinates and phthalates) can adopt a variety of coordination modes. The stereoselective and regioselective behavior of possible active Ti species with and without two succinate molecules coordinated in the proximity of the Ti atom have been investigated. Two succinate molecules give a remarkable stereoselectivity in both primary and secondary propene insertions. This study concluded that 1) Isolated Ti species on the  $\text{MgCl}_2(110)$  monolayer would lead to a substantially atactic polypropylene. 2) Ti species on the  $\text{MgCl}_2(110)$  monolayer flanked by two donors (110)-bridge coordinated would lead to a substantially isotactic polypropylene.

*In 2009*, Lee JW et al. [12] investigated the effect of the chemical structure of 1,3-diether in ZN catalyst for PP polymerization using the VWN functional corrected by the exchange functional of Becke and the correlation functional of Perdew in the ADF package and the MM using the universal force field in Cerius2 program. The

energy barriers during insertion of propylene have been calculated. It revealed that the isospecific active site created on the (100) surface of  $\text{MgCl}_2$  is more active than the aspecific active site which created on the (110) surface of  $\text{MgCl}_2$  for propylene polymerization. This work can concluded that the primary function of 1,3-diether is to prevent the formation of aspecific site on the  $\text{MgCl}_2$  (110) surface into isospecific site created on the  $\text{MgCl}_2$  (100) surface. Moreover, the analysis of the adsorption energy of various model compounds for 1,3-diether on the (110) and (100) surfaces of  $\text{MgCl}_2$  revealed that the substitution of highly branched hydrocarbon at the  $\text{C}_2$  position of 1,3-diether increases the adsorption energy difference as compared with the substitution of linear hydrocarbons, indicating that the substitution of highly branched hydrocarbons is more effective for better productivity and isotacticity of ZN catalyst.

In 2010, Vanka et al. [13] employed the PBE functional in TURBOMOLE program for investigation the roles of electron donors. Two phthalates (*di*-isobutyl and *di*-ethyl phthalates) and three alkoxy benzoates (*p*-isopropoxy, *p*-ethoxy, and *p*-*tert*-butoxy benzoates) as representative internal and external donors, respectively. Models for the  $\alpha$  and the  $\beta$  phases of the (110)  $\text{MgCl}_2$  lateral cut have been considered. The comparison of three different models of the  $\text{MgCl}_2$  support i.e., the fully fixed (where the atoms in the  $\text{MgCl}_2$  lateral cuts were kept fixed), the partially relaxed (some of the magnesium and chlorine atoms unfixed), and the fully relaxed (all atoms free) models indicates that the fully fixed model gave the best result. This work indicated that the phthalate donors would preferentially stabilize the  $\alpha$  phase of  $\text{MgCl}_2$ , while the alkoxy benzoate donors would stabilize the  $\beta$  phase more. Moreover, they proposed four adsorption models (mono, chelate, bridge, and zip modes) of phthalate donors. The results from comparison revealed that the zip mode is preferred over the mono and chelate modes whereas it is competitive with

the bridge mode. In addition, the presence of nearby zip-coordinated *di*-iso-butyl (DIBP) phthalate donor gives regioselectivity and stereoselectivity to the catalyst center, with the *si*-primary mode being the preferred route for insertion. Finally, the study of possible replacements to a zip-coordinated DIBP at the  $\text{MgCl}_2$  surface indicates that 1,3-diethers would serve as the best external donors to DIBP. The obtained results provide a basis for explaining why certain donor combinations are experimentally very effective in ZN polymerization systems.

In 2011, Wondimagegn *et al.* [14] have been investigated the effect of the structures of external alkoxysilane donors in ZN catalyst on stereoselectivity and molecular weight distributions of polypropylene by QM/MM calculations. The conclusions from this work, the molecular weight and the stereoselectivity are relying on the three factors: 1) the number of alkoxy groups. 2) the size and type of substituent ( $R_1$  and  $R_2$ ). 3) the nature of the hydrocarbon attached to the central silicon atom. Additionally, larger substituents, branched and cyclic hydrocarbons show highly isospecific catalyst performance. However, one bulky substituent on  $R_1$  or  $R_2$  does not produce highly isotactic PP polymers.

In 2012, Taniike *et al.* [15] have been conducted to clarify the mechanism for ethyl benzoate (EB) donors to influence polymerization performances of  $\text{MgCl}_2$ -supported ZN catalysts by periodic DFT calculations using GGA-PBE with DNP basis set which implemented in the DMol3 package. They conclude that  $\text{TiCl}_4$  preferentially adsorbs as mononuclear species on the  $\text{MgCl}_2$  (110) surface. Furthermore, when the absence of donors, the Ti mononuclear species on the (110) surface is aspecific. In addition, the coadsorption of EB can convert the aspecific Ti mononuclear species into the isospecific one by sterically controlling the orientation of the growing chain at the transition state. It also improves the regiospecificity as a result of the increase electrostatic repulsion for the 2,1 insertion. Moreover, the EB

donor prevents chain transfer to propylene, thus the molecular weight of the polypropylene increase.

### 1.2 Research Objectives

- 1) To investigate the relationships between the polypropylene activity/property and molecular properties of electron donors using the QSAR/QSPR techniques
- 2) To study the adsorption location of the malonate donors on the ZN catalyst
- 3) To investigate the ZN mechanism on the primary (1,2) and the secondary (2,1) both with *re* and *si* faces of insertion steps with the malonate donors by quantum chemical calculations

### 1.3 Scope of This Dissertation

The main goal of this research is to design new electron donors in heterogeneous Ziegler-Natta catalyst for PP polymerization by investigating the relationships between the activity/property and the electron donor structures using the QSAR/QSPR approaches. In this work, we are particularly interested in malonate donors because of this type of electron donors had never been theoretical studied. Then, the adsorption locations of the malonate donors on the ZN catalyst will be studied. After that, we will investigate the mechanism of ZN at the propylene in the primary (1,2) and the secondary (2,1) insertion steps with the malonate donors using quantum chemical calculations. Furthermore, we will also examine roles of malonate donors in the mechanism of the ZN catalyzed PP polymerization on activity and isotacticity.

## CHAPTER II

### THEORETICAL BACKGROUND

#### 2.1 Background on Ziegler-Natta Catalyst and Electron Donors in Polypropylene

##### 2.1.1 Ziegler-Natta Catalysts

The generations of ZN catalysts for the PP polymerization were reported in Table 1 [16].

**Table 1** Generations of ZN catalysts for the PP polymerization [16].

Generation	Catalyst system	Productivity (kg PP/g Cat.)	I.I. (wt%)	Morphology
First	$\text{TiCl}_3$ 0.33 $\text{AlCl}_3$ +DEAC	2-4	90-94	Powder
Second	$\text{TiCl}_3$ +DEAC	10-15	94-97	Granular
Third	$\text{TiCl}_4$ /Ester/ $\text{MgCl}_2$ + $\text{AlR}_3$ /Ester	15-30	90-95	Spherical
Fourth	$\text{TiCl}_4$ /Diester/ $\text{MgCl}_2$ + $\text{AlEt}_3$ /Silane	30-60	95-99	Spherical
Fifth	$\text{TiCl}_4$ /Diether/ $\text{MgCl}_2$ + $\text{AlEt}_3$	100-130	96-99	Spherical

Polymerization condition: bulk, 70 °C, 2 h.

DEAC = Diethylaluminum chloride,  $\text{AlR}_3$  = Alkyl aluminum,  $\text{AlEt}_3$ = Triethylaluminum,

I.I. = Isotactic Index



Several generations of ZN catalysts have been developed based on high yield productivity. The first and second generations of ZN catalysts were composed of crystalline  $\text{TiCl}_3$ . It can be activated with a DEAC co-catalyst. The third generation came when  $\text{TiCl}_4$  was supported on the  $\text{MgCl}_2$  particles. The third generation ( $\text{TiCl}_4/\text{MgCl}_2$ ) ZN catalysts had higher productivity than those of the first and second generations. The fourth generation ZN catalysts are also composed of  $\text{TiCl}_4$  supported on the  $\text{MgCl}_2$ , but with controlled morphology and with better productivity than the third generation. The fifth generation of catalysts used diether as internal donor with no requirement for an external donor, have become most successful in producing highly activity and isotacticity [16]. However, the use of 1,3-diethers donor leads to polypropylenes with narrow molecular weight distribution [17]. As the electron donors play a major role in the ZN catalyzed PP polymerization, therefore, the development of new electron donors becomes one of the key targets in designing of new generation polypropylene catalysts.

## 2.1.2 Mechanism for Ziegler-Natta Polymerization

### 2.1.2.1 Cossee-Arlman Mechanism

The most commonly accepted mechanism for the polymerization was proposed by Cossee and Arlman in 1964 as shown in Figure 1 [18, 19]. The first step, the coordination of the propene monomer at the vacant octahedral coordination site to the transition metal complex where the d-orbitals of the transition metal overlap with the  $\pi$  bonds of the monomer. This step called  $\pi$ -complex or the complexation step. The second step shows the formation of the transition state is assumed to be a four membered ring of Ti, the last carbon atom of the growing chain and the two carbon atoms forming the double bond of the monomer. Third step is the insertion step where the monomer is inserted between the transition metal atom and the

carbon atom of the alkyl group occurring as a syn addition (the insertion of propylene into Ti-C active centre). Finally, the migration step takes place, in which the alkyl group and the vacant site go back to their original position. For obtaining an isotactic polypropylene polymer, the next propylene monomer must undergo complexation and insertion after the migration occurs.

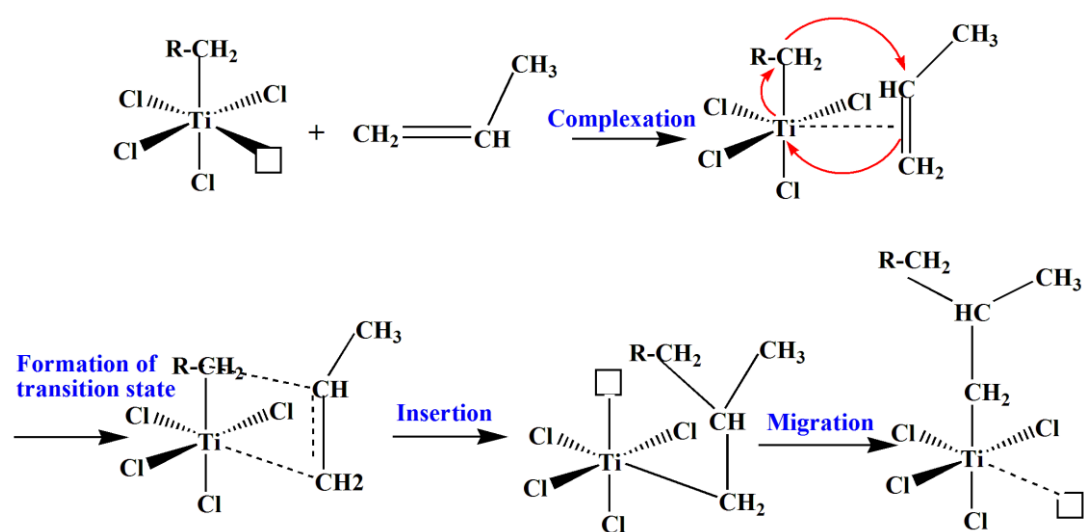


**Figure 1** The Cossee-Arlman mechanism for a heterogeneous Ziegler-Natta catalyst [18, 19].

### 2.1.2.2 Brookhart-Green Mechanism

An alternative and well-accepted mechanism to the Cossee-Arlman was proposed by Brookhart and Green in 1983 [20]. It is sketched in Figure 2, the insertion of the olefin proceeds from a  $\pi$ -complex configuration similar to the Cossee-Arlman but is assisted by the  $\alpha$ -agostic interaction of the Ti and nearby hydrogen belonging to the growing polymeric chain. This reduces steric repulsions between H atoms of the chain and those of the alkene.

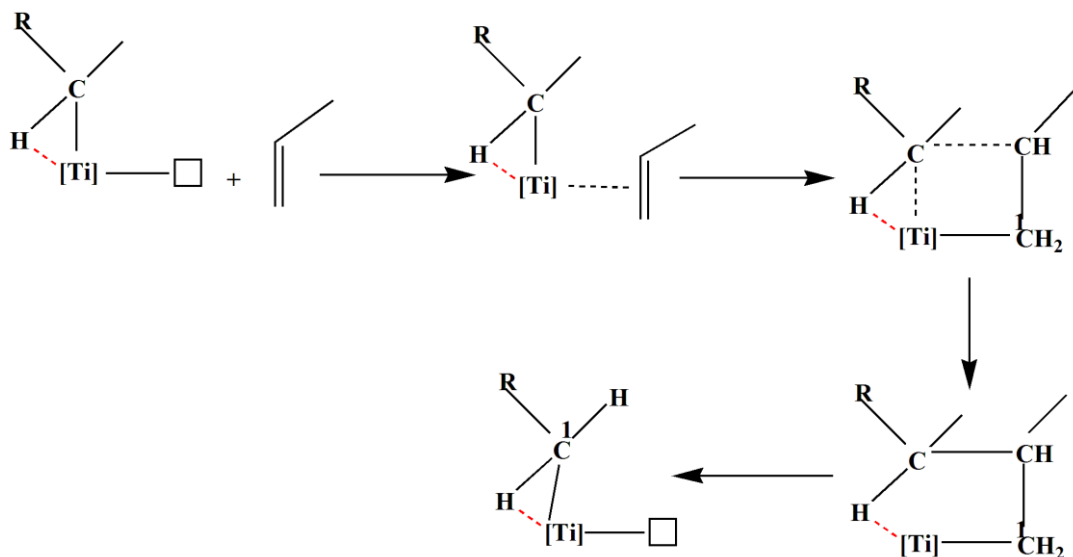


**Figure 2** The Brookhart-Green mechanism for a heterogeneous Ziegler-Natta catalyst [20].

In summary, the ZN catalyzed propylene polymerization is composed of three steps: insertion, propagation, and termination.

### 2.1.3 Electron Donors

It has been reported that the internal donor is bonded directly to the  $MgCl_2$  support [21]. This direct bond between the electron donor and  $MgCl_2$  support suggests that the internal donor has a higher impact on properties of the PP product than the external donor. The internal donor takes part in the active site formation, while the external donor only selectively poisons these sites and replaces the internal electron donors from the catalyst [22]. Specific combinations of internal donor and external donor have major influence on the activity of the catalyst, as well as the isotacticity of resultant polypropylene [23]. Figures 3 and 4 display the

most common chemical formulas for internal donors and external donor types, respectively.

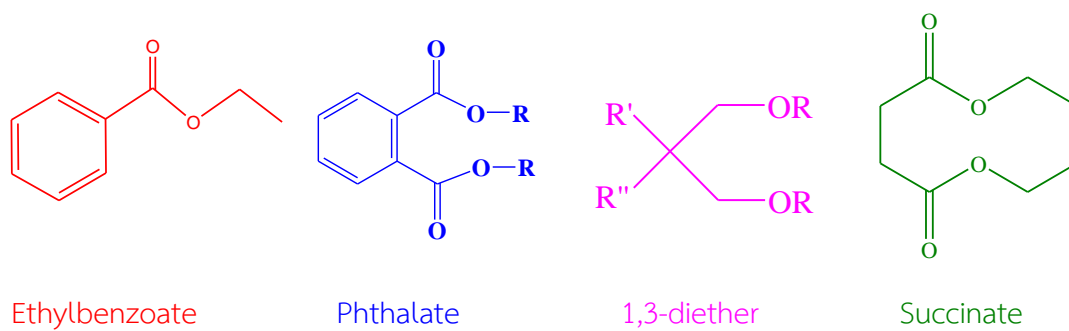


**Figure 3** Chemical formulas of the most common internal donor types.

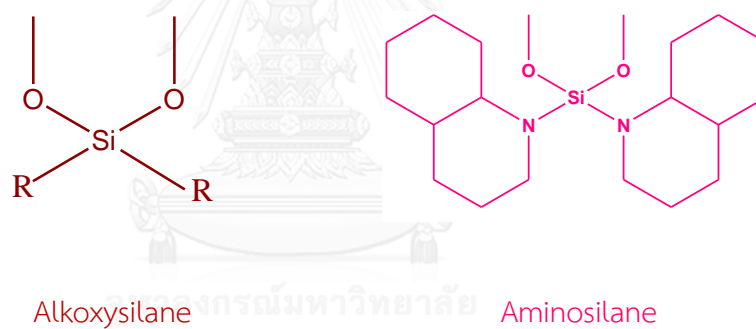


**Figure 4** Chemical formulas of the most common external donor types.

## 2.1.4 Polypropylene

### 2.1.4.1 Physical Properties of Polypropylene

The physical properties of polypropylene are displayed in Table 2 [24].

**Table 2** Physical properties of polypropylene [24].

No.	Properties	Value
1	Density (g/cm <sup>3</sup> )	0.90–0.91
2	Young Modulus (GPa)	1.4
3	Glass Transition Temperature (°C)	–20
4	Limiting oxygen index (LOI) (%)	17
5	Melting temperature (°C)	160
6	Specific Heat Capacity: Conventional (J/kg·K)	1900
7	Specific Heat Capacity: Volumetric (10 J/m·K)	1700
8	Speed of sound (10 m/s)	34–39
9	Stiffness to weight ratio: Tensile (MN·m/kg)	1.2–1.5
10	Stiffness to weight ratio: Tensile, Ultimate (KN·m/kg)	25–39
11	Tensile Strength: Ultimate (MPa)	23–36
12	Thermal Conductivity Ambient (W/m·K)	0.15

### 2.1.4.2 Polypropylene in the World and in Thailand

Polypropylene is one of the fastest growing commodity plastics in the world today. In 2012, the total for world polymer demand is 211 million metric tons. The low-density polyethylene (LDPE), high-density polyethylene (HDPE), linear low-density polyethylene (LLDPE) which types of Polyethylene (PE). Therefore, the PE is the most popular and widely used polymer worldwide and

the second is PP (37% of PE and 25% of PP), as presented in Figure 3 [25]. The PP consumption was greater than 100 million tons in 2006 and reached a total of 131 million metric tons in 2012 [26]. For polypropylene in Thailand, the PTT Chemical produces 2.89 million tons of olefins per year, comprising 2.38 million tons of ethylene and 512,000 tons of propylene [27]. Moreover, several company produces high quality polypropylene which are raw materials widely used in plastic industry such as Thai Polypropylene Co., Ltd. is a polyolefins manufacturer wholly owned by SCG Chemicals Co., Ltd., and IRPC Public Company Limited is a producer of integrated petrochemical products which included of HDPE, PP and etc. for sell as raw materials to plastic converters.

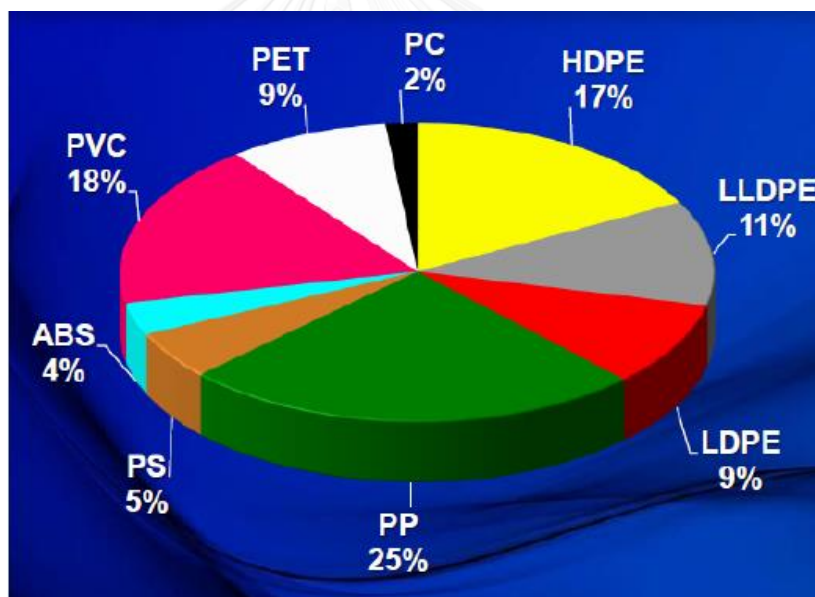


**Figure 5** A pie chart presenting world polymer usage [26].

#### 2.1.4.3 Tacticity of Polypropylene

Since propylene is an asymmetrical monomer, PP can be produced with different stereochemical configurations. Thus, tacticity is an important concept in understanding the link between PP structure and properties [28]. PP chain

structures have three stereoisomer as shown in Figure 4 [29], depending on how the methyl groups are positioned along the polymer backbone: if all of methyl groups are on the same side of the plane of the main backbone, the polymer is called isotactic; if the methyl groups are on alternating sides, the polymer is called syndiotactic; finally, if the methyl groups are randomly distributed on either side, the polymer is called atactic. Commercial isotactic PP has a melting point that ranges from 160 to 166°C, depending on atactic material and crystallinity. Syndiotactic PP with a crystallinity of 30% has a melting point of 130°C [30]. The fraction of isotactic chains in commercial PP is quantified with the isotacticity index, generally measured as the mass fraction of PP insoluble in boiling heptane or xylene. Hence, the stereoregularity of the PP structure influences crystallinity, melting temperature, solubility and mechanical properties. Moreover, the important factor which governs the quality of PP apart from tacticity of polymer is molecular weight (MW). A polymer usually does not consist of molecules with identical chain length thus distributions of chains with different molecular weight are present and the best way of representing the size of the chains is the molecular weight distribution (MWD) [31]. In general, the higher the molecular weight the tougher the polymer. However, a very high molecular weight can cause difficulties during the processing of the polymers. In addition, the MWD can control various properties of PP, such as temperature resistance, stiffness, strength, etc. [32].

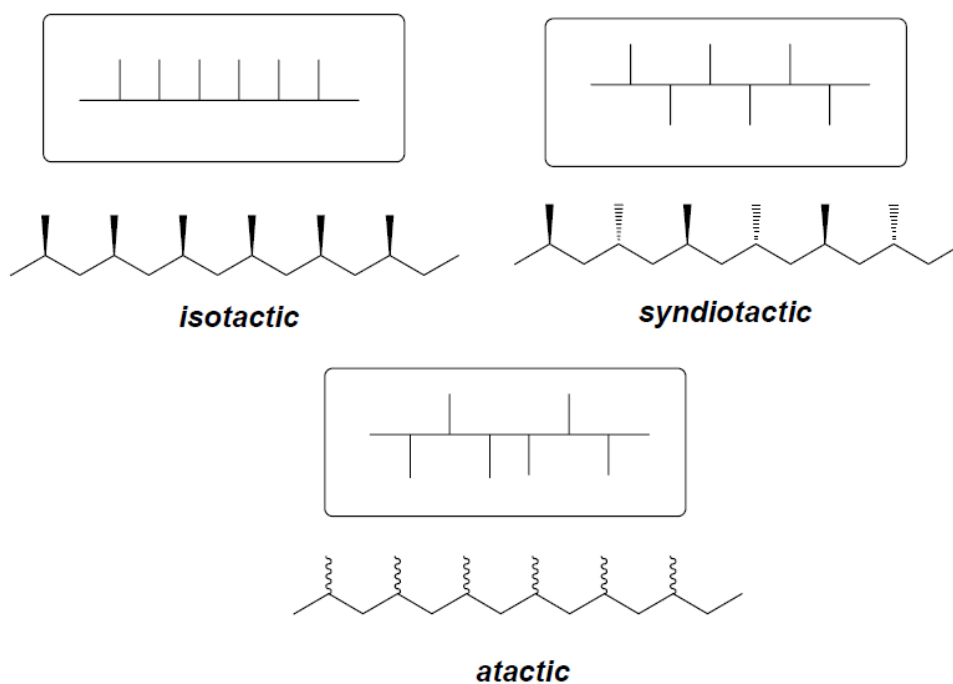


**Figure 6** Three stereoisomers of polypropylene structures; isotactic, syndiotactic, atactic [29].

## 2.2 Background on Quantum Chemistry

### 2.2.1 Density Functional Theory

The foundation of density functional theory (DFT) was laid by Hohenberg-Kohn and Kohn-Sham in 1964 [33]. They showed that the ground-state energy and other properties of a system are uniquely determined by the electron density based on one-electron orbitals [34-36]. Today, the most popular quantum chemical approaches are still DFT[25]. The DFT is based on the performance of approximate exchange correlation functionals [5-8]. Approximate functionals can be classified according to the number of ingredients contained in the recipe used for their development.

In DFT the energy of a system is given as a sum of six components:



$$\mathbf{E}_{\text{DFT}} = \mathbf{E}_{\text{NN}} + \mathbf{E}_{\text{T}} + \mathbf{E}_{\text{V}} + \mathbf{E}_{\text{Coul}} + \mathbf{E}_{\text{exch}} + \mathbf{E}_{\text{corr}} \quad (2.1)$$

Where  $E_{\text{NN}}$  is the nuclear-nuclear repulsion,  $E_{\text{T}}$  is the kinetic energy of the electrons,  $E_{\text{V}}$  is the nuclear-electron attraction,  $E_{\text{Coul}}$  is the classical electron-electron Coulomb repulsion,  $E_{\text{exch}}$  is the non-classical electron-electron exchange energies, however,  $E_{\text{exch}}$  different from those used in Hartree-Fock (HF) theory. The last term  $E_{\text{corr}}$  is the correlated movement of electrons of different spin and is not accounted for in HF theory.

In ground-state DFT one is interested in systems of  $N$  interacting electrons described by the Hamiltonian,  $\hat{\mathbf{H}}$  with the kinetic, potential and two particle interaction energy operators  $\hat{\mathbf{T}}$ ,  $\hat{\mathbf{V}}$  and  $\hat{\mathbf{V}}_{\text{ee}}$ , respectively. Where  $N$  is the number of electrons.

$$\hat{\mathbf{H}} = \hat{\mathbf{T}} + \hat{\mathbf{V}} + \hat{\mathbf{V}}_{\text{ee}} \quad (2.2)$$

$$\hat{\mathbf{H}} = -\sum_{i=1}^N \frac{\nabla_i^2}{2} + \sum_{i=1}^N v(\mathbf{r}_i) + \frac{1}{2} \sum_{i=1}^N \sum_{\substack{j=1 \\ i \neq j}}^N \frac{1}{|\mathbf{r}_i - \mathbf{r}_j|} \quad (2.3)$$

The Hohenberg-Kohn theorem states that the density  $\rho(\mathbf{r})$  of a non-degenerate ground state uniquely determines the external potential  $v(\mathbf{r})$  up to an arbitrary constant. This means one cannot find two potentials differing by more than a constant that yield the same density. Thus, the ground-state energy as a functional of the external potential  $v(\mathbf{r})$  according to

$$E(v) = \langle \Psi[v] | \hat{\mathbf{H}}_v | \Psi[v] \rangle \quad (2.4)$$

The ground-state energy  $E_0$  and the ground-state density  $\rho_0(\mathbf{r})$  of a system characterized by the potential  $v_0(\mathbf{r})$  can be obtained from a variational principle which involves only the density, thus, the ground state energy can be written as a functional of the density,  $E_{v_0}[\rho]$

$$E_0 = E_{v_0}[\rho_0] < E_{v_0}[\rho] \quad (2.5)$$

There exists a functional  $F[\rho]$  such that the energy functional can be written as

$$E_{v_0}[\rho] = F[\rho] + \int d^3r v_0(\mathbf{r})\rho(\mathbf{r}) \quad (2.6)$$

The functional  $F[\rho]$  is universal in the sense that, for a given particle-particle interaction, it is independent of the potential  $v_0(\mathbf{r})$  of the particular system under consideration, i.e., it has the same functional form for all systems.

The Hohenberg-Kohn theorem provides the basic theoretical foundation for the construction of an effective single-particle scheme which allows the calculation of the ground state density and energy of systems of interacting electrons. Therefore, the Kohn-Sham equations are at the heart of modern DFT. They have the form of the single-particle **Schrödinger** equation.

$$\left[ -\frac{\nabla^2}{2} + v_s(\mathbf{r}) \right] \varphi_i(\mathbf{r}) = \varepsilon_i \varphi_i(\mathbf{r}) \quad (2.7)$$

The density can then be computed from the  $N$  single-particle orbitals occupied in the ground state Slater determinant

$$\mathbf{n}(\mathbf{r}) = \sum_i^{\text{occ}} |\varphi_i(\mathbf{r})|^2 \quad (2.8)$$

The Kohn-Sham scheme is to construct the single-particle potential  $v_s(\mathbf{r})$  in such a way that the density of the auxiliary non-interacting system equals the density of the interacting system of interest. To this end one partitions the Hohenberg-Kohn functional in the following way

$$F[\mathbf{n}] = T_s[\mathbf{n}] + U[\mathbf{n}] + E_{\text{xc}}[\mathbf{n}] \quad (2.9)$$

Where,

$$U[\mathbf{n}] = \frac{1}{2} \int d^3r \int d^3r' \frac{\mathbf{n}(\mathbf{r})\mathbf{n}(\mathbf{r}')}{|\mathbf{r}-\mathbf{r}'|} \quad (2.10)$$

$U[\mathbf{n}]$  is the classical electrostatic energy of the charge distribution  $\mathbf{n}(\mathbf{r})$ , and

$E_{\text{xc}}[\mathbf{n}]$  is the so-called exchange-correlation energy which is formally defined by

$$E_{\text{xc}}[\mathbf{n}] = T[\mathbf{n}] + V_{\text{ee}}[\mathbf{n}] - U[\mathbf{n}] - T_s[\mathbf{n}] \quad (2.11)$$

### 2.2.2 DFT Functionals

Main functionals consist of 1. Local-density approximations (LDA)

2. Generalized gradient approximation (GGA) 3. Meta-GGA (MGGA) 4. Hybrid-GGA (HGGA) 5. Hybrid meta-GGA (HMGGGA) [37].

### 2.2.2.1 Local Density Approximations (LDA)

Local Density Approximations or LDA are a class of approximations to the exchange–correlation (XC) energy functional in density functional theory that depend on the value of the electronic density at each point in space [38].

In general, the exchange–correlation energy of a spin-unpolarized is obtained by assuming that its density can locally be treated as a uniform electron gas. Thus, the XC energy can be written as

$$E_{XC}^{LDA}[\rho] = \int \rho(\mathbf{r}) \varepsilon_{XC}(\rho(\mathbf{r})) d\mathbf{r} \quad (2.12)$$

where  $\rho$  is the electronic density and  $\varepsilon_{XC}$  is the exchange-correlation energy per particle of a homogeneous electron gas of charge density. The exchange-correlation energy can be split into exchange and correlation terms

$$\varepsilon_{XC}(\rho(\mathbf{r})) = \varepsilon_X(\rho(\mathbf{r})) + \varepsilon_C(\rho(\mathbf{r})) \quad (2.13)$$

Additionally, the exchange part is given by the Dirac expression

$$\varepsilon_X(\rho(\mathbf{r})) = -\frac{3}{4} \left( \frac{3}{\pi} \right)^{1/3} \rho(\mathbf{r})^{1/3} \quad (2.14)$$

The correlation component  $\varepsilon_C$  has been determined by Monte Carlo calculations for a uniform electron gas considering a number of different densities. For open-shell states with an unequal number of  $\alpha$  and  $\beta$  electrons, functionals of the two spin densities lead to more accurate results. However, for certain states with an even number of electrons, for instance the  $H_2$  molecule at larger separation, the unrestricted functionals perform significantly better because they allow symmetry

breaking. Up to this point the LDA was introduced as a functional depend on  $\rho(\mathbf{r})$ . If we extend the LDA to the unrestricted case, we arrive at the local spin-density approximation, or LSDA.

### 2.2.2.2 Generalized Gradient Approximation (GGA)

Because of inadequacies in the Local Density Approximation (LDA) method [38] which lead to a modified the exchange-correlation functional. They try to treat the non-uniformity of real systems by the inclusion of the derivatives of the density. In density, contains terms for the density gradient:

$$E_{XC}^{GGA}[\rho_\alpha\rho_\beta] = \int f(\rho_\alpha, \rho_\beta, \nabla\rho_\alpha, \nabla\rho_\beta)dr \quad (2.15)$$

$E_{XC}^{GGA}$  is usually split into its exchange and correlation contributions;

$$E_{XC}^{GGA} = E_X^{GGA} + E_C^{GGA} \quad (2.16)$$

One of the most commonly used non-empirical functionals is the Perdew-Becke- Ernzerhof (PBE) functional [39, 40], while Becke 1988 (B88)[41] is certainly the most commonly used empirical exchange functional. Other well-known functionals include Perdew 1986 (P86) [42] and Lee-Yang-Parr (LYP) correlation [43] and Perdew-Wang 1991 (PW91) exchange-correlation[44]. In all cases, the names of these functionals refer to their respective authors and the year of publication. All combinations of exchange and correlation functionals are possible, for example, the commonly used BLYP method [41, 43] which combines Becke's 1988 exchange functional with the correlation functional by Lee, Yang, and Parr.

### 2.2.2.3 Meta-GGA

The kinetic energy density,  $\tau(\mathbf{r})$ , is an additional Kohn–Sham contribution that can be calculated. In general, MGGA functionals [45] have the following form:

$$E_{XC}^{MGGA}[\rho] = \int \rho(\mathbf{r}) \varepsilon_{XC}(\rho(\mathbf{r}), \nabla \rho(\mathbf{r}), \tau(\mathbf{r})) d\mathbf{r} \quad (2.17)$$

In addition, the kinetic energy density,  $\tau(\mathbf{r})$  of the Kohn-Sham orbitals can be derived from,

$$\tau(\mathbf{r}) = \frac{1}{2} \sum_i^{\text{occ}} |\nabla \phi_i(\mathbf{r})|^2 \quad (2.18)$$

The main advantage of including kinetic energy densities is that it mostly eliminates self-interaction errors, causing inaccuracies with LDA and GGA functionals at low-density and strong interaction limits. In intermediate regions, however, MGGA functionals usually do not provide substantial improvement to corresponding GGAs. A non-empirical example is the Tao-Perdew-Staroverov-Scuseria (TPSS) functional [46], an empirical one is Truhlar and Zhao’s Minnesota 2006-Local (M06-L) [47].

### 2.2.2.4 Hybrid-GGA

Hybrid DFT with exact exchange: An entirely different approach to improve deficiencies in GGA functionals is to incorporate the so-called exact exchange energy contributions. The exact exchange energy  $E_x^{\text{exact}}$  is a derivative from the Hartree–Fock approximation, and is obtained by solving only the exchange part of the exchange-correlation functional exactly. The result is an energy value that when scaled according to provides a convenient cancellation of errors, making hybrid DFT methods surprisingly accurate. Based on this idea, the highly popular hybrid DFT method B3LYP[48] combines exact HF exchange with the Slater[49] local exchange functional.

$$E_{XC}^{\text{hybrid}} = E_X^{\text{GGA}} + a(E_X^{\text{exact}} - E_X^{\text{GGA}}) \quad (2.19)$$

As an example, the Becke-3-LYP (B3LYP) functional;

$$E_{xc}^{\text{B3LYP}} = a_{x0}E_x^S + (1 - a_{x0})E_x^{\text{HF}} + a_{x1}\Delta E_x^B + E_C^{\text{VWN}} + a_c\Delta E_C^{\text{LYP}} \quad (2.20)$$

With three scaling factors parameters  $a_{x0} = 0.80$ ,  $a_{x1} = 0.72$  and  $a_c = 0.81$ . These values were obtained from fitting of a selected set of thermochemical data. The term  $E_x^{\text{HF}}$  is calculated using the Kohn-Sham orbitals in the manner of HF procedure by computing the exchange integrals  $(\nu\mu|\mu\nu)$ ,  $E_x^S$  is Slater local density exchange,  $E_x^B$  is Becke's 1988 [50], the Slater exchange along with correction involving the gradient of the density.  $E_C^{\text{VWN}}$  is Vosko, Wilk and Nusair [51]. Correlation functional and  $E_C^{\text{LYP}}$  is the correction function of Lee, Yang and Parr [43]. Apart from B3LYP wide popularity use PBE0 [52], TPSS0[53] and B3LYP [41, 43].

#### 2.2.2.5 Hybrid Meta-GGA

One of the above types of functionals with a portion of exact exchange from Hartree-Fock theory added[54]. For example of Hybrid meta-GGA is TPSSh which probably improvement over PBE0; perhaps increase fraction of HF to 25% [53].

For instance; the hybrid form of TPSSh functional is obtained by mixing TPSS with exact exchange as follows:

$$E_{xc}^{\text{TPSSh}} = a_0 E_x^{\text{exact}} + (1 - a_0) E_x^{\text{TPSS}} + E_C^{\text{TPSS}} \quad (2.21)$$

TPSSh functional has one empirical parameter whose optimal value  $a_0 = 0.10$  [55].

The value of  $a_0 = 0.10$  in the TPSSh hybrid meta-GGA, being smaller than for a typical GGA hybrid (by about 20%), indicates that the TPSS meta-GGA is a better approximate exchange functional than the other GGAs. Furthermore, hybrid meta-GGA approaches can be considered as an improvement over the pure meta-GGA models, as the hybrid GGA have been an improvement over GGA's [56].

### 2.2.3 Dispersion Part in the Functionals

A general drawback of all common GGA functionals, including hybrids, that replace part of the local by nonlocal HF exchange, is that they cannot describe long-range electron correlations that are responsible for van derWaals (vdW, dispersive) forces. The vdW interactions between atoms and molecules play an important role in many chemical systems. The density functional theory including the empirical dispersion contributions was proposed by Grimme [57, 58]. For the dispersion part in the functional the total energy is given by

$$E_{\text{DFT-D}} = E_{\text{KS-DFT}} + E_{\text{disp}} \quad (2.22)$$

Where  $E_{\text{KS-DFT}}$  is the usual self-consistent Kohn–Sham energy as obtained from the chosen DF and  $E_{\text{disp}}$  is an empirical dispersion correction given by

$$E_{\text{disp}} = s_6 \sum_{\mathbf{g}} \sum_{ij} f(R_{ij,\mathbf{g}}) \frac{C_6^{ij}}{R_{ij,\mathbf{g}}^6} \quad (2.23)$$

Where the summation is over all atom pairs  $i,j$  and lattice vectors  $\mathbf{g}$  which define the cells of the  $j$ th atom, with the exclusion of the  $i = j$  contribution for  $\mathbf{g} = 0$ ;  $C_6^{ij}$  is the dispersion coefficient for the  $ij$ th pair of atoms;  $f$  is a damping function used to avoid near-singularities for small inter-atomic distances  $R_{ij,\mathbf{g}}^6$ ;  $s_6$  is a scaling factor that



depends on the adopted DFT method (for example, B3LYP  $S_6 = 1.0$  [59]; for PBE0  $S_6 = 0.6$  [60]).

## 2.3 Background on Quantitative Structure-Activity/Property Relationship

### 2.3.1 Theory in QSAR/QSPR Statistics

A wide variety of statistical techniques are used in QSAR/QSPR analysis. We select only we used in our thesis.

#### 2.3.1.1 Initial Data Analysis

The first step in statistical analysis of data should be to “look” at the data with appropriate graphical tools to get an idea about the quality of the data [61]. Most statistical techniques assume that data follows a normal distribution. If the input data diverges greatly from the expected distribution, the final results may have little statistical significance. Thus, the univariate analysis should be used to inspect the data, and see a number of statistics which will give the distribution details of the data. The initial analysis techniques is available in QSAR:

- 1) **Univariate analysis** [62] is a technique for generating statistics independently for a selected column of data. These statistics can be used to get an idea about the distribution of the data concerned.
- 2) **Standardizing data** [63] is a technique that involves the creation of a new column of data from another column of data, with those data being scaled and translated to meet certain specified standardization requirements.
- 3) **Transforming data** [64] is a technique that involves applying certain simple functions to the data with the idea of improving the distribution.

### 2.3.1.2 Data Reduction

In analysis of the large data set, it is often necessary to calculate or measure many variables as possible to describe the data samples. Although you can analyze all of the variables thus generated, there is an increased risk of over fitting the data. One way to reduce this risk is to look carefully at the data by using principle components analysis or PCA before performing the main statistical analysis [65]. PCA is a technique that involves the determination of the principal components of a multi-dimensional data set and the subsequent transformation of the data to a smaller number of columns with minimal loss of information [66]. Alternatively, a correlation matrix [67] is a table of all possible pairwise correlation coefficients for a set of variables. It can be used to help identify highly correlated pairs of variables, and thus identify redundancy in the data set. Correlation coefficient has value from -1.0 to 1.0. If a correlation coefficient nearly 1.0/-1.0 which indicated that two variables are perfectly correlated and if a coefficient equal 0.0 shows no correlation. A negative coefficient means inverse relationship between variables. Example of the correlation matrix for a group of four variables, i.e., a, b, c, and d as shown in Table 3 below;

**Table 3** Example of the correlation matrix for a group of four variables.

	a	b	c	d
a	1.00	0.85	0.21	0.96
b	0.85	1.00	-0.71	0.62
c	0.21	-0.71	1.00	0.46
d	0.96	0.62	0.46	1.00

This correlation matrix shows that ab and ad are highly correlated pairs of variables. It is likely that at least one of these four variables could be removed from the data set without losing useful information.

### 2.3.1.3 Model Building

Model building techniques allow you to generate parameters for a predictive QSA/PR model to describe response data in terms of explanatory variables. There are many statistical methods available to fit the model [68, 69]. Most used methods are Multiple Linear Regression (MLR), Partial Least Squares (PLS), and Genetic Function Approximation (GFA) techniques.

## 2.3.2 Regression Analysis for QSAR/QSPR Study

### 2.3.2.1 Multiple Linear Regression

MLR is a technique [70] that uses a stepping multiple linear regression algorithm to generate a model. In simple multiple regression, all the input x variables are used in the equation to predict y. In stepwise multiple regression, a selection algorithm is used to choose a subset of the input x variables. A choice of stepping algorithm to use for the selection of variables for the regression equation [71]. At each step of the algorithm, the partial F values are calculated for each variable, and these are then compared with user-defined parameters to determine which variable should enter or leave the calculation.

The overall F statistic for a model is:

$$F = \text{Explained Mean Square} / \text{Residual Mean Square} \quad (2.24)$$

Partial F values are an estimation of the contribution of each variable toward the F for the final model [72]. Stepwise selection of the candidate explanatory variables may be carried out with either a fixed number of steps or an automatically determined end point. Moreover, the forward and backward stepping algorithms may give regression equations that use different variables. This can be caused by collinearity of variables in the data set and may indicate instability in the model.

The major drawback of regression analysis is the danger of over fitting. This is the risk that an apparently good regression equation will be found which is based on a chance numerical relationship between the y variable and one or more of the x variables, rather than a genuine predictive relationship. When an over fitted model is used predictively, the predicted values for untested compounds can turn out to be very different from the true values, when these are eventually determined, even though the predicted values for the original tested compounds used to derive the regression equation were close to the true values. Such a regression equation has no predictive power.

#### 2.3.2.2 Partial Least Squares

PLS analysis [73, 74] is a popular regression technique which can be used to relate one or more dependent variable (Y) to several independent (X) variables. PLS relates a matrix Y of dependent variables to a matrix X of molecular structure descriptors. PLS is useful in situations where the number of independent variables exceeds the number of observation, when X data contain collinearity. PLS creates orthogonal components using existing correlations between independent variables and corresponding outputs while also keeping most of the variance of independent variables. Main aim of PLS regression is construct predictive models when factors are many and highly collinear by employed cross validation technique [75]. This technique used to estimate the true predictive power of every regression model to reduce the risk of chance over fitting.  $R^2_{CV}$  is derived from cross validation. Mostly use leave-one out cross validation. The comparison of  $R^2_{CV}$  with  $R^2$  can be used to help determine an appropriate number of vectors for the analysis. This is a key measure of the predictive power of a model. The closer the value is to 1.0, the better the predictive power. For a good model,  $R^2_{CV}$  should be fairly close to  $R^2$ . If  $R^2_{CV}$  is much less than  $R^2$ , the

regression is probably over fitting the data. A model with an  $R_{CV}^2$  value of 0.0 or less has no predictive power at all [ref]. To calculate  $R_{CV}^2$  following equation (1);

$$R_{CV}^2 = 1 - \frac{\sum(Y_{pred} - Y_{act})^2}{\sum(Y_{act} - Y_{mean})^2} \quad (2.25)$$

$Y_{pred}$ ,  $Y_{act}$ , and  $Y_{mean}$  are predicted, actual, and mean values of the activity, respectively.  $\sum(Y_{pred} - Y_{act})^2$  is the predictive residual error sum of squares (PRESS).

In addition, definitive validity of model is examined by mean of external validation also, which evaluates how well equation generalizes. Training set is used to derive an adjustment model that is used after to predict activities of test set. The predicted power of equations was validated using predictive squared correlation coefficients ( $R_{pred}^2$ ). To calculate the  $R_{pred}^2$  following equation (2);

$$R_{pred}^2 = 1 - \frac{\sum(Y_{pred(Test)} - Y_{Test})^2}{\sum(Y_{Test} - Y_{Training})^2} \quad (2.26)$$

Where  $Y_{Pred(Test)}$  and  $Y_{Test}$  are predicted and actual activity values, respectively, of test set compounds, and  $Y_{Training}$  is the mean activity value of training set.

### 2.3.2.3 Genetic Function Approximation

GFA is a technique [76] that uses genetic mutation of possible functions of the explanatory variables to obtain a model that best fits the response data. The genetic algorithms are search algorithms that take inspiration from natural genetics and evolution. The genetic algorithm works with a set of the string. Each string represents a location in the search space. These strings can be called a population. This population is evolved in a manner that leads it toward the objective of the

search. This requires that a measure of the fitness of each string, corresponding to a model in the GFA. The scoring criteria for GFA models are all related to the quality of the regression fit to the data. Thus, three operations for GFA approach are performed iteratively in succession: 1) Selection; two parents are selected from the present population, with probabilities proportional to their fitness. 2) Crossover; a crossover splices and rejoins the characters in the two parent strings to create a new child string. 3) Mutation; in the GFA algorithm, mutations are performed with a user-defined probability after each crossover. Furthermore, the GFA proceeds for a user-specified number of generations which means that a number of attempted crossovers equal to the size of the population. The GFA algorithm is assumed to have converged when no improvement is seen in the score of the population over a significant length of time, either that of the best model in each population or the average of all the models in each population. When this criterion has been satisfied, no further generations are calculated. The GFA algorithm approach has several advantages over other techniques: 1) it constructs multiple models rather than a single model. 2) It automatically selects which variables are to be used in the models. 3) It can be created non-linear models. 4) It includes Friedman's lack-of fit error which estimates the most appropriate number of variables by minimized least squares error, resists over fitting. However, disadvantages of GFA procedure is it takes too long to perform cross validation on each generation and, thus, you need to have a reasonable idea of how many terms to keep before you start.

## CHAPTER III

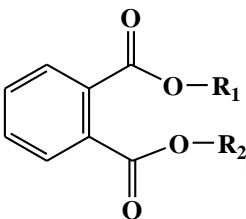
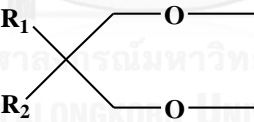
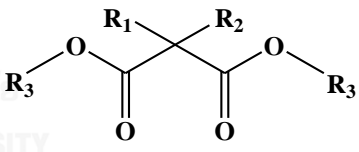
### STRUCTURE AND ACTIVITY DATA

#### 3.1 Chemical Structure of Electron Donors

##### 3.1.1 Data and Activity

There are three types of internal electron donors consisting of phthalates, 1,3-diethers, and malonates used in this study. Their structures and experimental activities are listed in Table 4. The activities for each group were obtained from different experiments.

**Table 4** Chemical structures of 29 internal electron donors with different substituents ( $R_1$ ,  $R_2$  and  $R_3$ ) [77-80]

					
Phthalate group (P1-P8)	1,3-diether group (D1-D9)	Malonate group (M1-M12)			
Name	R1	R2	R3	Activity (kg PP/g Cat.)	Ref.
P1	cyclohexyl	cyclohexyl	-	3.93	[77]
P2	ethyl	ethyl	-	10.01	[77]
P3	2-ethylhexyl	2-ethylhexyl	-	13.15	[77]
P4	octyl	octyl	-	15.83	[77]

P5	isobutyl	isobutyl	-	24.25	[77]
P6	isoheptyl	isoheptyl	-	24.79	[77]
P7	butyl	butyl	-	26.12	[77]
P8	isononyl	isononyl	-	20.63	[77]
D1	H	H	-	2.00	[78]
D2	methyl	H	-	15.00	[78]
D3	methyl	methyl	-	17.50	[78]
D4	isopropyl	methyl	-	20.00	[78]
D5	isopropyl	isopropyl	-	21.00	[78]
D6	propyl	propyl	-	16.50	[78]
D7	isobutyl	isobutyl	-	30.00	[78]
D8	cyclopentyl	cyclopentyl	-	26.00	[78]
D9	cyclohexyl		-	12.65	[78]
M1	H	H	butyl	0.30	[79]
M2	methyl	H	butyl	5.20	[79]
M3	cyclopropyl		butyl	12.0	[79]
M4	methyl	methyl	butyl	16.40	[79]
M5	cyclobutyl		butyl	15.20	[79]
M6	ethyl	ethyl	butyl	19.50	[79]
M7	cyclopentyl	H	butyl	24.80	[79]
M8	butyl	butyl	butyl	8.00	[79]
M9	cyclopentyl	F	ethyl	25.30	[80]
M10	cyclopentyl	Cl	ethyl	27.80	[80]
M11	cyclopentyl	methyl	ethyl	28.60	[80]
M12	cyclopentyl	H	ethyl	25.20	[80]



## CHAPTER IV

### QSAR

#### 4.1 Three Types of Electron Donors Groups

Because of electron donors have played a major role in the Ziegler-Natta catalyzed PP polymerization. Therefore, the relationships between molecular properties and activities of three types of electron donors groups consisting phthalate, 1,3-diether, and malonate groups have been investigated. In this chapter we are interested in designing new potent electron donors with high activity by QSAR technique.

Quantitative Structure Activity Relationship (QSAR) is the study of the quantitative relationship between the experimental activity of a set of compounds and their physicochemical properties using statistical methods. The experimental information associated with catalyst activity, which is used as dependent variables in building a QSAR model. The QSAR model assists the design of materials from diverse sample libraries. It provides *the in silico* screening of potential catalysts prior to the material synthesis and gives the insight into mechanisms. The QSAR approach has been evidenced as a reliable technique for finding correlations between the catalyst structure and its activity [81-85]. Although this technique could not predict the stereoregularity of the polymerized product, it is very useful as a screening study because of its ease of use and speed.

Yao et al. [86] used QSAR approach to study a set of 10 silane external donors of the ZN catalyst systems. The eleven molecular properties calculated from the MD and MM calculations by Discover program were used for fitting the QSAR model. The usage of models obtained from that work was limited because of the

small size of the training set and molecular properties. Tanase et al. [87] synthesized new malonate compounds ( $R_1R_2C(COOBu)_2$ ) with various substituents and investigated the relation between chemical structures of malonate compounds and isotacticity/activity by using properties obtained from a computational method. The results concluded that malonate catalysts with an appropriate molecular volume indicated high isotacticity and high activity. However, only few properties such as molecular volume, oxygen charge, and O-O distance were included in the model fitting.

#### 4.2 Geometry Optimization Details

All electron donor compounds were built by Materials Visualizer module as implemented in Materials Studio5.5. [88]. All structures were optimized by the generalized gradient approximation (GGA) [39] with the Perdew–Burke–Ernzerhof (PBE) [89] functional using the DMol3 module [90, 91]. A double numerical polarized (DNP) basis set [57] was employed. The convergence criteria for normal geometry optimization were set to 0.01255kcal/mol in energy and 0.6275 kcal/mol Å in force.

#### 4.3 Molecular Descriptors for QSAR

After obtained structural geometries of three types of electron donors then Fukui function (Nucleophilic and Electrophilic attack), orbitals (HOMO and LUMO), and population analysis (ESP, Mulliken, Hirshfeld charges) were computed to get more structural and electronic properties. Moreover, quantum chemical descriptors which give information about the electronic structure of the molecule were also calculated such as the energy of the highest occupied molecular orbital,  $E_{HOMO}$ , which is a quantitative measure for the chemical reactivity of the compound, the energy of the lowest unoccupied molecular orbital,  $E_{LUMO}$ , which accounts for the electron affinity. The  $E_{HOMO} - E_{LUMO}$  gap or ionization potential can be important descriptors for

predicting how molecules will react. Thus, totally 123 descriptors can be separated into six categories as follows: geometrical descriptors, fragment counts, atomistic descriptors, VAMP electrostatics descriptors, DMol3 molecular descriptors, force energetic descriptors, spatial descriptors were calculated using the QSAR module as implemented in Materials Studio5.5. [88]

Before construction of QSAR model, the distribution of the data must be first investigated. We used univariate analysis to evaluate the quality of the activity data in each group of electron donor that show acceptable normal distribution. If the data are not normally distributed, a numerical transformation to achieve a normal distribution is applied.

The QSAR model was built using the QSAR module of Material Studio5.5 program with the initial analysis to find the properties correlation matrix and model build to find the linear equation between activity and molecular properties. Due to many structural properties, the correlation matrix of all properties is performed to reduce the number of structural properties for the QSAR equation. Then, Genetic Algorithm (GA) [76] was used to find the QSAR model between PP activities and structural properties. Initial parameters were set with population parameter of 100, maximum generations of 500, mutation probability of 0.1 and scoring with Friedman LOF scale of 0.5.

## 4.4 Results and Discussions

### 4.4.1 QSAR model of Phthalate Group

The eight compounds of phthalate group were used to derive the model. Two dominant descriptors were statistically selected into the model as shown in equation 4.1.

$$\text{Activity} = - 3.3691 * \text{Torsion energy} + 322.8069 * \text{O charge} + 212.4315 \quad (4.1)$$

$$R^2 = 0.93, R^2_{CV} = 0.85, N = 8$$

**Table 5** Relationship between the two dominant descriptors from the best QSAR model of the eight compounds in phthalate group and experimental activity.

Name	Activity (kg PP/g Cat.)	=O charge (ESP)	Torsion energy (Forcite Energetics)
P1	3.93	-0.502	13.4125
P2	10.01	-0.524	9.9450
P3	13.15	-0.458	14.7822
P4	15.83	-0.462	13.9785
P5	24.25	-0.488	8.9252
P6	24.79	-0.486	9.9676
P7	26.12	-0.465	10.0274
P8	20.63	-0.457	14.0942

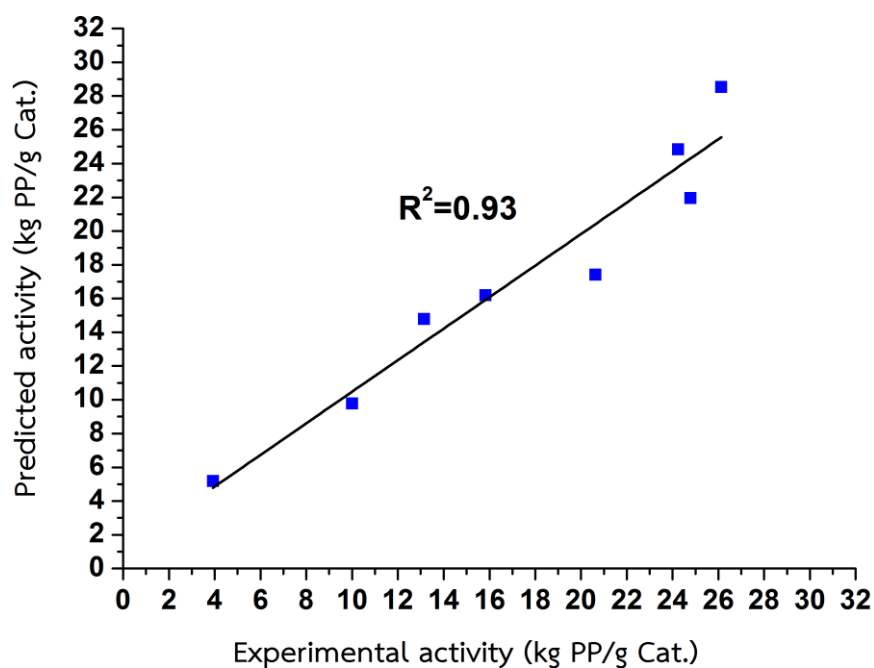
QSAR model in equation (4.1) has a correlation coefficient ( $R^2$ ) of 0.93 and a cross-validated correlation coefficient ( $R^2_{CV}$ ) of 0.85. Both values are considerably higher than the acceptable values ( $R^2 \geq 0.8$ ,  $R^2_{CV} \geq 0.5$ ) [92, 93]. The correlation coefficients between the oxygen carbonyl charge and torsion energy is 0.53 which less than 0.7, indicating no inter-correlation between variables in the model [94].

Table 6 shows the comparison between actual and predicted activity values of the eight phthalate compounds. The residual values indicated that based on predictive ability the model is satisfied. Moreover, the trend of predicted activities from QSAR equation was corresponding to the actual trend.

**Table 6** Predicted activity and residual values of the eight phthalate compounds by the best QSAR model.

Name	Actual activity (kg PP/g Cat.)	Predicted activity (kg PP/g Cat.)	Residual values
P1	3.93	5.19	-1.26
P2	10.01	9.77	0.24
P3	13.15	14.78	-1.63
P4	15.83	16.20	-0.37
P5	24.25	24.83	-0.58
P6	24.79	21.96	2.83
P7	26.12	28.54	-2.42
P8	20.63	17.42	3.21

The relationship between actual and predicted values of activity for the eight phthalate compounds using the best QSAR model was plotted in Figure 7.



**Figure 7** Plot of actual versus predicted activity values from the best QSAR model for the eight phthalate compounds with the GFA statistical method.

In QSAR study, the activity depends on all the variables presented in the model, therefore, using only one variable to predict the activity is not appropriate and it may not give a proper activity value. Then, we performed the analysis for two dominant variables from equation 4.1. This suggest that the activity can be higher when increase in the O charge (oxygen carbonyl atom) obtained from ESP method and decrease in the torsion energy which calculated from forcite energetics of phthalate donors. The phthalate compounds have the O charge in the range from -0.457 to -0.524. A positive coefficient of O charge parameter in the model indicates that the compounds with less negative O charge are designed to have more activity. For the torsion energy property in QSAR model, we can conclude that the PP activity will be increased with small amount of torsion energy, which can be implied that the

branch substituents (less torsion energy) are more active than alkyl chain or alkyl cyclic (high torsion energy).

#### 4.4.2 QSAR model of 1,3-Diether Group

The nine compounds of 1,3-diether group were used to derive the model. Two dominant descriptors were statistically selected into the model as shown in equation 4.2.

$$\text{Activity} = - 1253.1711 * \text{Fukui-Nucleophilic} + 21.5551 * \text{Dipole} + 23.1990 \quad (4.2)$$

$$R^2 = 0.94, R^2_{CV} = 0.84, N = 9$$

**Table 7** Relationship between the two descriptors from the best QSAR model of nine compounds in 1,3-diether group and experimental activity.

Name	Activity (kg PP/g Cat.)	Fukui-Nucleophilic at O atom	Total dipole (DMol3)
D1	2.00	0.035	1.0572
D2	15.00	0.025	1.0100
D3	17.50	0.020	0.9658
D4	20.00	0.021	0.9699
D5	21.00	0.013	0.6624
D6	16.50	0.012	0.3032
D7	30.00	0.008	0.7239
D8	26.00	0.014	0.9748
D9	12.65	0.016	0.6339

QSAR model in equation (4.2) has a correlation coefficient ( $R^2$ ) of 0.94 and a cross-validated correlation coefficient ( $R^2_{cv}$ ) of 0.84 which are higher than the acceptable values [92, 93]. The correlation coefficients between the Fukui-nucleophilic at O atom and total dipole variables was 0.60 which less than 0.7, indicating no inter-correlation between each pair of variables in the model [94].

The comparison between actual and predicted activity values of the nine 1,3-diether compounds is given in Table 8. The residual values indicated that the model is satisfied based on predictive ability.

**Table 8** Predicted activities and residual values of the nine 1,3-diether compounds by the best QSAR model.

Name	Actual activity (kg PP/g Cat.)	Predicted activity (kg PP/g Cat.)	Residual values
D1	2.00	2.13	-0.13
D2	15.00	13.64	1.36
D3	17.50	18.95	-1.45
D4	20.00	17.79	2.21
D5	21.00	21.19	-0.19
D6	16.50	14.70	1.80
D7	30.00	28.78	1.22
D8	26.00	26.67	-0.67
D9	12.65	16.81	-4.16

The relationship between the actual and predicted values of activities for the nine 1,3-diether compounds using the best QSAR model is depicted in Figure 8.



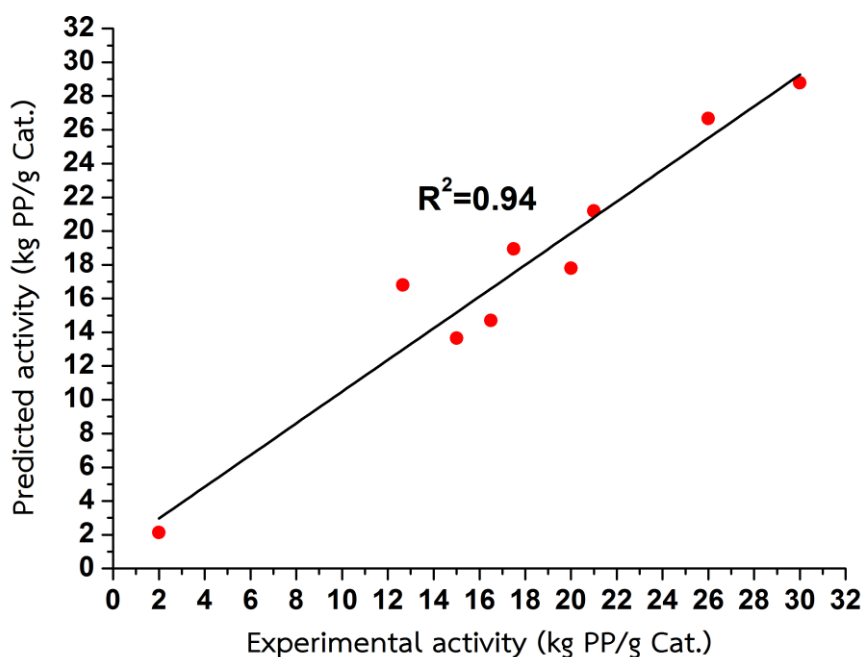


**Figure 8** Plot of actual versus predicted activity values from the best QSAR model for nine 1,3-diether compounds with the GFA statistical method.

Based on the obtained QSAR equation 4.2, there are two properties, total dipole moment and Fukui nucleophilic charge at O atom. The dipole moment representing the polarity of a polar covalent bond, shows positive coefficient value suggesting that the 1,3-diether type with high dipole moment could increase the activity. On the other hand, the PP activity will be increase with more negative Fukui nucleophilic charge of oxygen. This is probably because the oxygen with more negative Fukui nucleophilic charge has more reactivity to nucleophilic attack.

#### 4.4.3 QSAR model of Malonate Group

The halo-malonate compounds were excluded from the malonate group because they arrived from the different experiment.

Before construction of QSAR model of malonate group we used univariate analysis to evaluate the quality of the activity data. The result show not normally distributed, then, a numerical transformation to achieve a normal distribution was applied. The activity values were converted to the logarithm of the activity, which was used as the dependent variable in the QSAR analysis as presented in Table 9. After that, the eight compounds of malonate group were used to derive the model. Two dominant descriptors were statistically selected into the model as shown in equation 4.3.

$$\text{Log activity} = 43.2916 * E_{\text{HOMO}} - 5.6644 * R_{\text{og}} + 33.9396 \quad (4.3)$$

$$R^2 = 0.93, R^2_{\text{CV}} = 0.87, N = 8$$

**Table 9** Relationship between the two descriptors from the best QSAR model of eight compounds in malonate group and experimental activity.

Name	Log activity (kg PP/g Cat.)	Radius of gyration (Spatial Descriptors)	HOMO energy (DMol3)
M1	-0.523	4.3636	-0.225
M2	0.716	4.0868	-0.227
M3	1.079	4.1728	-0.214
M4	1.215	4.0747	-0.228
M5	1.182	4.0807	-0.223
M6	1.290	4.0155	-0.225
M7	1.394	4.0593	-0.226
M8	0.903	4.1049	-0.224

QSAR model in equation (4.3) has a correlation coefficient ( $R^2$ ) of 0.93 and a cross-validated correlation coefficient ( $R^2_{cv}$ ) of 0.87. Both values are higher than the acceptable values[92, 93]. The correlation coefficients between the radius of gyration and homo energy was 0.24 which less than 0.7, indicating no inter-correlation between each pair of variables in the model [94]. The comparison between actual and predicted activity values of malonate compounds is given in Table 10. The predictions are quite reasonable with the residual values in the range of 0.01-0.24.

**Table 10** Predicted log activities and residual values of the eight malonate compounds by the QSAR model.

Name	Actual log activity	Predicted log activity	Residual values
M1	-0.523	-0.515	-0.01
M2	0.716	0.952	-0.24
M3	1.079	1.057	0.02
M4	1.215	1.009	0.21
M5	1.182	1.177	0.01
M6	1.290	1.439	-0.15
M7	1.394	1.157	0.24
M8	0.903	0.980	-0.08

The relationships between actual and predicted values of activities for the 8 malonate compounds using the best QSAR model is shown in Figure 9.

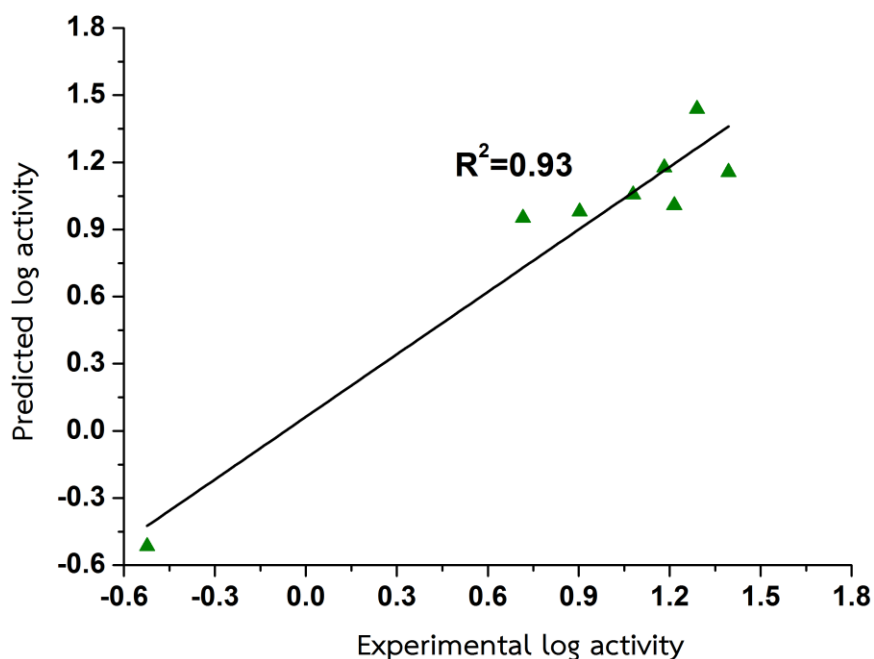


**Figure 9** Plot of actual versus predicted activity values from the best QSAR model for the eight malonate compounds with the GFA statistical method.

The equation 4.3 suggests that the activity can be higher when the radius of gyration and the highest occupied molecular orbital of malonate compounds are decreased. The malonate compounds have HOMO in the range from -0.172 to -0.184 Ha. A negative coefficient of HOMO parameter in the model indicates that compound with more negative HOMO is designed to gain higher activity.

The QSAR model for malonate compounds consists of radius of gyration and HOMO properties. The radius of gyration (Rog) represents the spatial distribution of atom in a molecule from its center of mass which shows negative coefficient, thus, we can imply that less values of radius of gyration of molecules will increase PP activity. HOMO is the highest occupied molecular orbital this property shows that the lower energy level of HOMO could increase the PP reactivity.

#### 4.5 QSAR Summary

The obtained QSAR models provide good relationship between catalytic activities and molecular properties of three types of electron donor groups with high predictive power. From the best QSAR model of phthalate group suggested that more potent phthalate compounds should contain the branch at  $R_1$ ,  $R_2$  substituents (less torsion energy) and substituents should increase in the O charge (oxygen carbonyl atom). Based on the obtained QSAR model of 1,3-diether group suggested that the potent 1,3-diether compounds with high dipole moment and the substituents at  $R_1$ ,  $R_2$  positions should increase the oxygen with more negative Fukui nucleophilic charge. The best QSAR model of malonate group can indicate that less values of radius of gyration of malonate molecules and the lower energy level of HOMO could increase the PP reactivity. The prediction from QSAR approach can be improved if number of compounds is large enough. Thus compounds can be classified into training set and test set. Unfortunately, the number of compounds in each group is rather small and not sufficient to divide into training and test sets.

Group	Statistics			QSAR model
	N	$R^2$	$R^2_{cv}$	
Phthalate	8	0.93	0.85	Activity = - 3.3691*Torsion energy + 322.8069*O charge + 212.4315
1,3-diether	9	0.94	0.84	Activity = - 1253.1711*Fukui-Nucleophilic + 21.5551*Dipole + 23.1990
Malonate	8	0.93	0.87	Log activity = 43.2916* $E_{HOMO}$ - 5.6644*Rog + 33.9396

## CHAPTER V

### QSPR

There has been limited numbers of QSAR studies on catalysts. This is probably due to difficulties in gathering the activity with same experimental conditions, i.e., from the same laboratory. The term of adsorption energy has been created to determine a good electron donor candidate. Since it has been successfully to investigate structural and functional relationship on the  $\text{MgCl}_2/\text{TiCl}_4/\text{Donors}$  complex system. In 2009, Lee et al. [95] found a good relationship between the adsorption energies of 1,3-diethers to  $\text{MgCl}_2$  surface and the isotacticity and the productivity of polypropylene. Thus, for 1,3-diethers the adsorption energy can represent the polypropylene activity. In this chapter, we would like to seek the relation between the adsorption energy of other electron donors and the activity of PP polymerization. If such the relation exists, the QSPR model with large data set from adsorption energies of electron donors could be made. The model could then be used for the design of more potent electron donors. Firstly the relation between adsorption energies and activities of three types of internal electron donors, phthalates, 1,3-diethers and malonates compounds was considered. Then, QSPR models between adsorption energies and molecular properties were sought and tested. Finally, the design of more potent electron donors for ZN catalyzed PP polymerization was suggested.

## 5.1 QSPR Model Setup

The cluster model was used for calculations of the ZN catalyst surface and the adsorption complex. From previous theoretical studies [96-98] it has been suggested that  $\text{TiCl}_4$  is predominantly adsorbed on the  $\text{MgCl}_2(110)$  lateral plane. In addition, Correa et al. [99] concluded that on the (110) surface the donor can coordinate close to the active site while on (104) surface the coordination of the donor is further away. Stukalov et al. [100] suggested the coordination of internal donors in the near proximity of Ti species is believed to be the most reliable molecular model for explaining the internal donors role in stereoregulation. Thus, the  $\text{MgCl}_2(110)$  lateral plane was selected as the adsorption plane for our study.

The ZN catalyst surface is modeled from the  $(\text{MgCl}_2)_{22}$  clusters in the  $\alpha$  crystalline phase with the active Ti atom replacing a Mg atom on the (110) plane (the active site [101]). This model is referred to as  $\text{TiCl}_4/\text{MgCl}_2(110)$ , Figure 10.

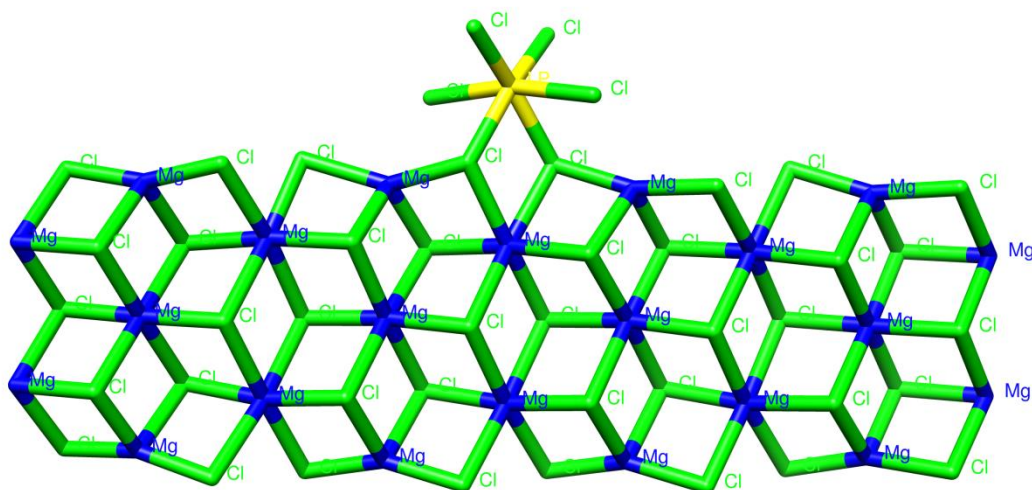


**Figure 10** The 3D-structure of  $\text{TiCl}_4$  on  $\text{MgCl}_2(110)$  surface used in this study. (The color codes are as follows: Ti (yellow), Cl (green), and Mg (blue)).

The adsorption complex structure was generated by aligning the electron donor over the  $\text{MgCl}_2(110)$  lateral plane and within the proximity of the active Ti species, Figure 11.

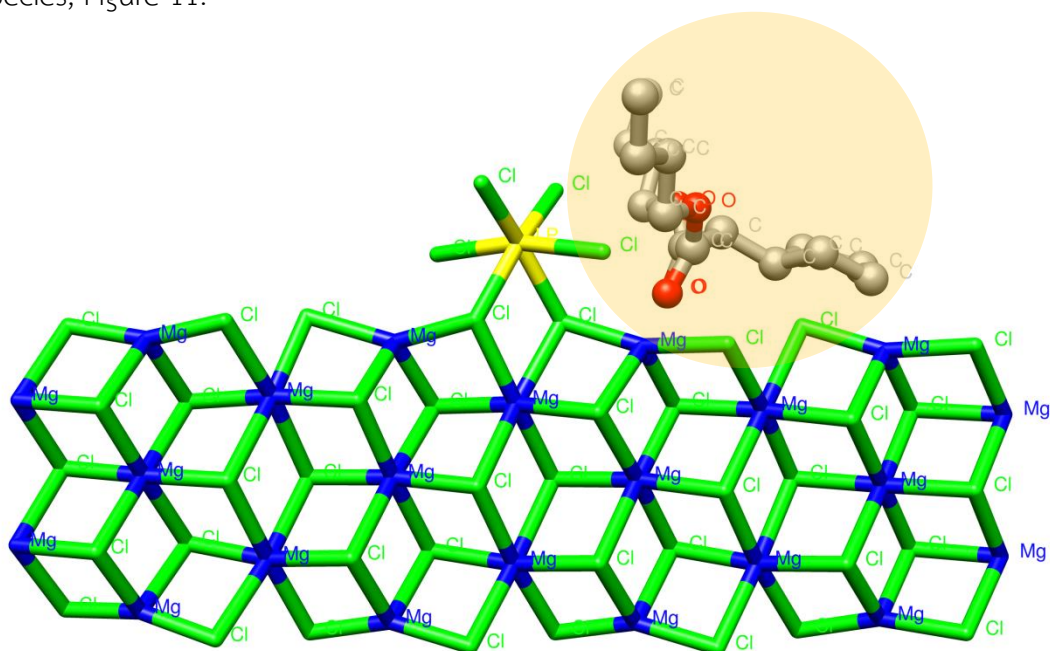


**Figure 11** The adsorption  $\text{TiCl}_4/\text{MgCl}_2(110)$  complex structure generated by aligning the electron donor (Hydrogen atoms of donor are not shown for clarity).

Because of electron donor can bind to the  $\text{MgCl}_2$  surface and adopt a variety of adsorption modes such as mono, chelate, bridge and zip modes [102]. Lee et al. [95] reported that all 1,3-diether donors are adsorbed on the  $\text{MgCl}_2(110)$  surface in the chelate mode. These results are in line with DFT calculations by Tanike et al. [103] and Correa et al. [102]. Moreover, Tanike et al. [103] who studied adsorption energies of four types of internal donors on the  $\text{MgCl}_2$  surface reported that phthalates also prefer to bind in the chelate mode. However, no study on the preferred adsorption mode has been performed for malonate donors. Ratanasak and Parasuk carried out calculations to investigate the preferred adsorption modes of malonate compounds and the calculations suggested the chelate mode [104].



Therefore, the chelate mode is selected as the adsorption mode for our study. The aim of our work is to compare different types of electron donors; we believe that our cluster model will provide a reliable chemical scenario.

## 5.2 Adsorption Energy Calculations

Adsorption energies ( $E_{\text{ads}}$ ) of electron donors on the  $\text{MgCl}_2$  (110) surface were calculated by equation (5.1).

$$E_{\text{ads}} = E(\text{surface}) + E(\text{donor}) - E(\text{complex}) \quad (5.1)$$

Adsorption energies calculations were calculated using the Perdew Burke Ernzerhof (PBE), Generalized Gradient Approximation (GGA) functional [105] and Double numerical with polarization (DNP) basis set [106] were employed together with effective core potentials (ECP) [107]. Geometries of donor molecules and the  $\text{MgCl}_2$ (110) surface were fully optimized while partial optimization were performed for the complex structure in which geometries of  $\text{MgCl}_2$  (110) surface was kept fixed. The convergence criteria for geometry optimization were set to 0.01255 kcal/mol in energy and 2.510 kcal/mol Å in force [1]. All calculations were performed by DMol3 module in the Material Studio 5.5 Suite [108].

## 5.3 QSPR Procedure

We define adsorption energy as the dependent variable Y and 47 molecular properties as the independent variable X which included structural descriptors, atomistic descriptors, spatial descriptors and quantum-chemical descriptors of electron donors were calculated (see Appendix Table A1). Then, we divided the data

set of 29 electron donors into a training set containing 24 compounds used for model development, and a test set of 5 randomly selected compounds (P2, P7, D8, M4, and M10) in Table 4 from three types of electron donors for model validation. After that, we use the Partial Least Squares (PLS) technique for fitting the QSPR models [109].

## 5.4 Results and Discussion

### 5.4.1 Adsorption Energy of Electron Donor on Catalyst Surface

Adsorption energy of electron donor on  $\text{TiCl}_4/\text{MgCl}_2(110)$  surface ( $E_{\text{ads}}$ , kcal/mol) and their energy components of 29 electron donors in the phthalate (P1-P8), 1,3-diether (D1-D9) and malonate (M1-M12) groups are listed in Table 11. Phthalate groups showed adsorption energies ranging from 16 to 29 kcal/mol while 1,3-diether groups are in the range of 7-16 kcal/mol and malonate group are in the range 16 to 30 kcal/mol. The average adsorption energy of phthalate, 1,3-diether, and malonate compounds are 22.80, 12.27, and 24.53 kcal/mol, respectively. Hence, malonate compounds gave higher adsorption energies than two types of electron donors group.

**Table 11** Calculated adsorption energy of electron donor on  $\text{TiCl}_4/\text{MgCl}_2(110)$  surface ( $E_{\text{ads}}$ , kcal/mol) and their energy components of 29 electron donors in the phthalate (P1-P8), 1,3-diether (D1-D9) and malonate (M1-M12) groups.

Name	E(complex) (au)	E(surface) (au)	E(donor) (au)	$E_{\text{ads}}$ (kcal/mol)
P1	-25781.61	-24703.81	-1077.77	16.09
P2	-25469.83	-24703.81	-765.99	17.55
P3	-25941.06	-24703.81	-1237.21	20.95
P4	-25941.06	-24703.81	-1237.21	21.42
P5	-25626.91	-24703.81	-923.06	25.89
P6	-25862.53	-24703.81	-1158.68	26.26
P7	-25705.46	-24703.81	-1001.6	28.99
P8	-26019.6	-24703.81	-1315.75	25.23
D1	-25051.69	-24703.81	-347.86	7.60
D2	-25090.95	-24703.81	-387.13	9.88
D3	-25130.23	-24703.81	-426.4	10.94
D4	-25248.02	-24703.81	-544.19	13.03
D5	-25287.29	-24703.81	-583.46	13.80
D6	-25287.3	-24703.81	-583.47	12.93
D7	-25365.83	-24703.81	-661.99	15.88
D8	-25441.97	-24703.81	-738.13	14.89
D9	-25246.84	-24703.81	-543.01	11.52
M1	-25435.35	-24703.81	-731.52	16.36
M2	-25474.63	-24703.81	-770.78	18.48
M3	-25512.67	-24703.81	-808.82	25.12
M4	-25513.9	-24703.81	-810.05	26.15
M5	-25551.94	-24703.81	-848.09	26.99
M6	-25592.43	-24703.81	-888.58	27.50
M7	-25630.51	-24703.81	-926.66	29.77
M8	-25749.51	-24703.81	-1045.66	24.82
M9	-25572.62	-24703.81	-868.77	24.10
M10	-25932.87	-24703.81	-1229.02	25.26
M11	-25512.7	-24703.81	-808.85	26.11
M12	-25473.43	-24703.81	-769.58	23.71

### 5.4.2 Adsorption Energy and Experimental Activity

Relationship between adsorption energies and experimental activities for each experimental set of three types of internal electron donors, phthalates, 1,3-diethers and malonates compounds was studied. We found the correlation between the experimental PP activity and  $E_{ads}$  for each group of internal electron donor. The squared correlation coefficient ( $R^2$ ) of 0.88, 0.96, and 0.89 for the malonates excluding halo-malonate, phthalates, and 1,3-diethers, respectively was obtained from plotted in Figure 12. The halo-malonate compounds were excluded from the malonate group because they arrived from the different experiment.

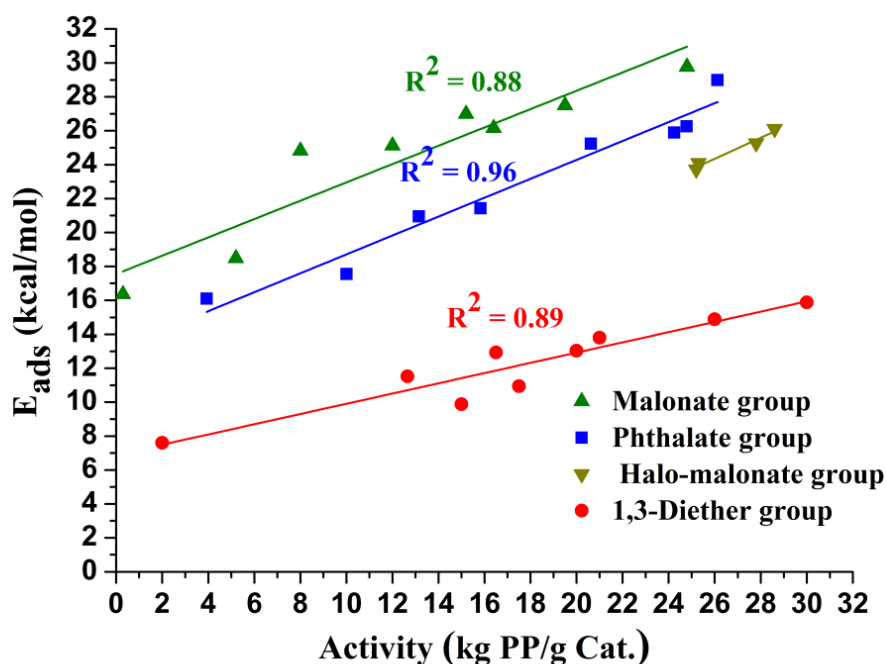


**Figure 12** Plotting graph relationship between the adsorption energy ( $E_{ads}$ ) and the experimental PP activity for the three types of internal electron donor: malonate (halo-malocate), phthalate, and 1,3-diether.

From Figure 12, the high  $R^2$  value suggests that there exhibits the linear relation between adsorption energies of the three donors and PP activities. This is in the same light to that reported by Lee et al. for 1,3-diether compounds [95]. Thus, the compound with the strongest adsorption energy will have the highest activity. Since malonate compounds have stronger adsorption energies among the three groups of electron donors, they should also have higher PP activities. Adsorption energies of 24 electron donors can be used to construct the QSPR model. The prediction of this model will be more reliable than the model obtained from the QSAR model of less than 10 compounds.

#### 5.4.3 QSPR Model on the Adsorption Energy

The PLS analyses of equations with one, two, three, four, five, and six descriptors were performed. The best regression equations with one, two and three descriptors were listed in Table 12. Also, the correlation matrix between various descriptors was constructed and used to identify highly correlated descriptors.

**Table 12** The best QSPR models on the adsorption energy ( $E_{ads}$ ) of 24 electron donors with one, two, three, four, five, and six descriptors shown with the square correlation coefficient ( $R^2$ ) and the square cross-validated value ( $R^2_{cv}$ ).

Des.	Equations	$R^2$	$R^2_{cv}$	s	F
1	$E_{ads} = 1.8204BE + 6.1337$	0.66	0.66	3.93	43.56
2	$E_{ads} = 3.4071Rog + 1.2591BE - 3.4834$	0.84	0.83	2.79	54.44
3	$E_{ads} = 2.3141Rog + 1.6036Dipole + 0.8552BE + 0.9902$	<b>0.84</b>	<b>0.83</b>	<b>2.61</b>	<b>64.00</b>
4	$E_{ads} = 1.6711Rog + 1.1580 Dipole + 0.6175BE - 0.0393Hf - 0.4987$	0.83	0.82	2.61	64.00

5	$E_{\text{ads}} = 1.3356\text{Rog} + 0.9255\text{Dipole} + 0.4935\text{BE}$ - 0.0314Hf - 110.0500HOMO - 20.2945	0.80	0.79	2.61	64.00
6	$E_{\text{ads}} = 1.0954\text{Rog} + 0.7591\text{Dipole} + 0.4048\text{BE}$ - 0.0257Hf - 90.2639HOMO - 25.8824LUMO-HOMO - 8.1784	0.78	0.77	2.61	64.00

\* Des. = Descriptor(s) , BE = Forcite bond energy,

Dipole = VAMP dipole moment Y component, Rog = Radius of gyration,

Hf = Heat of formation (VAMP Electrostatics),

HOMO = HOMO energy (DMol3), LUMO-HOMO = LUMO-HOMO energy (DMol3)

Considering the one-descriptor model with the BE descriptor has the squared correlation coefficient ( $R^2$ ) lower than the acceptable value (0.80 [110]) while it has the squared cross-validated value ( $R^2_{\text{cv}}$ ) exceeding the acceptable value (0.50 [111]). Thus, the one-descriptor model was excluded. For the two-descriptor model with the BE and the Rog descriptors, both  $R^2$  and  $R^2_{\text{cv}}$  of the equation are higher than the acceptable values, however both of Rog and BE are steric descriptors. The two-descriptor model still lacks the electronic descriptor. "Cruz and co-workers [83] studied the catalytic activity of the 25 metallocene catalysts data set by the 3D QSPR model. That model was used to successfully predict the activity of three additional catalysts within the experimental error. The study suggested that the compound which can constitute the stronger LUMO field will have an enhanced polymerization activity. Finally, we choose three-descriptor model with the BE, the Rog, and Dipole descriptors. The meanings of descriptors in the best QSPR model with three-descriptor are 1) the forcite bond energy (BE) reflects the stability of the molecule due to the atomic alignment (molecular geometry) or molecular stress and strain 2) The Vamp dipole y (Dipole) indicates the strength of the dipole interaction

and the orientation of the molecule in the y-direction 3) the radius of gyration ( $R_{og}$ ) represents the spatial distribution of atom in a molecule from its center of mass.

Apart from  $R^2$  and  $R^2_{cv}$  we found the standard deviation ( $s$ ) of the three-descriptor model ( $s = 2.61$ ) is lower than that of the two-descriptor model ( $s = 2.79$ ) while the Fisher  $F$  statistic value of the three-descriptor model ( $F = 64.00$ ) is greater than that of the two-descriptor model ( $F = 54.44$ ). The lower  $s$  and greater  $F$  values suggest the three-descriptor model as the better regression model. Moreover, from the Table 12, it can be seen that the  $R^2$  and  $R^2_{cv}$  values are not improved when more descriptors were added for the fitting. This suggests the over fitting for the models with 4, 5, and 6 descriptors. Additionally, this equation has the value of  $R^2_{cv}$  very close to  $R^2$  indicating the robustness of the equation. It implies that the statistic of the equation is not dominated by just a few molecules.

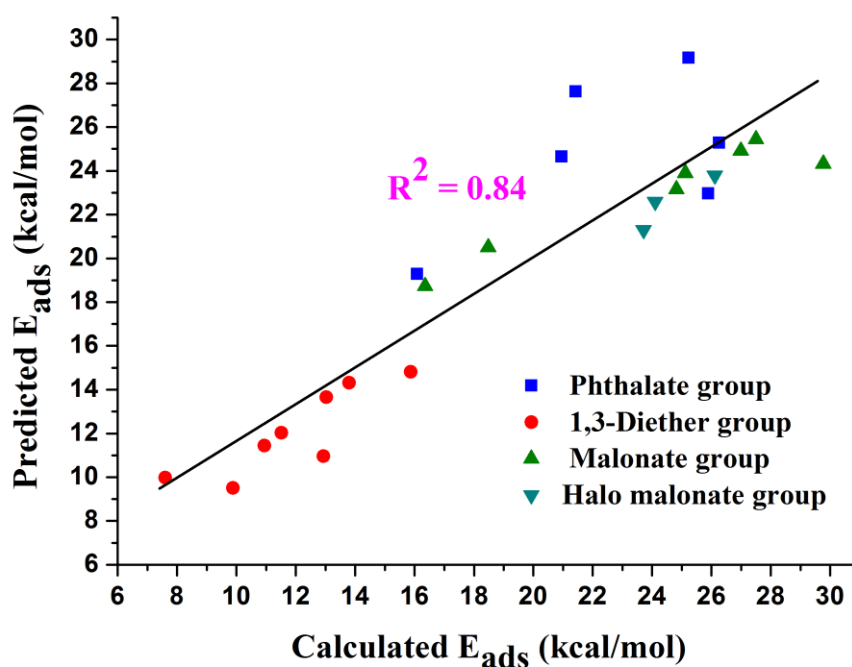


**Figure 13** Relationship between calculated and predicted values of adsorption energies for the 24 compounds as training set using the best QSPR model.

The coefficient in front of the descriptor times the descriptor value suggests the contribution of a particular descriptor to the activity/property. Then, we calculated the % contribution of the 3 dominant descriptors in our QSPR model. The results founded that  $R_{og}$  have 50% contribution of the adsorption energy while BE and Dipole have 34% and 16% contribution, respectively. Hence, the  $R_{og}$  designates the value of the adsorption energy. It could be seen that the adsorption energy of the complex between donor and surface as well as the activity of propylene polymerization by ZN mainly depends on the steric hindrance. Values of these three molecular descriptors from 24 electron donors were presented in Table 13.

**Table 13** List of three dominant molecular properties of 24 electron donors as training set from the best QSPR model.

Name	$R_{og}$ (Å)	Dipole (e Å)	BE (kcal/mol)
P1	4.0187	1.1100	8.4526
P3	4.4971	3.4340	9.0536
P4	5.6039	4.1940	8.1278
P5	4.3500	2.8080	8.6669
P6	5.4137	2.4360	9.1858
P8	5.9430	4.2690	8.8689
D1	2.7582	0.5650	1.9831
D2	2.6572	0.3500	2.1213
D3	2.7193	1.1650	2.6761
D4	2.8867	0.2900	6.4599
D5	2.9604	-0.3740	8.2722
D6	3.2288	-0.9530	4.7067
D7	3.2503	-0.3130	7.9555



D9	2.9600	0.6170	3.7525
M1	4.5790	2.2080	4.2111
M2	4.9675	1.6890	6.2102
M3	4.9704	3.7620	6.2860
M5	4.7776	2.5010	10.3581
M6	4.6386	3.2380	9.9743
M7	4.7066	2.6140	9.6469
M8	4.6493	2.6100	8.4526
M9	3.6357	1.3630	12.8591
M11	3.5660	2.5790	12.1826
M12	3.6165	2.5040	9.2609

Considering the sign of the coefficient which tell the direction for improvement of the activity/property. Coefficients of all three descriptors have positive sign signifying that the compound with large values of Rog, BE, and Dipole will have large adsorption energy and high activity.

In Table 13, Rog and BE values of phthalate and malonate compounds are comparable, while those of 1,3-diethers are smaller. This signifies the smaller molecular size of 1,3-diether as compared to other donors. The size of the compound is also controlled by substituents  $R_1$ ,  $R_2$ , and  $R_3$ . The Rog and BE increase as the substituent becomes bulkier. Although both Rog and BE give the same trend, their values arrive from different sources. Dipole values do not follow the same trend. For phthalate and malonate donors, values of Dipole are comparable, while they are much smaller for 1,3-diether. Dipole is a vector quantity. The positive sign also suggests the preferred spatial alignment of atoms in the molecule. As it can be

noticed compounds D5-D7 have negative Dipole values which are probably due to the symmetric substitution at R<sub>1</sub> and R<sub>2</sub> positions.

Along with Rog, BE and Dipole values of 1,3-diether compounds have lower adsorption energies and hence lower PP activities. In case of malonate compounds have somewhat slightly lower Rog, BE and Dipole than phthalate compounds. Nevertheless, phthalate compounds have very large R<sub>1</sub> and R<sub>2</sub> substituents causing large values of Rog. Thus, the activity of the malonate donor could be improved by using same substituents for R<sub>1</sub> and R<sub>2</sub> as those of the phthalate compound. In addition, one could also replace *n*-Bu moiety of the malonates by other substituents which could also enhance Rog, BE, and Dipole. Therefore, the more potent electron donor could be yet developed from the malonate compounds than the other two types of electron donors.

#### 5.4.4 Validation of QSPR Model

As for the five compounds in the test set (P2, P7, D8, M4, and M10), three dominant descriptors which consist of Rog, Dipole, and BE descriptors were calculated as displayed in Table 14.

**Table 14** The three dominant descriptors were calculated and predicted adsorption energy for five compounds in the test set from the best QSPR model.

Name	Rog (Å)	Dipole (e Å)	BE (kcal/mol)	Predicted Eads (kcal/mol)
P2	3.8162	1.5240	6.2668	17.62
P7	4.3988	1.8640	8.1836	21.16
D8	3.3023	-0.6920	10.0367	16.11
M4	4.8677	2.1450	8.8170	23.23
M10	3.6553	1.4140	13.6253	23.37

Predicted versus calculated  $E_{\text{ads}}$  for test set is depicted in Figure 14. The test set has  $r^2$  of 0.77 which indicates the good predictive ability of the model. To justify the three-descriptor over the two descriptor model,  $E_{\text{ads}}$  of compounds in the test set were also predicted using the two-descriptor model and the  $r^2$  of 0.42 was obtained.

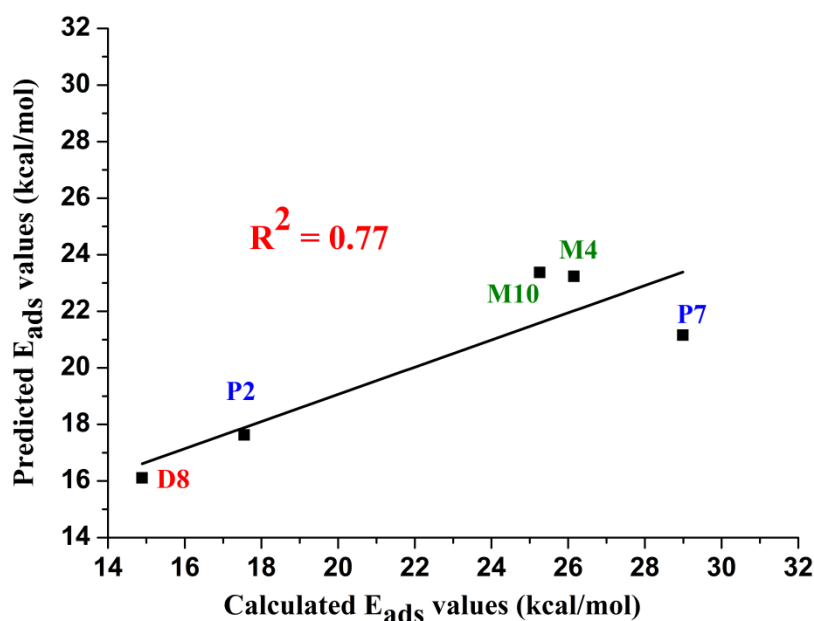
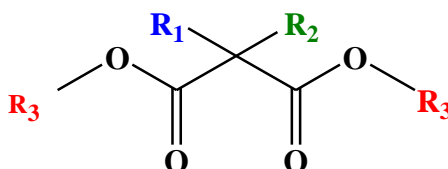


**Figure 14** The predicted versus the calculated  $E_{\text{ads}}$  values for test set using the best QSPR model.

#### 5.4.5 Suggestions for Potent Electron Donors

Based on the best QSAR model, more potent electron donors particularly for malonate donors should have all substituents at  $R_1$ ,  $R_2$  and  $R_3$  positions with bulky groups and more electron-donating groups. As can be observed that the size of the substituent increases values of  $R_{\text{og}}$  and BE are raised. Moreover, the increase of  $R_{\text{og}}$  by changing  $R_3$  substitution is more obvious. It should be noted that the substitution of electron withdrawing group at  $R_2$  position should be avoided because it will reduce Dipole. In addition, the electron donating group could help enhance the

Dipole value as evident by values of Dipole in M11 and M12 compared to M9 and M10. The potent malonate donors are illustrated in Figure 15.



$R_1$ ,  $R_2$ ,  $R_3$  should contain more bulky and electron-donating groups

**Figure 15** Summary of structure for design new potent electron donors based on malonate template by our QSPR model.

### 5.5 QSPR Summary

In this chapter, the QSAR between adsorption energies of 3 groups which consists of phthalate, 1,3-diether and malonate, groups totally 29 internal electron donors of the ZN catalyzed propylene polymerization and PP activities was investigated. From this study revealed that adsorption energies of donors and catalytic surface show a good correlation with experimental PP activities. Then, QSPR model between adsorption energies and 47 molecular properties of the 24 electron donors as training set were sought. The best QSPR model which contains 3 molecular descriptors, the radius of gyration (Rog), the force bond energy (BE), and the Vamp dipole  $\gamma$  (Dipole) has the  $R^2=0.84$  and  $R_{CV}^2=0.83$ . The Rog, BE, and Dipole have the contribution to the adsorption energy of 50%, 34% and 16%, respectively. Therefore, the adsorption energy and hence the activity of PP polymerization is more directly relevant to the steric contribution than the electronic contribution of electron donors. The accuracy of our QSPR model was assessed by prediction of the test set

of 5 compounds from three different electron donors groups. We obtained  $R^2_{\text{predict}} = 0.77$  which indicating a good predictive ability of the model. Moreover, based on our QSPR model, the malonate group is the most promising template for preparing potent electron donors. In summary, more potent malonate donors should have both bulky and electron donating groups for  $R_1$ ,  $R_2$ , and  $R_3$  substituents. This work can confirmed that the QSPR technique can be used to design potent electron donors which saves a lot time and also reduces experimental research cost.



## CHAPTER VI

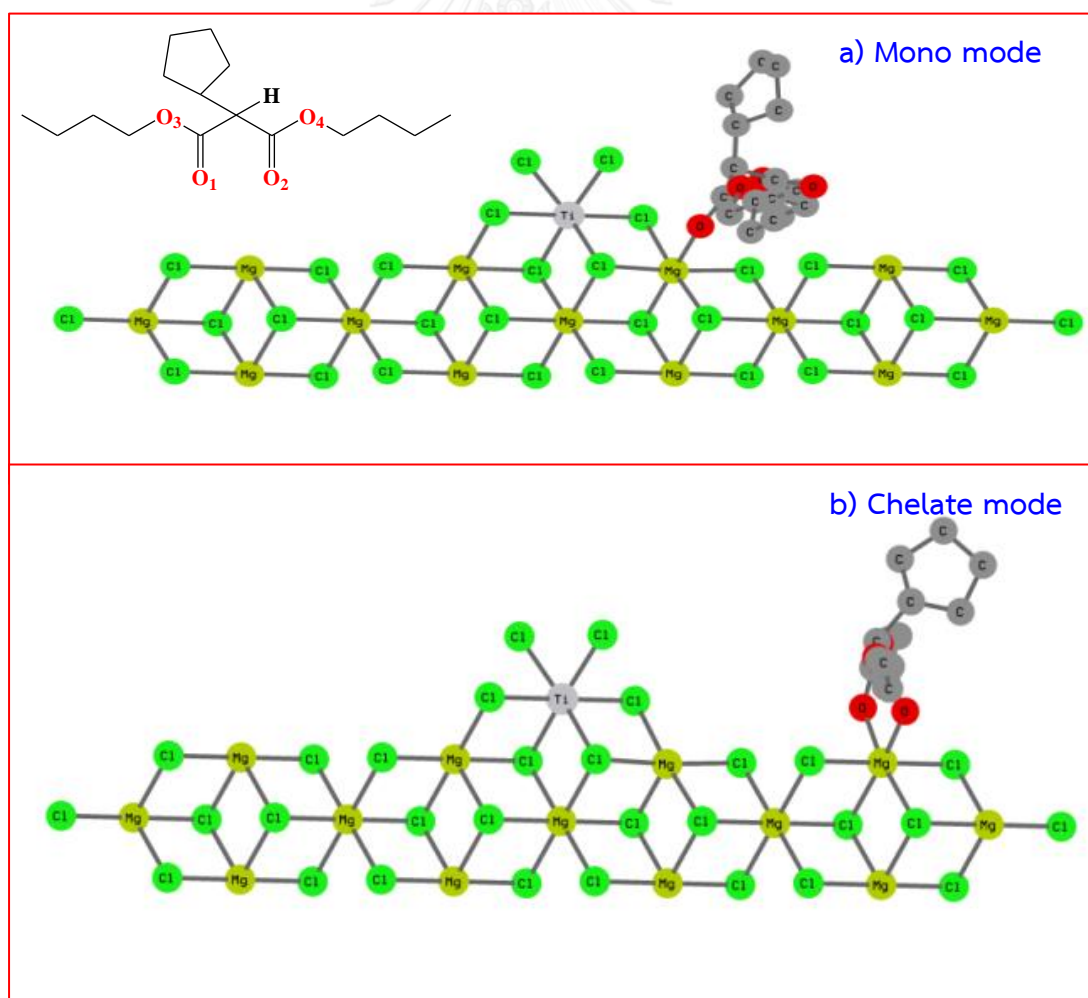
### Mechanistic Study

#### 6.1 Introduction

A catalyst is used to reduce the activation energy for the polymerization process thereby speeding up the reaction and allowing it to proceed even under mild conditions [25]. Also, a catalyst does not change the thermodynamics of a reaction, meaning that the equilibrium remains unchanged. The rate of the reaction is enhanced as a new and a more favorable reaction pathway is established. For example, in the absence of the catalyst, ethylene does not undergo polymerization in mild conditions and requires high-energy particle collisions to react. Hence, the proportion of different structures formed is reliant on the relative rates of their formation [112]. In the PP industry, ZN catalysts play a vital role in production; however, to date the working mechanism of ZN systems have not been understood completely. An understanding of this behavior would help in designing and developing catalysts with desirable properties.

Many experimental [8-10, 97, 113-119] and theoretical studies [14, 100, 120-125] have been carried out to study the mechanism underlying the role of the electron donors in ZN catalyst of polypropylene. Most of the works have been focused on ethylbenzoates [15, 116, 120, 126, 127], phthalates[13], succinates[122], alkoxysilanes [14, 128] and 1,3-diethers [12, 129, 130]. Malonate compounds as internal electron donor have been reported to be very potent electron donors which show good activity and high isotacticity [79, 131]. However, there have not been through studies on the role of this class of electron donors. More importantly, the

molecular structure of malonate donors is different from phthalates and 1,3-diethers and hence it could lead to the different mechanism. From the previous studied by Correa group [122] they analyzed and separated electron donors into two classes. The first class consists of alkoxy silanes and 1,3-diethers which have a short spacer between their two oxygen atoms and could be adsorbed only at the  $\text{MgCl}_2(110)$  surface with chelate mode. The second class contains phthalates and succinates which could be adsorbed at both the (100) and (110) planes of  $\text{MgCl}_2$  with bridge or chelate or zip coordination modes due to a longer spacer between the coordinating O atoms. In this work, we investigated the four possible adsorption modes are mono, chelate, bridge and zip modes (see Figure 15) for malonate donor on the  $\text{MgCl}_2$  (110) surface.



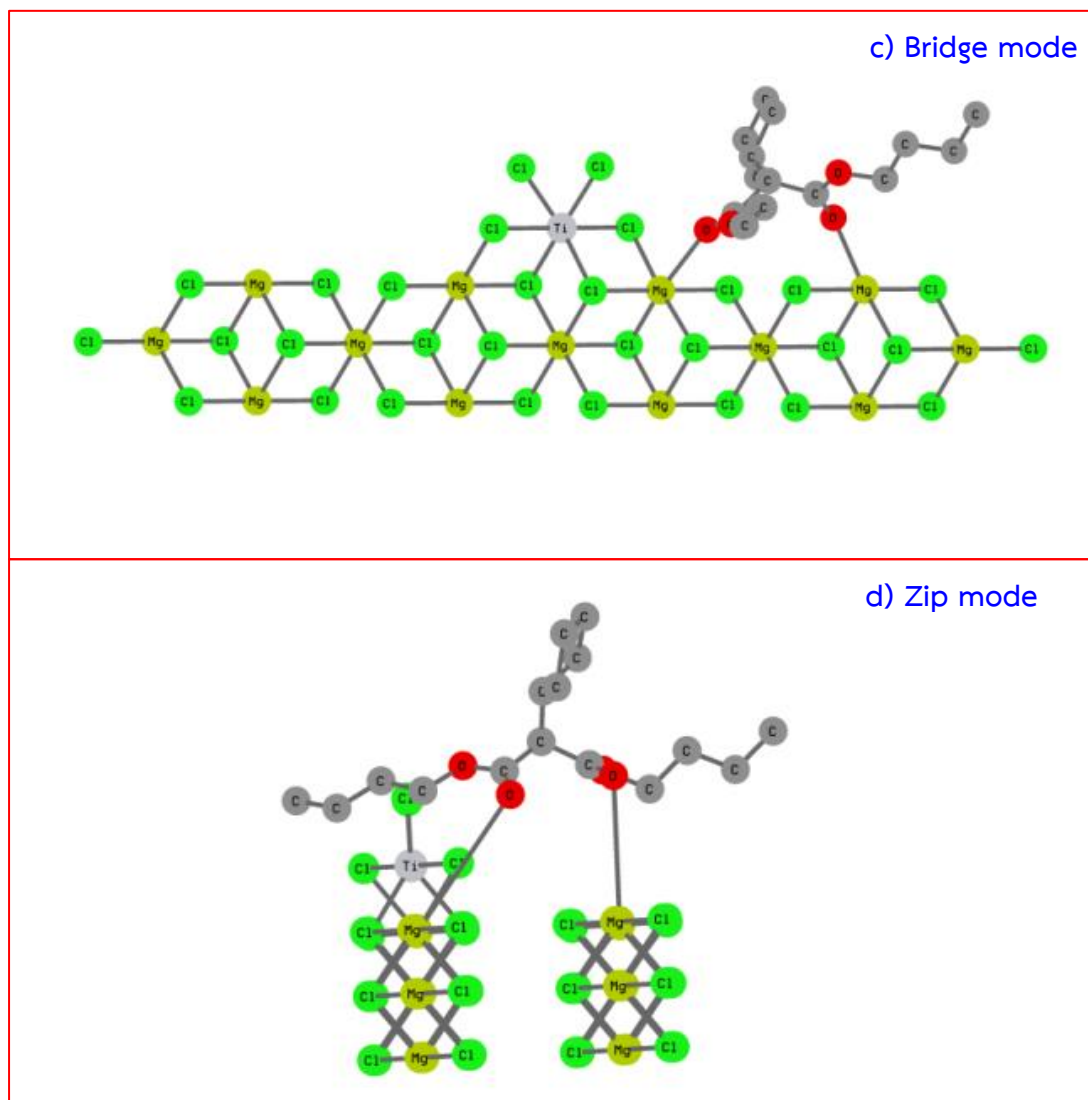


**Figure 16** Four adsorption modes of the malonate donor on the  $\text{MgCl}_2(110)$  surface (all hydrogens are not shown for purposes of clarity).

From the literature reviews have been reported the regio- and stereoselectivity of the polymerized product are controlled by the insertion step [132-134]. Thus, the role of the malonate donors for regio- and stereoselectivity in the ZN catalyzed propylene polymerization at the propylene insertion step was investigated. We choose the propylene insertion step for studying due to this step is the rate determining step [135, 136]. For propylene, there are four possible modes



of the insertion, the primary (1,2) and the secondary (2,1) both with *re* and *si* faces, as presented in Figure 16. There are different orientation of methyl groups in propylene monomer.

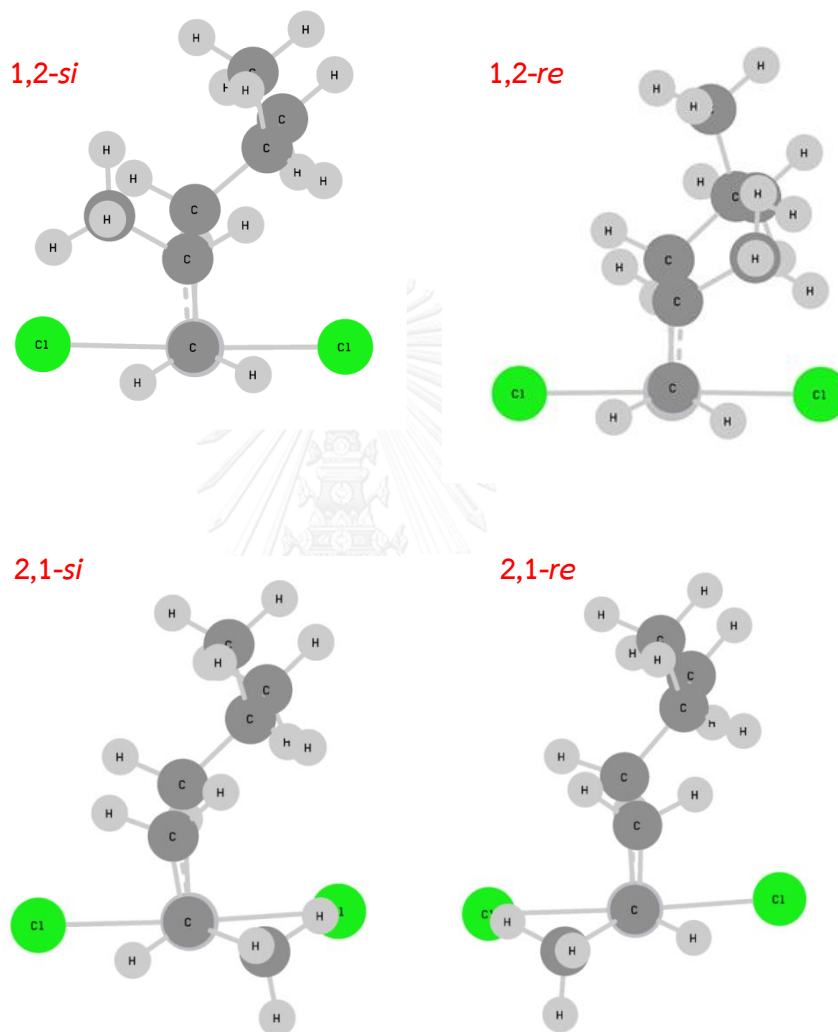


**Figure 17** Four possible insertion modes of propylene monomer into a Ti-*i*Bu growing chain of polypropylene.

From Figure 16 the primary (1,2)-*re* have the steric interactions between the alkyl group of growing polymer chain and the methyl group of the propylene monomer. Therefore, in order to reduce steric interactions in the case of the primary



## 6.2 Models and Computational Details

### 6.2.1 Four Adsorption Mode of Malonate Donor

Many theoretical studies have reported that the interaction of  $\text{TiCl}_4$  with the  $\text{MgCl}_2(110)$  face is strong [138, 139] while that with  $\text{MgCl}_2(100)$  and  $(104)$  faces are weak [123, 140]. Therefore, the  $\text{MgCl}_2(110)$  lateral plane was selected over  $(100)$  and  $(104)$ . Also, the interaction between the Lewis bases and the  $\text{MgCl}_2$  support noticeably indicates that the electron donor could stabilize the  $(110)$  greater than the  $(104)$   $\text{MgCl}_2$  surface [100]. The cluster was represented by  $\text{Mg}_{13}\text{Cl}_{26}$  to model the Corradini site  $(110)$  [141]. Thus, the  $[\text{Mg}_{13}\text{Cl}_{26}\text{Cl}_2\text{Ti}]$  cluster model was used for the pre-activated  $\text{MgCl}_2(110)$  surface. Four possible adsorption modes, i.e., mono, chelate, bridge and zip of the di-*n*-butyl 2-cyclopentyl malonate donor displayed in Figure 15, were investigated. In addition, the positions of atoms of the  $\text{MgCl}_2$  cluster were kept fixed. Assuming that atoms on the surface present a structure close to that in the bulk of the crystal, the Mg-Cl distances and all the Cl-Mg-Cl angles were set to X-ray values of 2.49 Å and  $90^\circ$ , respectively [142]. Besides, the  $\alpha$ - $\text{MgCl}_2(110)$  surface has been selected for the studies, with the distance of 5.9 Å between the layers as suggested by Vanka and co-worker [13]. Adsorption energies have been obtained using the DFT method with B3LYP-D3 functional [143] and 6-31G(d, p) basis set for C, H, O, Mg and Cl, and LANL2DZ basis set and ECP function for Ti atom [144]. All calculations were carried out using the GAUSSIAN09 package [145].

The adsorption energy of malonate donor, represented as  $E_{\text{ads}}$  is calculated from equation (6.1)

$$E_{\text{ads}} = E(\text{complex}) - [E(\text{surface}) + E(\text{donor})] \quad (6.1)$$

Where  $E_{\text{ads}}$  is the adsorption energy of malonate donor,  $E(\text{complex})$  is the energy of the complex formed by the malonate donor coordinating to the  $\text{TiCl}_4/\text{MgCl}_2(110)$  cluster, while  $E(\text{surface})$  and  $E(\text{donor})$  are energies of the  $\text{TiCl}_4/\text{MgCl}_2(110)$  cluster and the malonate donor compound, respectively.

### 6.2.2 Reaction Model Without Electron Donors

The growing chain was modeled by isobutyl (*i*Bu) since it is the minimal unit which can describe the growing chain as suggested by Taniike et al.[15]. The small alkyl group such as methyl ( $\text{CH}_3\text{-Ti}$ ) does not have sufficient repulsion with the bulky ligand, leading to the lower stereoselectivity as compared to isobutyl (*i*Bu-Ti) [15]. The stereoselectivity of the propylene insertion into *i*Bu-Ti is similar to those of the polypropylene growing chain as observed by  $^{13}\text{C}$  NMR[6, 146]. Therefore, the  $[\text{Mg}_{13}\text{Cl}_{26}\text{Cl}_2\text{Ti-}i\text{Bu}]$  was employed for the active surface model [122]. For the titanium atom has the +3 oxidation state and contains one unpaired electron. Consequently, doublet spin state was set for the calculations and spin-unrestricted calculations for the open shell systems have been carried out throughout this investigation using DFT calculations at the same level of theory as those in section 6.2.1. We have calculated the vibrational frequencies for confirming the transition state. In addition, the top four  $\text{MgCl}_2$  units involved in donor and Ti coordination were relaxed. The remaining  $\text{MgCl}_2$  units were frozen at the bulk  $\text{MgCl}_2$  value[147].

### 6.2.3 Reaction Model With Malonate Donor

We use the same set up as in section 6.2.2 for the study of the reaction with malonate donor. However, the active surface was modeled from the adsorption complex between  $[\text{Mg}_{13}\text{Cl}_{26}\text{Cl}_2\text{Ti-}i\text{Bu}]$  surface and di-*n*-butyl 2-cyclopentyl malonate obtained from 6.2.1. Only the structure that yields the lowest adsorption energy

where the malonate donor is coordinated close to the growing chain and the active Ti atom was selected.

## 6.3 Results and Discussion

### 6.3.1 Favorable Adsorption Mode of Malonate Donor

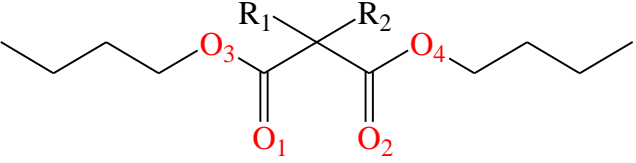
The adsorption energies ( $E_{ads}$ ) and their energy components, the main interatomic distances for the di-*n*-butyl 2-cyclopentyl malonate adsorbed on the pre-activated  $MgCl_2$  (110) surface were given in Table 15 and Table 16, respectively.

**Table 15** Calculated adsorption energy ( $E_{ads}$ , kcal/mol) and their energy components of di-*n*-butyl-2-cyclopentyl malonate adsorbed on the pre-activated  $MgCl_2$  (110) surface.

Name	E(complex) (au)	E(surface) (au)	E(donor) (au)	$E_{ads}$ (kcal/mol)
Mono	-17395.3414	-16467.6573	-927.6025	-51.19
Chelate	-17395.3633	-16467.6573	-927.6002	-66.38
Bridge	-17395.3166	-16467.6528	-927.5951	-43.08
Zip	-31963.9687	-31036.3328	-927.6048	-19.48

Adsorption energies of the mono, the chelate, the bridge, and the zip coordination modes of the di-*n*-butyl 2-cyclopentyl malonate donor adsorbed to the pre-activated  $MgCl_2$  (110) surface are -51.19, -66.38, -43.08, and -19.48 kcal/mol, respectively. When comparison of the mono coordination mode with chelate, bridge and zip coordination modes. The calculations from Table 15 indicated that the chelate coordination mode was the most favorable adsorption mode.

**Table 16** The main interatomic distances for the di-*n*-butyl-2-cyclopentyl malonate adsorbed on the pre-activated MgCl<sub>2</sub> (110) surface.

Coordination Mode	 $R_1 = \text{Cyclopentyl}, R_2 = \text{H}$			
	Interatomic distance (Å)			
	=O <sub>1</sub> ...Mg	=O <sub>2</sub> ...Mg	-O <sub>3</sub> -...Mg	-O <sub>4</sub> ...Mg
Mono	2.15	5.07	4.52	5.13
Chelate	2.07	2.11	4.17	4.08
Bridge	2.51	2.43	5.36	4.12
Zip	6.02	5.86	5.34	4.77

From Table 16, the coordination modes of mono, chelate, and bridge modes have distances between oxygen and Mg atoms of surface are 2.07-2.51 Å for the carbonyl O<sub>1</sub>/O<sub>2</sub> and 4.08-5.36 Å for the ether O<sub>3</sub>/O<sub>4</sub>. For the bridge mode, the O<sub>2</sub> atom coordinates with another Mg atom on the surface, see Figure 15. Thus, the malonate donor uses carbonyl oxygens to coordinate with the MgCl<sub>2</sub> (110) surface. This is reasonable since not only the ether oxygen has less electron density but there are also lots of steric hindrance between the ether moiety and the surface. For the zip coordination, the O<sub>1</sub>/O<sub>2</sub> to Mg distances are larger than 5 Å. This suggests that the donor molecule does not bind to MgCl<sub>2</sub>(110) surface. In addition, the zip coordination mode is impossible because the malonate donor has the distance of 3.10 Å between two coordinating carbonyl oxygens while the distance between neighboring adsorption sites on the MgCl<sub>2</sub>(110) surface is 6.36 Å.

### 6.3.2 Ziegler-Natta Reaction Without Electron Donor

The results of our calculations are given in Table 17 and 18. The  $\pi$ -complex formation energy ( $\Delta E_{\pi}$ ) in Table 17 denotes the energy gained due to complexation of the propylene to the Ti(III) catalyst center on the  $MgCl_2$  surface. It was computed from the relative energy of the  $\pi$ -complex with respect to the sum of the energies of a separated monomer and an active site. For  $\Delta E_{TS}$  refers to the difference in energy between the transition state and the  $\pi$ -complex and  $\Delta E_{product}$  refers to the difference in energy between the product and the  $\pi$ -complex (or reactant complex). And the intrinsic activation energy ( $E_a$ ) obtained from the difference between energies of the four-membered ring transition state and the  $\pi$ -complex.

Despite similar structures for 1,2-*re*- and 1,2-*si* insertion, the energetics of propylene insertion was different from each other. The activation energy for *re*-insertion (6.52 kcal/mol) was much higher than that for *si*-insertion (4.28 kcal/mol). However, the  $\pi$ -complex and the final product from *re*-insertion more stable than that of *si*-insertion by 2.47 and 3.39 kcal/mol, respectively, as can be seen in Table 17. This overall energetics indicates that the *re*-insertion more favorable rather than the *si*-insertion in the first insertion step.

**Table 17** The  $\pi$ -complex formation energy ( $\Delta E_{\pi}$ ), The energy difference between the transition state and the  $\pi$  complex ( $\Delta E_{TS}$ ), and The energy difference between the product and the  $\pi$  complex ( $\Delta E_{product}$ ), and the intrinsic activation energy ( $E_a$ ) when absence malonate donor.

Type of insertion	$\Delta E_{\pi}$ (kcal/mol)	$\Delta E_{TS}$ (kcal/mol)	$E_a$ (kcal/mol)	$\Delta E_{product}$ (kcal/mol)
<b>Primary insertion (1,2)</b>				
<i>si</i> face	-30.68	-26.40	4.28	-39.88
<i>re</i> face	-33.15	-26.63	6.52	-43.27
<b>Secondary insertion (2,1)</b>				
<i>si</i> face	-30.72	-24.05	6.67	-40.88
<i>re</i> face	-30.10	-24.23	6.87	-44.84

The energy difference between the primary (1,2) and secondary (2,1) insertion of propene into the Ti-*i*Bu bond at transition states can indicate the regioselectivity of this active site. And the energy difference between two enantiofaces (*si* and *re* faces) of transition states structures can also indicate the stereoselectivity of this active site. From the Table 18, the small energy difference between the two transition states, 0.2 kcal/mol, indicates that there is no preference for one of the two propene enantiofaces (nonstereoselective). Moreover, two transition states of the secondary (2,1) insertion are about 2.4-2.6 kcal/mol which higher in energy relative to the transition states of primary (1,2) insertion. Therefore, the primary (1,2) insertion take place more easily than the secondary (2,1) insertion. These theoretical results were in good qualitative agreement with other theoretical results [13, 122, 148, 149]. Furthermore, it was notable that the transition state structure exhibit a



strong  $\alpha$ -agostic interaction which is obvious from an elongated C $\alpha$ -H $\alpha$  bond distance (1.14 Å) as compared with the normal C-H bond distance (1.10 Å).

**Table 18** The relative barriers of the insertion step of ZN catalyzed propylene polymerization in the absence of the electron donor together with values of TS imaginary frequencies.

Type of insertion	Relative barriers* (kcal/mol)	TS imaginary frequency (cm <sup>-1</sup> )
Primary insertion (1,2)		
<i>si</i> face	0.2	-355.98
<i>re</i> face	0.0	-371.62
Secondary insertion (2,1)		
<i>si</i> face	2.6	-423.34
<i>re</i> face	2.4	-494.94

\* the relative insertion barriers for the four cases, with the lowest insertion barrier (that of the *re*-primary insertion) taken as 0.0 kcal/mol.

Relative energy profile in kcal/mol for PP primary and secondary (both *re* and *si* faces) insertion into Ti-C bond when absence malonate donor is shown in Figure 19. This graph use relative energy of  $\pi$ -complex with respect to the sum of the energies of a separated propylene monomer and an active site.

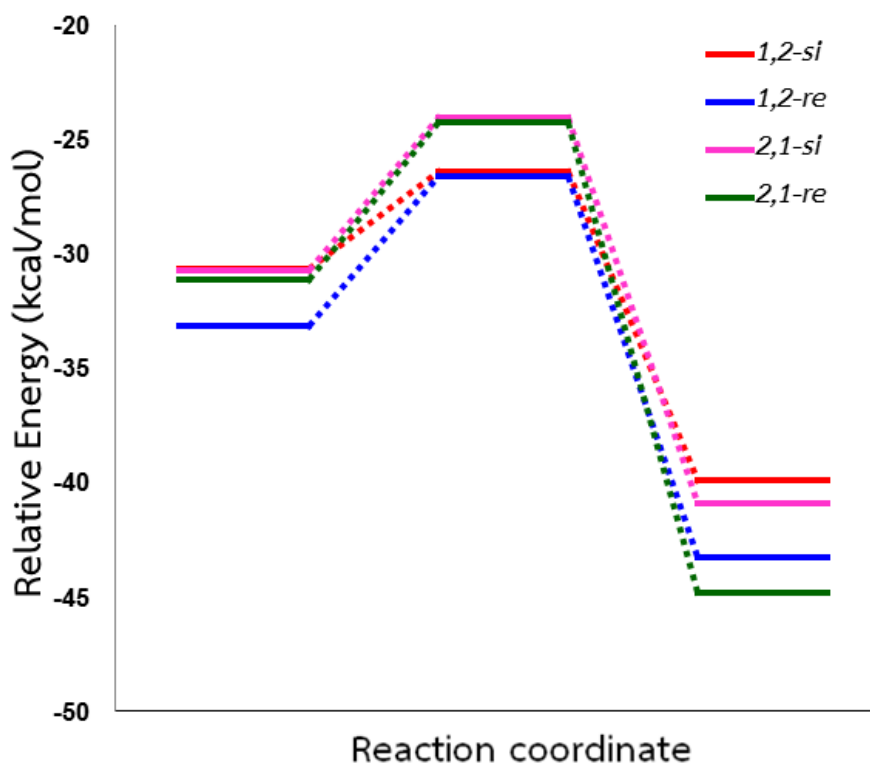


**Figure 19** Relative energy profiles (kcal/mol) for PP primary and secondary (both *re* and *si* faces) insertion into Ti-C bond when absence malonate donor.

### 6.3.3 Influence of Malonate Donor on Ziegler-Natta Reaction

From the adsorption energy calculations revealed that the chelate coordination mode was the most stable coordination mode. Consequently, we investigate the effect of adsorbed malonate donor in chelate mode on the activity, the stereo-, and regio-selectivity of the active site created on the  $\text{MgCl}_2$  (110) surface by performed calculation for the propylene insertion. The results of our calculations were collected together in Table 19 and 20. In our case, only one malonate donor was coordinated close to the active Ti atom and also close to the growing chain used set up the model. We found that the primary insertion(1,2) was stereoselective, while the secondary(2,1) insertion was nonstereoselective which in line with Correa

et al. [150] were proposed. If the situation with the growing chain close to the donor more stable, an isotactic polypropylene will be produced [150].

**Table 19** The  $\pi$ -complex formation energy ( $\Delta E_{\pi}$ ), The energy difference between the transition state and the  $\pi$  complex ( $\Delta E_{TS}$ ), and The energy difference between the product and the  $\pi$  complex ( $\Delta E_{product}$ ), and the intrinsic activation energy ( $E_a$ ) when presence malonate donor.

Type of insertion	$\Delta E_{\pi}$ (kcal/mol)	$\Delta E_{TS}$ (kcal/mol)	$E_a$ (kcal/mol)	$\Delta E_{product}$ (kcal/mol)
<b>Primary insertion (1,2)</b>				
<i>si</i> face	-40.94	-38.48	2.46	-52.66
<i>re</i> face	-42.55	-36.97	5.59	-51.52
<b>Secondary insertion (2,1)</b>				
<i>si</i> face	-41.15	-35.72	5.43	-52.46
<i>re</i> face	-42.37	-35.66	6.71	-56.52

From Table 17 and 19, we found the  $\Delta E_{\pi}$  for insertion reactions with the di-*n*-butyl 2-cyclopentyl malonate was lower than without donors in all cases of insertions. Hence, the first role of malonate donor was observed it can be stabilized the  $\pi$ -complex. Also, we observed that the  $\pi$ -complex for 1,2-*re* insertion was the most stable this situation similar to the insertion reactions without electron donors. This situation can be also explained by the steric interaction between the methyl group of the propylene and the alkyl moiety of the catalyst. Nevertheless, the stabilization owing to the coordination with the malonate donor also plays roles in the stability of the  $\pi$ -complex. Besides, the  $\pi$ -complex for the secondary (2,1)-*re*

insertion has a comparable stability to that for the primary (1,2)-*re* insertion. This is probably due to the position of the adsorbed malonate donor. Thus, the *re* face insertion is better stabilized by the electron donor. The same reasoning could be as well applied to the stability of the TS of the insertion reaction.

The primary insertion(1,2) with the malonate donor has lower activation energy ( $E_a$ ) than the secondary(2,1) insertion with the malonate donor. Moreover, the large difference between the activation energy for propylene insertion of 1,2-*si* and 1,2-*re* complexes while the small difference between the activation energy for propylene insertion of 2,1-*si* and 2,1-*re* complexes were observed. When comparison of the corresponding  $E_a$  values in the absence and presence of malonate donor (Tables 17 and 19) revealed that the coadsorption of malonate donor decreased the  $E_a$  values. Thus, coadsorption of malonate donor can convert the aspecific Ti mononuclear species (non-stereoselective, Table 18) into isospecific one (stereoselective, Table 20) by sterically controlling the orientation of the growing chain at the transition state.

**Table 20** The relative barriers of the insertion step of ZN catalyzed propylene polymerization in the presence of the di-*n*-butyl 2-cyclopentyl malonate donor together with values of TS imaginary frequencies.

Type of insertion	Relative barrier* (kcal/mol)	TS imaginary frequency ( $\text{cm}^{-1}$ )
Primary insertion (1,2)		
<i>si</i> face	0.0	-336.28
<i>re</i> face	1.5	-343.56
Secondary insertion (2,1)		
<i>si</i> face	1.2	-445.79
<i>re</i> face	1.3	-527.05

\* the relative insertion barriers for the four cases, with the lowest insertion barrier (that of the *si*-primary insertion) taken as 0.0 kcal/mol.

The relative barriers of the insertion step of ZN catalyzed propylene polymerization in the presence of the malonate donor together with values of TS imaginary frequencies is given in Table 20. Also, only one imaginary frequency was obtained for each TS structure of the four kinds of insertion by malonate donor. From Table 20, the 1,2-*re* has the highest relative barriers which can be explain by steric interactions between the methyl group of the propene close to the malonate donor.

Energy profile in kcal/mol for PP primary and secondary (both *re* and *si* faces) insertion into Ti-C bond when presences malonate donor is presented in Figure 21. This graph use relative energy of  $\pi$ -complex with respect to the sum of the energies of a separated propylene monomer, an active site, and malonate donor. The transition states structures for primary and secondary propene insertion (both *re* and *si* faces) with malonate donor in chelate mode into the Ti-*i*Bu bond of this model are displayed in Figure 20 and 21.

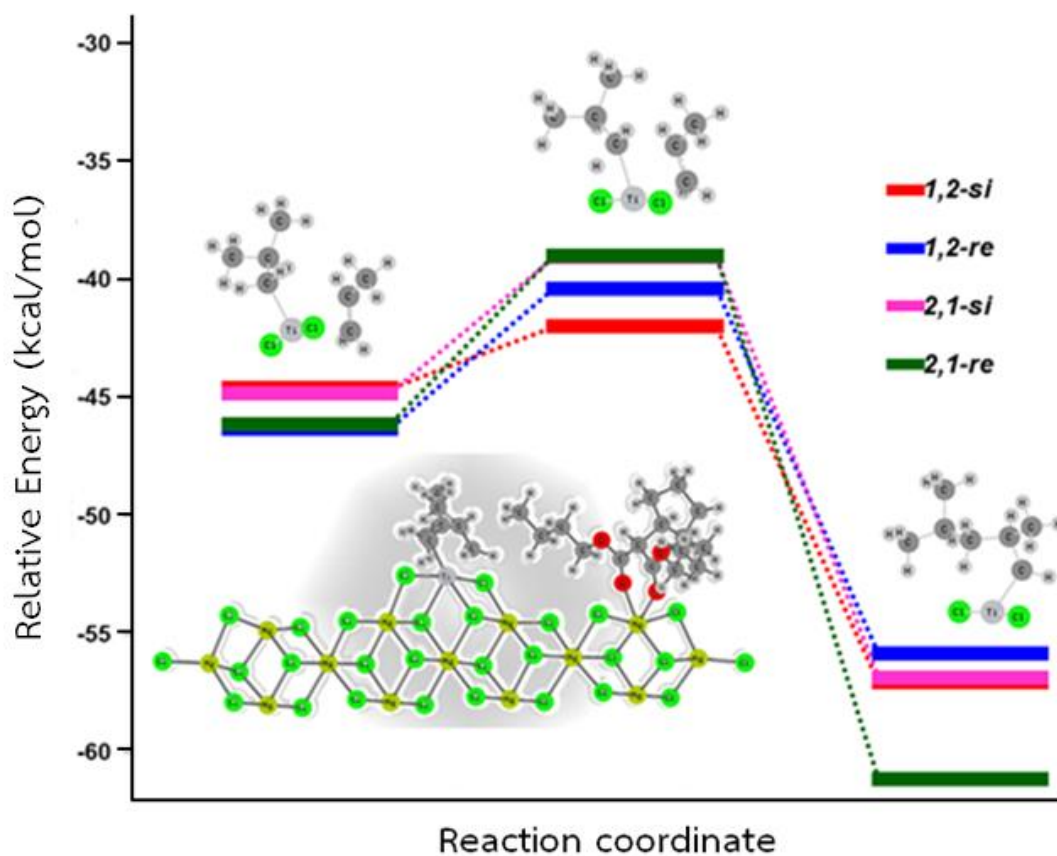


**Figure 20** Energy profiles (kcal/mol) for PP primary and secondary (both *re* and *si* faces) insertion into Ti-C bond when presence malonate donor.

From Table 20, the relative insertion barriers for the primary (1,2)-*si* and insertion was 1.2 and 1.3 kcal/mol more stable than those for the secondary (2,1)-*si* and *-re*, respectively, while it is 1.5 kcal/mol more stable than that for the primary (1,2)-*re* (see Table 20).

While the steric interaction between the methyl group of propylene and the alkyl moiety of the catalyst destabilizes the TSs of the secondary (2,1)-*re* and *-si* insertion, the repulsion between the propylene and the malonate donor in the primary (1,2)-*re* insertion raises its TS energy. For in case of the primary (1,2)-*re* insertion can be clarified by steric effect of the chelate-coordinated malonate donor and the propylene monomer as can be seen in Figure 21. Moreover, we observed

the energy difference between the TSs for the secondary (2,1)-*si* and -*re* propylene insertion to be just 0.1 kcal/mol, which signifies the secondary (2,1) insertion to be nonstereoselective. The TSs of the secondary (2,1)-*re* and -*si* are less hindered by the donor as shown in Figure 20. The presence of the malonate donor in the chelate mode favors the primary (1,2)-*si* insertion similarly to cases for the zip[13] and the bridge[122] coordination modes. Hence, co-adsorption of the di-*n*-butyl 2-cyclopentyl malonate converts the aspecific (nonstereoselective) Ti mononuclear species into isospecific (stereoselective) one by sterically controlling the orientation of the growing chain at the transition state. This finding is in line with DFT calculations for phthalate donor by Vanka et al.[13], for ethyl benzoate donor by Taniike et al.[15] for succinate donor by Correa et al.[122] and in agreement with the temperature rising elution fractionation (TREF) experiment of polypropylene where it was found that the inclusion of the electron donor causes the ZN catalyst to be moderately isospecific[79].

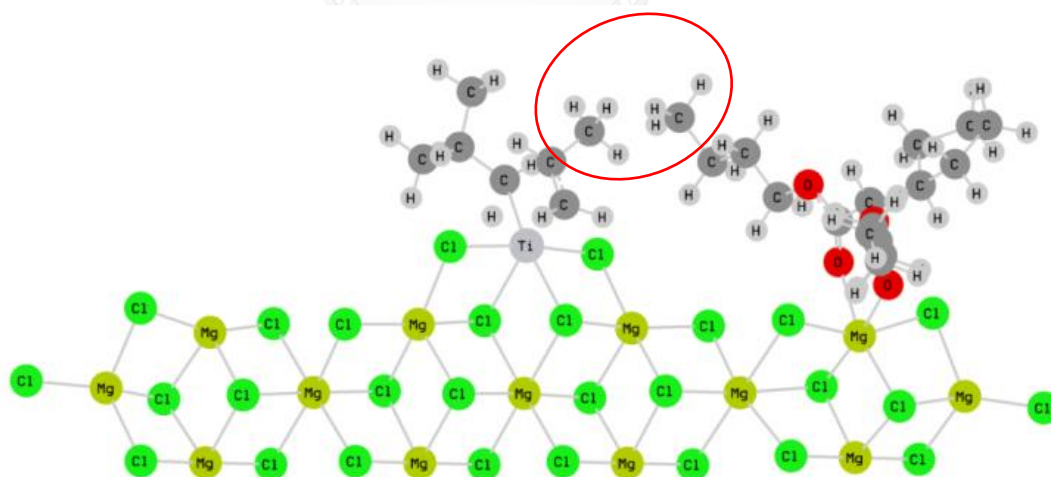


**Figure 21** Steric effect of the chelate-coordinated malonate donor at the transition state on the primary (1,2)-*re* insertion: the repulsion between the propylene and the malonate donor.

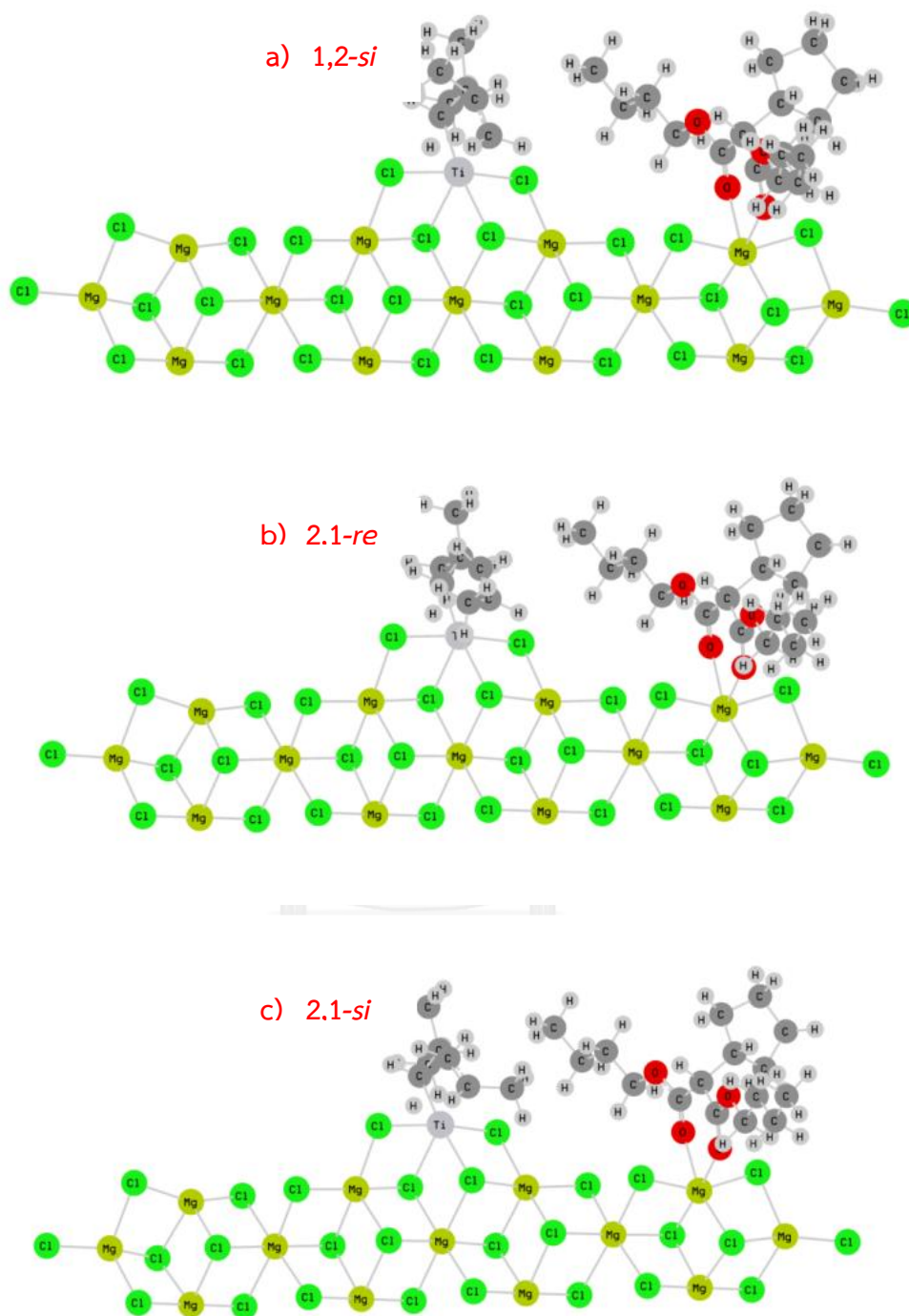


**Figure 22** Structures of the chelate-coordinated malonate donor at the transition states for a) the primary (1,2)-*si*; b) the secondary (2,1)-*re*; c) the secondary (2,1)-*si* insertion.



Finally, we also founded that the di-*n*-butyl 2-cyclopentyl malonate reduces the intrinsic activation energy ( $E_a$ ) of the insertion step. Thus, the influence of the malonate donor on the activity was the result of the electron transfer from the malonate donor to the  $MgCl_2(110)$  surface as evident by the enhancement of charge density of the Ti species on the  $MgCl_2(110)$  surface as can be seen in Table 22. This observation is in agreement with periodic calculations by Taniike et al.[126] Since the donor sits beside Ti species, the donor with the larger substituents will yield the more stereoselective catalyst. Therefore, the potent electron donor should provide electron to Ti species to enhance the activity.

**Table 21** Comparison of transition state structure of the Ti active ZN catalyst when absence and presence of malonate donor and their charge transfer through the  $MgCl_2(110)$  support.

Transition state structure	Mulliken Charges			
	Ti	Mg	O1	O2
<b>Absence</b> malonate donor with the lowest relative insertion barrier (1,2- <i>re</i> )	-0.119	0.408	-	-
<b>Presence</b> malonate donor. with the lowest relative insertion barrier (1,2- <i>si</i> )	-0.125	0.330	-0.420	-0.417

#### 6.4 Mechanistic Study Summary

The conclusion from this chapter, we founded that the malonate donor preferable coordinates to the  $\text{MgCl}_2(110)$  surface of ZN catalyst in the chelate mode. When absence of the malonate donor, the ZN catalyst was regioselective in favor of the primary (1,2) insertion but nonstereoselective. Hence, the regioselectivity was controlled by the steric repulsion between the methyl group of propylene and the alkyl moiety of the catalyst. When the presence of the malonate donor, it was found that the ZN catalyst was both stereo- and regioselective. In case of regioselectivity with malonate donor can clarified by similar as in the case without donor. However, in case of the stereoselectivity was elucidated by the steric hindrance between the propylene and the malonate donor. There is less steric repulsion between the propylene and the malonate donor in the primary (1,2)-*si* insertion and, hence, the reaction proceeds in the direction of this insertion mode. Moreover, we found that the malonate donor reduces the intrinsic activation energy by the electron transfer to the Ti species (more negative charge) on the  $\text{MgCl}_2$  support. Therefore, the role of the malonate donor is clearly seen.

## CHAPTER VII CONCLUSIONS

Electron donors play an important role in the Ziegler-Natta catalyzed propylene polymerization. Consequently, a main goal for improvements of ZN catalysts is to find more potent electron donors. Therefore, relationships between the activity/property and the electron donor structures were investigated by using the QSAR/QSPR techniques. The statistical coefficients ( $R^2$  and  $R^2_{CV}$ ) of QSAR/QSPR models show good relationships between activities and molecular properties with good predictive power for Ziegler-Natta polypropylene catalysts. From all three QSAR models of 3 groups of compounds which obtained from different experiments, phthalates, 1,3-diethers and malonates donors showed satisfactory statistical quality and good predictive abilities as show the  $R^2 > 0.93$  and  $R^2_{CV} > 0.84$ . However, the usages of QSAR models obtained were limited because the number of compounds in each group is rather small and not sufficient to divide into training and test sets. Hence, the prediction could be improved if number of compounds is large enough. In this work, we use the adsorption energies of electron donors to catalyst surface which related to the experimental PP activities for construct QSPR model. We divided the data set of electron donors into a training set containing 24 compounds used for model development and a test set of 5 randomly selected compounds from 3 different groups for model validation. The QSPR model between donor-surface adsorption energies shows high correlation ( $R^2 = 0.84$ ,  $R^2_{CV} = 0.83$ ,  $R^2_{predict} = 0.77$ ). Moreover, the QSPR model suggested that the steric effect (84%) which obtained the radius of gyration (50%), and the forcite bond energy (34%) has more contributions to the catalyst activity than the electronic effect (dipole moment, 16%). Among three groups of electron donors, malonate compounds possess the strongest binding affinity to the catalyst surface and hence are the most promising template for preparing potent electron donors. Based on our QSPR model, potent malonate donors should have both bulky and electron donating groups for  $R_1$ ,  $R_2$ , and  $R_3$

substituents. Lastly, the roles of malonate donor were investigated by DFT using B3LYP-D3 calculations. Adsorption energy calculations revealed that malonate compound on the  $\text{TiCl}_4/\text{MgCl}_2(110)$  surface was preferred in the chelate mode over mono, bridge, and zip modes. From main results obtained in mechanistic studied the roles of the malonate donor is evidently seen by in the presence of the malonate donor, the ZN catalyst is both stereo- and regioselective. For that reason the stereoselectivity is elucidated by the steric hindrance between the propylene and the malonate donor and the regioselectivity is controlled by the steric repulsion between the methyl group of propylene and the alkyl moiety of the catalyst. Furthermore, with malonate donor, the reaction for primary or 1,2-*si* is favored and hence, the reaction proceeds in the direction of this insertion mode. In addition, we found that the malonate donor also stabilized the transition state structure by transferring electrons to Ti resulting in the reduction of the activation energy and hence the catalyst becomes more active.

In conclusion, the results from QSPR model and mechanistic studied gave good agreement the catalyst activity of propylene polymerization mainly depended on steric effect. Our theoretical investigation is highly consistent with experiments and previous theoretical results and this research provided the valuable information for molecular design of better electron donors to yield highly isotactic polypropylene which save time and experimental costs

## REFERENCES

- [1] J.J. Eisch, Fifty Years of Ziegler–Natta Polymerization: From Serendipity to Science. A Personal Account, *Organometallics*, 31 (2012) 4917-4932.
- [2] J.P. Claverie, F. Schaper, Ziegler-Natta catalysis: 50 years after the Nobel Prize, *MRS Bulletin*, 38 (2013) 213-218.
- [3] Market Study: Polypropylene - 2nd ed. overview (UC-4205) Ceresana 2012. Accessed on September 15, 2014, <http://www.ceresana.com/en/market-studies/plastics/polypropylene/>.
- [4] Z. Wang, Ziegler-Natta Polymerization, in: *Comprehensive Organic Name Reactions and Reagents*, John Wiley & Sons, Inc., 2010.
- [5] J.M. Gómez-Elvira, P. Tiemblo, M. Elvira, L. Matisova-Rychla, J. Rychly, Relaxations and thermal stability of low molecular weight predominantly isotactic metallocene and Ziegler–Natta polypropylene, *Polymer Degradation and Stability*, 85 (2004) 873-882.
- [6] M.C. Sacchi, I. Tritto, P. Locatelli, Stereochemical investigation of the effect of Lewis bases in heterogeneous Ziegler-Natta initiator systems, *Prog. Polym. Sci.*, 16 (1991) 331-360.
- [7] J. Xu, Y. Yang, L. Feng, X. Kong, S. Yang, Microtacticity of polypropylene fractions produced by different active sites of heterogeneous Ziegler–Natta catalyst, *Journal of Applied Polymer Science*, 62 (1996) 727-731.
- [8] A. Andoni, J.C. Chadwick, H.J.W. Niemantsverdriet, P.C. Thüne, The role of electron donors on lateral surfaces of MgCl<sub>2</sub>-supported Ziegler–Natta catalysts: Observation by AFM and SEM, *Journal of Catalysis*, 257 (2008) 81-86.
- [9] H.-X. Zhang, Y.-J. Lee, J.-R. Park, D.-H. Lee, K.-B. Yoon, Control of molecular weight distribution for polypropylene obtained by commercial ziegler-natta catalyst: Effect of electron donor, *Macromol. Res.*, 19 (2011) 622-628.

- [10] J. Guo, G. Hu, Z. Chen, Synthesis of novel electron donors and their application to propylene polymerization, *Trans. Tianjin Univ.*, 18 (2012) 8-14.
- [11] A. Correa, F. Piemontesi, G. Morini, L. Cavallo, Key elements in the structure and function relationship of the MgCl<sub>2</sub>/TiCl<sub>4</sub>/Lewis base Ziegler-Natta catalytic system, *Macromolecules*, 40 (2007) 9181-9189.
- [12] J.W. Lee, W.H. Jo, Chemical structure–stereospecificity relationship of internal donor in heterogeneous Ziegler–Natta catalyst for propylene polymerization by DFT and MM calculations, *Journal of Organometallic Chemistry*, 694 (2009) 3076-3083.
- [13] K. Vanka, G. Singh, D. Iyer, V.K. Gupta, DFT Study of Lewis Base Interactions with the MgCl<sub>2</sub> Surface in the Ziegler–Natta Catalytic System: Expanding the Role of the Donors, *The Journal of Physical Chemistry C*, 114 (2010) 15771-15781.
- [14] T. Wondimagegn, T. Ziegler, The Role of External Alkoxysilane Donors on Stereoselectivity and Molecular Weight in MgCl<sub>2</sub>-Supported Ziegler–Natta Propylene Polymerization: A Density Functional Theory Study, *The Journal of Physical Chemistry C*, 116 (2011) 1027-1033.
- [15] T. Taniike, M. Terano, Coadsorption model for first-principle description of roles of donors in heterogeneous Ziegler–Natta propylene polymerization, *Journal of Catalysis*, 293 (2012) 39-50.
- [16] E. Albizzati, M. Galimberti, Catalysts for olefins polymerization, *Catal. Today*, 41 (1998) 159-168.
- [17] J.C. Chadwick, F.P.T.J. van der Burgt, S. Rastogi, V. Busico, R. Cipullo, G. Talarico, J.J.R. Heere, Influence of Ziegler–Natta Catalyst Regioselectivity on Polypropylene Molecular Weight Distribution and Rheological and Crystallization Behavior, *Macromolecules*, 37 (2004) 9722-9727.
- [18] P. Cossee, Ziegler-Natta catalysis I. Mechanism of polymerization of  $\alpha$ -olefins with Ziegler-Natta catalysts, *Journal of Catalysis*, 3 (1964) 80-88.
- [19] E.J. Arlman, Ziegler-Natta catalysis II. Surface structure of layer-lattice transition metal chlorides, *Journal of Catalysis*, 3 (1964) 89-98.
- [20] M. Brookhart, M.L.H. Green, CARBON-HYDROGEN-TRANSITION METAL BONDS, *Journal of Organometallic Chemistry*, 250 (1983) 395-408.

- [21] K. Matyjaszewski, S. Gaynor, D. Greszta, D. Mardare, T. Shigemoto, Synthesis of well defined polymers by controlled radical polymerization, *Macromolecular Symposia*, 98 (1995) 73-89.
- [22] E. Albizzati, U. Giannini, G. Morini, M. Galimberti, L. Barino, R. Scordamaglia, Recent advances in propylene polymerization with  $MgCl_2$  supported catalysts, *Macromol. Symp.*, 89 (1995) 73-89.
- [23] E.G. Albizzati, U.; Collina, G.; Noristi, L.; Resconi, L., In *Polypropylene Handbook*, Hanser: Munich, Vienna, New York, 1966.
- [24] B.M. Mandal, *Fundamentals of polymerization*, World Scientific Pub. Co., Singapore ;, 2013.
- [25] A. Shamiri, M. Chakrabarti, S. Jahan, M. Hussain, W. Kaminsky, P. Aravind, W. Yehye, The Influence of Ziegler-Natta and Metallocene Catalysts on Polyolefin Structure, Properties, and Processing Ability, *Materials*, 7 (2014) 5069-5108.
- [26] E. Sagel, Polyethylene Global Overview, in: P.a. IHS (Ed.), Mexico City, 2012, pp. Presentation.
- [27] Industry News, PTT Chemical and PTT Aromatics and Refining to Merge, Accessed on September 15, 2014, <http://www.chemicals-technology.com/news/news111593.html>.
- [28] A. Andoni, J.C. Chadwick, H. Niemantsverdriet, P.C. Thune, A Flat Model Approach to Ziegler-Natta Catalysts for Propylene Polymerization and a Preparation Method of Well-defined Crystallites of  $MgCl_2$ -supported Catalysts, *Macromolecular Symposia*, 260 (2007) 140-146.
- [29] C.C. Maier, Teresa, *Polypropylene: the definitive user's guide and databook*, 1998.
- [30] Q. T. H. Shubhra, A.K.M.M. Alam, M.A. Quaiyyum, Mechanical properties of polypropylene composites: A review, *Journal of Thermoplastic Composite Materials*, (2011).
- [31] T. Shiono, H. Hagihara, T. Ikeda, K. Soga, Control of molecular weight distribution of isotactic polypropylene obtained by a  $MgCl_2$ -supported  $TiCl_4$  catalyst, *Polymer*, 38 (1997) 6409-6411.

- [32] W. Yoon, Y. Kim, I. Kim, K. Choi, Recent advances in polymer reaction engineering: Modeling and control of polymer properties, *Korean J. Chem. Eng.*, 21 (2004) 147-167.
- [33] P. Hohenberg, W. Kohn, Inhomogeneous Electron Gas, *Physical Review*, 136 (1964) B864-B871.
- [34] C.J. Cramer, *Essentials of Computational Chemistry: Theories and Models*, Wiley, 2005.
- [35] W. Kohn, A.D. Becke, R.G. Parr, Density Functional Theory of Electronic Structure, *The Journal of Physical Chemistry*, 100 (1996) 12974-12980.
- [36] C.J. Cramer, D.G. Truhlar, Density functional theory for transition metals and transition metal chemistry, *Physical Chemistry Chemical Physics*, 11 (2009) 10757-10816.
- [37] J.A. Keith, J. Anton, P. Kaghazchi, T. Jacob, Modeling Catalytic Reactions on Surfaces with Density Functional Theory, in: *Modeling and Simulation of Heterogeneous Catalytic Reactions*, Wiley-VCH Verlag GmbH & Co. KGaA, 2011, pp. 1-38.
- [38] R.E. Watson, G.W. Fernando, M. Weinert, Y.J. Wang, J.W. Davenport, Local-density approximation: Cohesion in the transition metals and  $s \rightarrow d$  promotion in the transition-metal atoms, *Physical Review B*, 43 (1991) 1455-1462.
- [39] J.P. Perdew, K. Burke, M. Ernzerhof, Generalized Gradient Approximation Made Simple, *Physical Review Letters*, 77 (1996) 3865-3868.
- [40] J.P. Perdew, K. Burke, M. Ernzerhof, Generalized Gradient Approximation Made Simple [*Phys. Rev. Lett.* 77, 3865 (1996)], *Physical Review Letters*, 78 (1997) 1396-1396.
- [41] A.D. Becke, Density-functional exchange-energy approximation with correct asymptotic behavior, *Physical Review A*, 38 (1988) 3098-3100.
- [42] J.P. Perdew, W. Yue, Accurate and simple density functional for the electronic exchange energy: Generalized gradient approximation, *Physical Review B*, 33 (1986) 8800-8802.



- [43] C. Lee, W. Yang, R.G. Parr, Development of the Colle-Salvetti correlation-energy formula into a functional of the electron density, *Physical Review B*, 37 (1988) 785-789.
- [44] J.P. Perdew, J.A. Chevary, S.H. Vosko, K.A. Jackson, M.R. Pederson, D.J. Singh, C. Fiolhais, Atoms, molecules, solids, and surfaces: Applications of the generalized gradient approximation for exchange and correlation, *Physical Review B*, 46 (1992) 6671-6687.
- [45] J.P. Perdew, J. Tao, V.N. Staroverov, G.E. Scuseria, Meta-generalized gradient approximation: Explanation of a realistic nonempirical density functional, *The Journal of Chemical Physics*, 120 (2004) 6898-6911.
- [46] J. Tao, J.P. Perdew, V.N. Staroverov, G.E. Scuseria, Climbing the Density Functional Ladder: Nonempirical Meta-Generalized Gradient Approximation Designed for Molecules and Solids, *Physical Review Letters*, 91 (2003) 146401.
- [47] Y. Zhao, D. Truhlar, The M06 suite of density functionals for main group thermochemistry, thermochemical kinetics, noncovalent interactions, excited states, and transition elements: two new functionals and systematic testing of four M06-class functionals and 12 other functionals, *Theoretical Chemistry Accounts*, 120 (2008) 215-241.
- [48] A.D. Becke, Density-functional thermochemistry. III. The role of exact exchange, *The Journal of Chemical Physics*, 98 (1993) 5648-5652.
- [49] J.C. Slater, *Quantum theory of molecules and solids*, McGraw-Hill, New York, 1963.
- [50] A.D. Becke, Density-functional exchange-energy approximation with correct asymptotic behavior, *Physical Review A*, 38 (1988) 3098-3100.
- [51] S.H. Vosko, L. Wilk, M. Nusair, Accurate spin-dependent electron liquid correlation energies for local spin density calculations: a critical analysis, *Canadian Journal of Physics*, 58 (1980) 1200-1211.
- [52] C. Adamo, V. Barone, Toward reliable density functional methods without adjustable parameters: The PBE0 model, *The Journal of Chemical Physics*, 110 (1999) 6158-6170.

- [53] F. Neese, Prediction of molecular properties and molecular spectroscopy with density functional theory: From fundamental theory to exchange-coupling, *Coordination Chemistry Reviews*, 253 (2009) 526-563.
- [54] R. Peverati, D.G. Truhlar, Improving the Accuracy of Hybrid Meta-GGA Density Functionals by Range Separation, *The Journal of Physical Chemistry Letters*, 2 (2011) 2810-2817.
- [55] F. Allouti, L. Manceron, M.E. Alikhani, On the performance of the hybrid TPSS meta-GGA functional to study the singlet open-shell structures: A combined theoretical and experimental investigations of the Ni<sub>2</sub>O<sub>2</sub> molecule, *Journal of Molecular Structure: THEOCHEM*, 903 (2009) 4-10.
- [56] J. Toulouse, C. Adamo, A new hybrid functional including a meta-GGA approach, *Chemical Physics Letters*, 362 (2002) 72-78.
- [57] S. Grimme, Accurate description of van der Waals complexes by density functional theory including empirical corrections, *Journal of Computational Chemistry*, 25 (2004) 1463-1473.
- [58] S. Grimme, J. Antony, S. Ehrlich, H. Krieg, A consistent and accurate ab initio parametrization of density functional dispersion correction (DFT-D) for the 94 elements H-Pu, *The Journal of Chemical Physics*, 132 (2010) -.
- [59] B. Civalleri, C.M. Zicovich-Wilson, L. Valenzano, P. Ugliengo, B3LYP augmented with an empirical dispersion term (B3LYP-D\*) as applied to molecular crystals, *CrystEngComm*, 10 (2008) 405-410.
- [60] R. Huenerbein, B. Schirmer, J. Moellmann, S. Grimme, Effects of London dispersion on the isomerization reactions of large organic molecules: a density functional benchmark study, *Physical Chemistry Chemical Physics*, 12 (2010) 6940-6948.
- [61] P. Filzmoser, K. Hron, C. Reimann, Univariate statistical analysis of environmental (compositional) data: Problems and possibilities, *Science of The Total Environment*, 407 (2009) 6100-6108.
- [62] R. Viertl, Univariate statistical analysis with fuzzy data, *Computational Statistics & Data Analysis*, 51 (2006) 133-147.

- [63] O. Spjuth, E. Willighagen, R. Guha, M. Eklund, J. Wikberg, Towards interoperable and reproducible QSAR analyses: Exchange of datasets, *Journal of Cheminformatics*, 2 (2010) 5.
- [64] G.E.P. Box, D.R. Cox, An Analysis of Transformations, *Journal of the Royal Statistical Society. Series B (Methodological)*, 26 (1964) 211-252.
- [65] R. Todeschini, V. Consonni, P. Gramatica, 4.05 - Chemometrics in QSAR, in: S.D.B.T. Walczak (Ed.) *Comprehensive Chemometrics*, Elsevier, Oxford, 2009, pp. 129-172.
- [66] N. Brauner, Mordechai, Considering precision of data in reduction of dimensionality and PCA, *Computers & Chemical Engineering*, 24 (2000) 2603-2611.
- [67] H. Joe, Generating random correlation matrices based on partial correlations, *Journal of Multivariate Analysis*, 97 (2006) 2177-2189.
- [68] P. Gramatica, Principles of QSAR Models Validation: Internal and External, *QSAR Comb Sci*, 26 (2007) 694 - 701.
- [69] P. Geddeck, R. Lewis, Exploiting QSAR models in lead optimization, *Curr Opin Drug Discov Devel*, 11 (2008) 569 - 575.
- [70] B. Manly, *Multivariate statistical methods: a primer*, 1986, in, Chapman and Hall, London.
- [71] T. Haga, T. Okuno, Selection of variables in multiple regression analysis, in: G. Maruyama, J. Prokhorov (Eds.) *Proceedings of the Third Japan — USSR Symposium on Probability Theory*, Springer Berlin Heidelberg, 1976, pp. 713-722.
- [72] W. Leland, G.E. Dallal, Tests of Significance in Forward Selection Regression with an F-to-Enter Stopping Rule, *Technometrics*, 23 (1981) 377-380.
- [73] S. Brandmaier, U. Sahlin, I.V. Tetko, T. Öberg, PLS-Optimal: A Stepwise D-Optimal Design Based on Latent Variables, *Journal of Chemical Information and Modeling*, 52 (2012) 975-983.
- [74] I. Frank, J. Feikema, N. Constantine, B. Kowalski, Prediction of Product Quality from Spectral Data Using the Partial Least-Squares Method, *Journal of Chemical Information and Computer Sciences*, 24 (1984) 20-24.

- [75] M. Stone, Cross-Validatory Choice and Assessment of Statistical Predictions, *Journal of the Royal Statistical Society. Series B (Methodological)*, 36 (1974) 111-147.
- [76] D. Rogers, A.J. Hopfinger, Application of Genetic Function Approximation to Quantitative Structure-Activity Relationships and Quantitative Structure-Property Relationships, *Journal of Chemical Information and Computer Sciences*, 34 (1994) 854-866.
- [77] Research and Development Department, IRPC Public Company Limited, Thailand.
- [78] E. Albizzati, M. Galimberti, Catalysts for olefins polymerization, *Catalysis Today*, 41 (1998) 159-168.
- [79] S. Tanase, K. Katayama, N. Yabunouchi, T. Sadashima, N. Tomotsu, N. Ishihara, Design of novel malonates as internal donors for MgCl<sub>2</sub>-supported TiCl<sub>4</sub> type polypropylene catalysts and their mechanistic aspects, Part 1, *Journal of Molecular Catalysis A: Chemical*, 273 (2007) 211-217.
- [80] L. Chen, T.W. Leung, T. Tao, Catalyst Composition with Halo-Malonate Internal Electron Donor and Polymer From Same, in, Google Patents, 2012.
- [81] V.L. Cruz, S. Martinez, J. Ramos, J. Martinez-Salazar, 3D-QSAR as a Tool for Understanding and Improving Single-Site Polymerization Catalysts. A Review, *Organometallics*, 33 (2014) 2944-2959.
- [82] S. Martínez, V.L. Cruz, J. Ramos, J. Martínez-Salazar, Polymerization Activity Prediction of Zirconocene Single-Site Catalysts Using 3D Quantitative Structure-Activity Relationship Modeling, *Organometallics*, 31 (2012) 1673-1679.
- [83] V.L. Cruz, J. Ramos, S. Martinez, A. Muñoz-Escalona, J. Martinez-Salazar, Structure-Activity Relationship Study of the Metallocene Catalyst Activity in Ethylene Polymerization, *Organometallics*, 24 (2005) 5095-5102.
- [84] T.A. Manz, J.M. Caruthers, S. Sharma, K. Phomphrai, K.T. Thomson, W.N. Delgass, M.M. Abu-Omar, Structure-Activity Correlation for Relative Chain Initiation to Propagation Rates in Single-Site Olefin Polymerization Catalysis, *Organometallics*, 31 (2012) 602-618.

- [85] G. Occhipinti, H.-R. Bjørsvik, V.R. Jensen, Quantitative Structure–Activity Relationships of Ruthenium Catalysts for Olefin Metathesis, *Journal of the American Chemical Society*, 128 (2006) 6952-6964.
- [86] S. Yao, Y. Tanaka, Theoretical Consideration of the External Donor of Heterogeneous Ziegler–Natta Catalysts Using Molecular Mechanics, Molecular Dynamics, and QSAR Analysis, *Macromol. Theory Simul.*, 10 (2001) 850-854.
- [87] S. Tanase, K. Katayama, N. Yabunouchi, T. Sadashima, N. Tomotsu, N. Ishihara, Design of novel malonates as internal donors for MgCl<sub>2</sub>-supported TiCl<sub>4</sub> type polypropylene catalysts and their mechanistic aspects, Part 1, *J. Mol. Catal. A: Chem.*, 273 (2007) 211-217.
- [88] Materials Studio, Release 5.5; Accelrys Software, Inc.: San Diego, CA, (2009).
- [89] J.P. Perdew, Y. Wang, Accurate and simple analytic representation of the electron-gas correlation energy, *Physical Review B*, 45 (1992) 13244-13249.
- [90] B. Delley, An all-electron numerical method for solving the local density functional for polyatomic molecules, *The Journal of Chemical Physics*, 92 (1990) 508-517.
- [91] B. Delley, From molecules to solids with the DMol3 approach, *The Journal of Chemical Physics*, 113 (2000) 7756-7764.
- [92] R.D. Cramer, J.D. Bunce, D.E. Patterson, I.E. Frank, Crossvalidation, Bootstrapping, and Partial Least Squares Compared with Multiple Regression in Conventional QSAR Studies, *Quantitative Structure-Activity Relationships*, 7 (1988) 18-25.
- [93] R. Guha, P.C. Jurs, Determining the Validity of a QSAR Model – A Classification Approach, *Journal of Chemical Information and Modeling*, 45 (2004) 65-73.
- [94] A. Tropsha, Chapter 7 Variable Selection QSAR Modeling, Model Validation, and Virtual Screening, in: C.S. David (Ed.) *Annual Reports in Computational Chemistry*, Elsevier, 2006, pp. 113-126.
- [95] J.W. Lee, W.H. Jo, Chemical structure–stereospecificity relationship of internal donor in heterogeneous Ziegler–Natta catalyst for propylene polymerization by DFT and MM calculations, *J. Organomet. Chem.*, 694 (2009) 3076-3083.
- [96] (!!! INVALID CITATION !!!).

- [97] D.V. Stukalov, V.A. Zakharov, A.G. Potapov, G.D. Bukatov, Supported Ziegler–Natta catalysts for propylene polymerization. Study of surface species formed at interaction of electron donors and  $\text{TiCl}_4$  with activated  $\text{MgCl}_2$ , *Journal of Catalysis*, 266 (2009) 39-49.
- [98] R.-h. Cheng, J. Luo, Z. Liu, J.-w. Sun, W.-h. Huang, M.-g. Zhang, J.-j. Yi, B.-p. Liu, Adsorption of  $\text{TiCl}_4$  and electron donor on defective  $\text{MgCl}_2$  surfaces and propylene polymerization over Ziegler-Natta catalyst: A DFT study, *Chin J Polym Sci*, 31 (2013) 591-600.
- [99] A. Correa, R. Credendino, J.T.M. Pater, G. Morini, L. Cavallo, Theoretical Investigation of Active Sites at the Corners of  $\text{MgCl}_2$  Crystallites in Supported Ziegler–Natta Catalysts, *Macromolecules*, 45 (2012) 3695-3701.
- [100] D.V. Stukalov, V.A. Zakharov, I.L. Zilberberg, Adsorption Species of Ethyl Benzoate in  $\text{MgCl}_2$ -Supported Ziegler–Natta Catalysts. A Density Functional Theory Study, *The Journal of Physical Chemistry C*, 114 (2009) 429-435.
- [101] N. Bahri-Laleh, A. Correa, S. Mehdipour-Ataei, H. Arabi, M.N. Haghighi, G. Zohuri, L. Cavallo, Moving up and down the Titanium Oxidation State in Ziegler–Natta Catalysis, *Macromolecules*, 44 (2011) 778-783.
- [102] A. Correa, F. Piemontesi, G. Morini, L. Cavallo, Key Elements in the Structure and Function Relationship of the  $\text{MgCl}_2/\text{TiCl}_4/\text{Lewis Base}$  Ziegler–Natta Catalytic System, *Macromolecules*, 40 (2007) 9181-9189.
- [103] T. Taniike, M. Terano, Coadsorption model for first-principle description of roles of donors in heterogeneous Ziegler–Natta propylene polymerization, *Catal. Today*, 293 (2012) 39-50.
- [104] M. Ratanasak, V. Parasuk, Roles of malonate donor on activity and stereoselectivity of Ziegler–Natta catalyzed propylene polymerization, *Journal of Organometallic Chemistry*, 775 (2015) 6-11.
- [105] J.P. Perdew, K. Burke, M. Ernzerhof, Generalized Gradient Approximation Made Simple, *Phys. Rev. Lett.*, 77 (1996) 3865-3868
- [106] B. Delley, An all electron numerical method for solving the local density functional for polyatomic molecules, *J. Chem. Phys*, 92 (1990) 508-517.

- [107] A. Bergner, M. Dolg, W. Küchle, H. Stoll, H. Preuß, Ab initio energy-adjusted pseudopotentials for elements of groups 13–17, *Mol. Phys.*, 80 (1993) 1431-1441.
- [108] Materials Studio, Release 5.5; Accelrys Software, Inc.: San Diego, CA, 2009.
- [109] S. Wold, A. Ruhe, H. Wold, I. Dunn, W., The Collinearity Problem in Linear Regression. The Partial Least Squares (PLS) Approach to Generalized Inverses, *SIAM J. Sci. Comput.*, 5 (1984) 735-743.
- [110] H. Kubinyi, Statistical Methods, in: *QSAR: Hansch Analysis and Related Approaches*, Wiley-VCH Verlag GmbH, 2008, pp. 91-107.
- [111] S. Wold, L. Eriksson, S. Clementi, Statistical Validation of QSAR Results, in: *Chemometric Methods in Molecular Design*, Wiley-VCH Verlag GmbH, 2008, pp. 309-338.
- [112] Y. Nie, J. Sun, W. Yin, L. Wang, Z. Shi, H. Schumann, Novel diphenyl thioether-bridged binuclear metallocenes of Ti and Zr for synthesis of polyethylene with broad molecular weight distribution, *Journal of Applied Polymer Science*, 120 (2011) 3530-3535.
- [113] J. Xu, L. Feng, S. Yang, Formation Mechanism of Stereoblocks in Polypropylene Produced by Supported Ziegler–Natta Catalysts, *Macromolecules*, 30 (1997) 2539-2541.
- [114] M.C. Sacchi, F. Forlini, I. Tritto, P. Locatelli, Stereochemistry of the initiation step in Ziegler-Natta catalysts containing dialkyl propane diethers: A tool for distinguishing the role of internal and external donors, *Macromolecular Symposia*, 89 (1995) 91-100.
- [115] V. Busico, P. Corradini, L. De Martino, A. Proto, V. Savino, E. Albizzati, Polymerization of propene in the presence of MgCl<sub>2</sub>-supported Ziegler-Natta catalysts, 1. The role of ethyl benzoate as “internal” and “external” base, *Die Makromolekulare Chemie*, 186 (1985) 1279-1288.
- [116] B. Liu, R. Cheng, Z. Liu, P. Qiu, S. Zhang, T. Taniike, M. Terano, K. Tashino, T. Fujita, Experimental and Computational Approaches on the Isospecific Role of Monoester-Type Internal Electron Donor for TiCl<sub>4</sub>/MgCl<sub>2</sub> Ziegler-Natta Catalysts, *Macromolecular Symposia*, 260 (2007) 42-48.

- [117] Y.V. Kissin, X. Liu, D.J. Pollick, N.L. Brungard, M. Chang, Ziegler-Natta catalysts for propylene polymerization: Chemistry of reactions leading to the formation of active centers, *Journal of Molecular Catalysis A: Chemical*, 287 (2008) 45-52.
- [118] H. Mori, K. Hasebe, M. Terano, XPS study of the interaction of titanium species with internal electron donors on MgCl<sub>2</sub>-supported Ziegler catalysts, *Journal of Molecular Catalysis A: Chemical*, 140 (1999) 165-172.
- [119] M.d.F.V. Marques, R.d.S. Cardoso, M.G. da Silva, Preparation of MgCl<sub>2</sub>-supported Ziegler-Natta catalyst systems with new electron donors, *Applied Catalysis A: General*, 374 (2010) 65-70.
- [120] T. Taniike, M. Terano, Density Functional Calculations for Electronic and Steric Effects of Ethyl Benzoate on Various Ti Species in MgCl<sub>2</sub>-Supported Ziegler-Natta Catalysts, *Macromolecular Symposia*, 260 (2007) 98-106.
- [121] A.P. de Oliveira Filho, U. Schuchardt, R. Custodio, Hartree-Fock and density functional theory analysis of propylene insertion in Al(CH<sub>3</sub>)<sub>3</sub>/TiCl<sub>3</sub>/TiO<sub>2</sub> (red.) in the presence of a Lewis base, *Journal of Molecular Catalysis A: Chemical*, 146 (1999) 191-198.
- [122] L. Cavallo, S. Del Piero, J.-M. Duc  r  , R. Fedele, A. Melchior, G. Morini, F. Piemontesi, M. Tolazzi, Key Interactions in Heterogeneous Ziegler-Natta Catalytic Systems: Structure and Energetics of TiCl<sub>4</sub>-Lewis Base Complexes, *The Journal of Physical Chemistry C*, 111 (2007) 4412-4419.
- [123] R.-h. Cheng, J. Luo, Z. Liu, J.-w. Sun, W.-h. Huang, M.-g. Zhang, J.-j. Yi, B.-p. Liu, Adsorption of TiCl<sub>4</sub> and electron donor on defective MgCl<sub>2</sub> surfaces and propylene polymerization over Ziegler-Natta catalyst: A DFT study, *Chin J Polym Sci*, 31 (2013) 591-600.
- [124] Z. Flisak, T. Ziegler, DFT Study of Ethylene and Propylene Copolymerization over a Heterogeneous Catalyst with a Coordinating Lewis Base, *Macromolecules*, 38 (2005) 9865-9872.
- [125] Z. Flisak, Multidentate Tetrahydrofurfuryloxy Ligand in a Ziegler-Natta Catalyst Studied by Molecular Modeling, *Macromolecules*, 41 (2008) 6920-6924.
- [126] T. Taniike, M. Terano, Coadsorption and Support-Mediated Interaction of Ti Species with Ethyl Benzoate in MgCl<sub>2</sub>-Supported Heterogeneous Ziegler-Natta



- Catalysts Studied by Density Functional Calculations, *Macromolecular Rapid Communications*, 28 (2007) 1918-1922.
- [127] T. Taniike, M. Terano, A Density Functional Study on the Influence of the Molecular Flexibility of Donors on the Insertion Barrier and Stereoselectivity of Ziegler-Natta Propylene Polymerization, *Macromolecular Chemistry and Physics*, 210 (2009) 2188-2193.
- [128] X.-r. Shen, Z.-s. Fu, J. Hu, Q. Wang, Z.-q. Fan, Mechanism of Propylene Polymerization with MgCl<sub>2</sub>-Supported Ziegler-Natta Catalysts Based on Counting of Active Centers: The Role of External Electron Donor, *The Journal of Physical Chemistry C*, 117 (2013) 15174-15182.
- [129] M. Toto, G. Morini, G. Guerra, P. Corradini, L. Cavallo, Influence of 1,3-Diethers on the Stereospecificity of Propene Polymerization by Supported Ziegler-Natta Catalysts. A Theoretical Investigation on Their Adsorption on (110) and (100) Lateral Cuts of MgCl<sub>2</sub> Platelets, *Macromolecules*, 33 (2000) 1134-1140.
- [130] L. Brambilla, G. Zerbi, F. Piemontesi, S. Nascetti, G. Morini, Structure of Donor Molecule 9,9-Bis(Methoxymethyl)-Fluorene in Ziegler-Natta Catalyst by Infrared Spectroscopy and Quantum Chemical Calculation, *The Journal of Physical Chemistry C*, 114 (2010) 11475-11484.
- [131] M. Ratanasak, T. Rungrotmongkol, O. Saengsawang, S. Hannongbua, V. Parasuk, Towards the design of new electron donors for Ziegler-Natta catalyzed propylene polymerization using QSPR modeling, *Polymer*, 56 (2015) 340-345.
- [132] G. Talarico, V. Busico, L. Cavallo, Origin of the Regiochemistry of Propene Insertion at Octahedral Column 4 Polymerization Catalysts: Design or Serendipity?, *Journal of the American Chemical Society*, 125 (2003) 7172-7173.
- [133] A. Correa, G. Talarico, L. Cavallo, Regiochemistry of propene insertion with group 4 polymerization catalysts from a theoretical perspective, *Journal of Organometallic Chemistry*, 692 (2007) 4519-4527.
- [134] V. Busico, R. Cipullo, R. Pellicchia, S. Ronca, G. Roviello, G. Talarico, Design of stereoselective Ziegler-Natta propene polymerization catalysts, *Proceedings of the National Academy of Sciences*, 103 (2006) 15321-15326.

- [135] O.N. Shumilo, N.N. Bulgakov, V.A. Likholobov, On the mechanism of ethylene and propylene insertion into metal-hydroxo bonds, *React Kinet Catal Lett*, 22 (1983) 87-93.
- [136] Y. Doi, S. Suzuki, F. Nozawa, K. Soga, T. Keii, Structure and Reactivity of "Living" Polypropylene., In *Studies in Surface Science and Catalysis*, (1986).
- [137] P. Corradini, G. Guerra, L. Cavallo, Do New Century Catalysts Unravel the Mechanism of Stereocontrol of Old Ziegler–Natta Catalysts?, *Accounts of Chemical Research*, 37 (2004) 231-241.
- [138] M. Boero, M. Parrinello, K. Terakura, First Principles Molecular Dynamics Study of Ziegler–Natta Heterogeneous Catalysis, *Journal of the American Chemical Society*, 120 (1998) 2746-2752.
- [139] M. Seth, T. Ziegler, Polymerization Properties of a Heterogeneous Ziegler–Natta Catalyst Modified by a Base: A Theoretical Study, *Macromolecules*, 36 (2003) 6613-6623.
- [140] M. D'Amore, R. Credendino, P.H.M. Budzelaar, M. Causá, V. Busico, A periodic hybrid DFT approach (including dispersion) to MgCl<sub>2</sub>-supported Ziegler–Natta catalysts – 1: TiCl<sub>4</sub> adsorption on MgCl<sub>2</sub> crystal surfaces, *Journal of Catalysis*, 286 (2012) 103-110.
- [141] P. Corradini, G. Guerra, V. Villani, Stereoselectivity of the model catalytic site proposed for the isospecific Ziegler-Natta polymerization of the .alpha.-olefins, *Macromolecules*, 18 (1985) 1401-1406.
- [142] D.E. Partin, M. O'Keeffe, The structures and crystal chemistry of magnesium chloride and cadmium chloride, *Journal of Solid State Chemistry*, 95 (1991) 176-183.
- [143] S. Grimme, Density functional theory with London dispersion corrections, *Wiley Interdisciplinary Reviews: Computational Molecular Science*, 1 (2011) 211-228.
- [144] M. Dolg, U. Wedig, H. Stoll, H. Preuss, Energy-adjusted abinitio pseudopotentials for the first row transition elements, *The Journal of Chemical Physics*, 86 (1987) 866-872.

- [145] M.J. Frisch, G.W. Trucks, H.B. Schlegel, G.E. Scuseria, M.A. Robb, J.R. Cheeseman, G. Scalmani, V. Barone, B. Mennucci, G.A. Petersson, H. Nakatsuji, M. Caricato, X. Li, H.P. Hratchian, A.F. Izmaylov, J. Bloino, G. Zheng, J.L. Sonnenberg, M. Hada, M. Ehara, K. Toyota, R. Fukuda, J. Hasegawa, M. Ishida, T. Nakajima, Y. Honda, O. Kitao, H. Nakai, T. Vreven, J.A. Montgomery, J.E. Peralta, F. Ogliaro, M. Bearpark, J.J. Heyd, E. Brothers, K.N. Kudin, V.N. Staroverov, R. Kobayashi, J. Normand, K. Raghavachari, A. Rendell, J.C. Burant, S.S. Iyengar, J. Tomasi, M. Cossi, N. Rega, J.M. Millam, M. Klene, J.E. Knox, J.B. Cross, V. Bakken, C. Adamo, J. Jaramillo, R. Gomperts, R.E. Stratmann, O. Yazyev, A.J. Austin, R. Cammi, C. Pomelli, J.W. Ochterski, R.L. Martin, K. Morokuma, V.G. Zakrzewski, G.A. Voth, P. Salvador, J.J. Dannenberg, S. Dapprich, A.D. Daniels, Farkas, J.B. Foresman, J.V. Ortiz, J. Cioslowski, D.J. Fox, Gaussian 09, Revision B.01, in, Wallingford CT, 2009.
- [146] A. Zambelli, P. Ammendola, Stereospecific polymerization of  $\alpha$ -olefins: End groups, polymer structure and reaction mechanism, *Progress in Polymer Science*, 16 (1991) 203-218.
- [147] R. Credendino, V. Busico, M. Causa, V. Barone, P.H.M. Budzelaar, C. Zicovich-Wilson, Periodic DFT modeling of bulk and surface properties of  $MgCl_2$ , *Physical Chemistry Chemical Physics*, 11 (2009) 6525-6532.
- [148] J.W. Lee, W.H. Jo, Theoretical investigation on the model active site for isotactic polypropylene in heterogeneous Ziegler–Natta catalyst: A density functional study, *Journal of Organometallic Chemistry*, 692 (2007) 4639-4646.
- [149] S. Mukhopadhyay, S.A. Kulkarni, S. Bhaduri, Density functional study on the role of electron donors in propylene polymerization using Ziegler–Natta catalyst, *Journal of Organometallic Chemistry*, 690 (2005) 1356-1365.
- [150] A. Correa, F. Piemontesi, G. Morini, L. Cavallo, Key Elements in the Structure and Function Relationship of the  $MgCl_2/TiCl_4$ /Lewis Base Ziegler–Natta Catalytic System, *Macromolecules*, 40 (2007) 9181-9189.

## APPENDIX-A

Table A1 Input molecular properties of QSPR model analysis.

Donor	Methoxy (Fragment Counts)	Butyl (Fragment Counts)	Ethyl (Fragment Counts)	Isobutyl (Fragment Counts)	Isopropyl (Fragment Counts)	Methyl (Fragment Counts)	Propyl (Fragment Counts)
P1	0	0	0	0	0	0	0
P3	0	2	4	0	0	4	2
P4	0	2	2	0	0	2	2
P5	0	0	0	2	2	4	0
P6	0	0	0	2	2	4	0
P8	0	0	0	2	2	4	0
D1	2	0	0	0	0	2	0
D2	2	0	0	0	0	3	0
D3	2	0	0	0	0	4	0
D4	2	0	0	0	0	6	0
D5	2	0	0	0	2	6	0
D6	2	0	2	0	0	4	2
D7	2	0	0	0	2	6	0
D9	2	0	0	0	0	2	0
M1	0	2	2	0	0	2	2
M2	0	2	2	0	0	3	2
M3	0	2	2	0	0	2	2
M5	0	2	2	0	0	2	2
M6	0	2	4	0	0	4	2
M7	0	2	2	0	0	2	2
M8	0	4	4	0	0	4	4
M9	0	0	2	0	0	2	0
M11	0	0	2	0	0	3	0
M12	0	0	2	0	0	2	0

**Table A1** Input molecular properties of QSPR model analysis (con't).

Donor	Cyclohexane (Fragment Counts)	Total molecular mass (Atomistic Descriptors)	Molecular area (vdW area) (Spatial Descriptors)	Molecular volume (vdW volume) (Spatial Descriptors)
P1	2	330.424	388.2381	318.3656
P3	0	390.564	513.7978	409.2019
P4	0	390.564	522.6805	410.2128
P5	0	278.348	350.2051	274.7323
P6	0	362.510	478.6491	375.9589
P8	0	418.618	562.0794	442.6283
D1	0	104.149	158.0200	113.3358
D2	0	118.176	179.0118	130.4929
D3	0	132.203	196.6395	147.1442
D4	0	174.284	247.7814	196.6577
D5	0	188.311	264.0508	213.2042
D6	0	188.311	278.2692	214.2932
D7	0	216.365	315.5442	248.0816
D9	0	172.268	239.5806	185.4034
M1	0	216.277	293.2051	219.5355
M2	0	230.304	313.4778	237.1220
M3	0	242.315	318.9370	244.9146
M5	0	256.342	337.8499	260.4916
M6	0	272.385	368.2985	286.7648
M7	0	284.396	378.1584	293.4801
M8	0	328.493	455.4640	354.2877
M9	0	246.278	296.0774	230.4086
M11	0	242.315	305.4217	242.4994
M12	0	228.288	291.4950	226.0303

**Table A1** Input molecular properties of QSPR model analysis (con't).

Donor	Molecular density (Spatial Descriptors)	Radius of gyration (Spatial Descriptors)	Atom count (Atomistic Descriptors)	Element count (Atomistic Descriptors)
P1	1.0379	4.0187	50	20
P3	0.9545	4.4971	66	24
P4	0.9521	5.6039	66	24
P5	1.0132	4.3500	42	16
P6	0.9642	5.4137	60	22
P8	0.9458	5.9430	72	26
D1	0.9189	2.7582	19	5
D2	0.9056	2.6572	22	6
D3	0.8985	2.7193	25	7
D4	0.8862	2.8867	34	10
D5	0.8832	2.9604	37	11
D6	0.8788	3.2288	37	11
D7	0.8722	3.2503	43	13
D9	0.9292	2.9600	32	10
M1	0.9852	4.5790	35	11
M2	0.9712	4.9675	38	12
M3	0.9894	4.9704	39	13
M5	0.9841	4.7776	42	14
M6	0.9499	4.6386	47	15
M7	0.9690	4.7066	48	16
M8	0.9272	4.6493	59	19
M9	1.0689	3.6357	36	12
M11	0.9992	3.5660	39	13
M12	1.0100	3.6165	26	12

**Table A1** Input molecular properties of QSPR model analysis (con't).

Donor	Principal moments			
	of inertia (magnitude) (Spatial Descriptors)	Principal moment of inertia X (Spatial Descriptors)	Principal moment of inertia Y (Spatial Descriptors)	Principal moment of inertia Z (Spatial Descriptors)
P1	5111.1540	1969.3430	2490.5940	4005.3120
P3	7714.2190	2809.4840	4485.6000	5612.0730
P4	12177.5300	3894.7120	6510.1090	9525.8590
P5	4640.3780	1078.8050	2909.8640	3449.9250
P6	10314.9600	2457.9680	6331.7840	7763.0800
P8	14979.6500	4744.8700	7999.2950	11742.5500
D1	774.6049	67.1008	524.3691	566.1689
D2	676.8947	194.6458	403.5960	507.3556
D3	786.2871	303.1326	418.1427	592.8868
D4	1192.4130	589.7524	604.6508	841.6881
D5	1416.6520	604.4416	874.5208	936.3588
D6	1703.9930	825.5802	910.9765	1179.8870
D7	2023.5680	929.5988	1135.7140	1393.1360
D9	1302.2050	453.1223	751.4633	962.1440
M1	4284.2910	601.2599	2782.5920	3201.6900
M2	5420.4140	288.9071	3779.4280	3874.7060
M3	5721.1970	324.3324	3910.1150	4163.8810
M5	5543.5490	409.4737	3836.4100	3980.6070
M6	5691.3460	649.7478	3937.1140	4058.1260
M7	5818.6700	1207.3080	3638.8090	4377.0300
M8	6735.0260	1500.6940	4498.9670	4782.0270
M9	2630.2604	997.1116	1366.6247	2014.0445
M11	2671.7237	981.6454	1403.2654	2050.6892
M12	2580.0561	953.8792	1326.3293	1996.9112

**Table A1** Input molecular properties of QSPR model analysis (con't).

Donor	Total energy (VAMP Electrostatics)	Electronic energy (VAMP Electrostatics)	Heat of formation (VAMP Electrostatics)	HOMO eigenvalue (VAMP Electrostatics)
P1	-4201.9310	-33047.8900	-175.8403	-10.1236
P3	-4879.6470	-43104.3000	-197.5476	-10.2305
P4	-4880.0830	-39909.3600	-207.6093	-10.2771
P5	-3633.6430	-24406.3500	-158.3285	-10.1441
P6	-4568.4620	-35629.1500	-195.0456	-10.1499
P8	-5191.5030	-44057.7200	-215.5503	-10.2864
D1	-1446.8770	-5893.9060	-104.0479	-10.4507
D2	-1602.3760	-7372.3480	-103.1524	-10.3330
D3	-1758.0100	-8843.4620	-105.3479	-10.3183
D4	-2224.6260	-13898.0300	-105.4080	-10.2952
D5	-2380.4500	-15667.8400	-112.0204	-10.2472
D6	-2381.0990	-15111.1800	-126.9774	-10.3531
D7	-2691.7830	-19153.4300	-117.9533	-10.3036
D9	-2197.7860	-13203.4400	-116.2781	-10.2399
M1	-2967.2840	-16440.3500	-206.3821	-11.2994
M2	-3122.9300	-18211.2800	-208.8824	-11.1778
M3	-3249.4070	-19635.7500	-168.5454	-11.1254
M5	-3405.5290	-21941.1100	-182.0094	-10.9926
M6	-3589.6980	-24808.8300	-212.4340	-10.9064
M7	-3718.1590	-25920.5400	-217.8668	-11.0969
M8	-4213.0050	-33726.5800	-239.0888	-10.8388
M9	-3565.8846	-21966.5101	-227.6133	-11.0167
M11	-3250.4196	-21524.5844	-191.8953	-10.9250
M12	-3094.9893	-19155.1466	-194.3762	-11.0954



**Table A1** Input molecular properties of QSPR model analysis (con't).

Donor	LUMO eigenvalue (VAMP Electrostatics)	Molecular surface area (VAMP Electrostatics)	Total dipole (VAMP Electrostatics)	Dipole x (VAMP Electrostatics)
P1	-0.4866	390.0814	2.7020	1.4480
P3	-0.6724	514.2071	6.1470	-2.3300
P4	-0.6096	524.6824	5.1020	-1.3900
P5	-0.4703	351.0854	3.6650	0.3220
P6	-0.5923	477.5395	3.7100	-0.0720
P8	-0.6160	563.9319	4.9530	-1.8530
D1	2.8985	159.7732	1.7720	-1.5130
D2	3.0907	180.3738	2.0900	-2.0450
D3	3.0229	199.8834	2.0410	-1.4830
D4	3.0051	248.8046	2.0150	-1.9250
D5	2.7748	265.4429	1.1660	-0.4670
D6	2.8694	277.6669	1.6910	-1.2310
D7	2.6800	315.9147	1.3440	0.8390
D9	2.9364	237.9783	2.1030	-1.7890
M1	0.8168	292.8988	2.9120	-1.8020
M2	0.8513	316.4191	2.1810	1.3800
M3	0.8120	320.2358	4.3110	0.2890
M5	1.0139	338.6166	3.3120	1.7080
M6	1.0244	369.6437	4.1220	0.1000
M7	0.9121	380.7596	3.3700	-0.9450
M8	0.9728	457.0896	3.4140	1.2320
M9	0.6994	295.2733	1.8650	-0.2740
M11	1.0175	305.0293	3.4580	-0.9320
M12	0.9320	291.9105	3.2800	-0.8570

**Table A1** Input molecular properties of QSPR model analysis (con't).

Donor	Dipole y (VAMP Electrostatics)	Dipole z (VAMP Electrostatics)	Total energy (DMol3 Molecular)	Binding energy (DMol3 Molecular)
P1	1.1100	-1.9920	-1069.7640	-9.9435
P3	3.4340	-4.5350	-1227.8570	-12.4424
P4	4.1940	-2.5520	-1227.8520	-12.4371
P5	2.8080	-2.3330	-916.2621	-8.2129
P6	2.4360	-2.7970	-1149.9630	-11.3898
P8	4.2690	-1.6950	-1305.7550	-13.4990
D1	0.5650	0.7280	-345.3272	-3.2203
D2	0.3500	-0.2510	-384.2739	-3.7463
D3	1.1650	-0.7800	-423.2272	-4.2789
D4	0.2900	-0.5190	-540.0727	-5.8624
D5	-0.3740	-1.0010	-579.0209	-6.3900
D6	-0.9530	0.6610	-579.0261	-6.3952
D7	-0.3130	-1.0020	-656.9120	-7.4398
D9	0.6170	-0.9160	-538.9171	-5.6623
M1	2.2080	-0.5970	-726.2111	-6.4431
M2	1.6890	0.0420	-765.1613	-6.9727
M3	3.7620	-2.0870	-802.9074	-7.2536
M5	2.5010	-1.3400	-841.8588	-7.7844
M6	3.2380	-2.5500	-882.0039	-8.5533
M7	2.6140	-1.9050	-919.7906	-8.8748
M8	2.6100	-1.8230	-1037.8090	-10.6755
M9	1.3630	-1.2430	-862.6670	-6.8008
M11	2.5790	-2.1060	-802.9448	-7.2911
M12	2.5040	-1.9370	-763.9951	-6.7620

**Table A1** Input molecular properties of QSPR model analysis (con't).

Donor	HOMO energy			Total dipole (DMol3 Molecular)
	(DMol3 Molecular)	LUMO energy (DMol3 Molecular)	LUMO-HOMO energy (DMol3 Molecular)	
P1	-0.2255	-0.0839	0.1416	1.2623
P3	-0.2153	-0.0929	0.1225	2.3716
P4	-0.2237	-0.0886	0.1351	1.9382
P5	-0.2260	-0.0829	0.1432	1.5226
P6	-0.2268	-0.0920	0.1348	1.5167
P8	-0.2240	-0.0890	0.1350	1.8869
D1	-0.2057	0.0500	0.2557	0.6536
D2	-0.1987	0.0399	0.2385	0.7139
D3	-0.1984	0.0410	0.2394	0.6550
D4	-0.1999	0.0347	0.2345	0.7252
D5	-0.2035	0.0384	0.2420	0.3884
D6	-0.2037	0.0403	0.2441	0.7282
D7	-0.2086	0.0322	0.2408	0.5848
D9	-0.1970	0.0410	0.2380	0.6687
M1	-0.2338	-0.0440	0.1899	1.2314
M2	-0.2306	-0.0459	0.1847	0.7272
M3	-0.2151	-0.0361	0.1791	1.7096
M5	-0.2220	-0.0426	0.1794	1.0438
M6	-0.2157	-0.0387	0.1770	1.4488
M7	-0.2262	-0.0465	0.1797	1.3559
M8	-0.2250	-0.0379	0.1870	1.0588
M9	-0.2297	-0.0543	0.1754	0.7599
M11	-0.2224	-0.0425	0.1799	1.2659
M12	-0.2270	-0.0481	0.1789	1.3225

**Table A1** Input molecular properties of QSPR model analysis (con't).

Donor	Dipole x (DMol3 Molecular)	Dipole y (DMol3 Molecular)	Dipole z (DMol3 Molecular)	Total energy (Forcite Energetics)
P1	0.8647	0.4324	-0.8116	50.8149
P3	-0.7317	1.1987	-1.9111	145.8020
P4	-0.2352	1.6351	-1.0138	120.3419
P5	0.3650	1.0874	-1.0013	77.9906
P6	0.1699	0.9064	-1.2041	48.5579
P8	-0.4231	1.7039	-0.6916	64.6455
D1	-0.5571	0.1848	0.2875	6.8050
D2	-0.7057	0.0437	-0.0981	36.5093
D3	-0.4460	0.4485	-0.1700	37.5068
D4	-0.7102	-0.0844	-0.1202	37.9030
D5	-0.1176	-0.2592	-0.2642	74.9133
D6	-0.4614	-0.5086	0.2423	73.9923
D7	0.4445	-0.2403	-0.2943	33.6166
D9	-0.6001	0.0778	-0.2846	63.1020
M1	-0.6867	0.9954	-0.2323	-24.8617
M2	0.4315	0.5853	0.0064	52.5953
M3	0.0659	1.4761	-0.8600	395.2334
M5	0.6534	0.7091	-0.3998	199.7786
M6	0.1451	1.1083	-0.9217	151.5775
M7	-0.5459	0.9077	-0.8464	33.8008
M8	0.6250	0.6569	-0.5468	135.8764
M9	-0.3079	0.3933	-0.5727	168.1902
M11	-0.5732	0.7416	-0.8508	79.4904
M12	-0.5276	0.8624	-0.8526	-5.8107

**Table A1** Input molecular properties of QSPR model analysis (con't).

Donor	Non bond energy (Forcite Energetics)	van der Waals energy (Forcite Energetics)	Electrostatic energy (Forcite Energetics)	Bond energy (Forcite Energetics)
P1	12.5718	30.0002	-17.4283	8.4526
P3	98.1972	28.1260	70.0713	9.0536
P4	72.6767	22.2029	50.4738	8.1278
P5	32.0841	24.0654	8.0187	8.6669
P6	3.7697	30.3697	-26.6000	9.1858
P8	15.0986	27.3019	-12.2033	8.8689
D1	-1.8396	5.2898	-7.1294	1.9831
D2	26.3164	6.9025	19.4139	2.1213
D3	27.6746	10.6114	17.0631	2.6761
D4	17.3274	26.8952	-9.5678	6.4599
D5	47.0588	27.8042	19.2546	8.2722
D6	56.7836	16.1734	40.6102	4.7067
D7	-9.9433	22.6154	-32.5587	7.9555
D9	49.6796	16.5794	33.1002	3.7525
M1	-53.1707	9.0015	-62.1722	4.2111
M2	26.5236	11.2148	15.3088	6.2102
M3	93.3248	18.3144	75.0104	6.2860
M5	86.8153	15.0673	71.7480	10.3581
M6	112.4079	21.3345	91.0734	9.9743
M7	-16.6305	12.2144	-28.8449	9.6469
M8	94.1888	20.0310	74.1578	8.4526
M9	122.4574	12.7694	109.6880	12.8591
M11	33.8890	20.3882	13.5008	12.1826
M12	-51.7069	11.4014	-63.1083	9.2609

**Table A1** Input molecular properties of QSPR model analysis (con't).

Donor	Angle energy (Forcite Energetics)	Torsion energy (Forcite Energetics)	Inversion energy (Forcite Energetics)	Valence energy (Forcite Energetics)
P1	16.6269	13.0901	0.0735	38.2431
P3	23.5853	14.4821	0.4838	47.6048
P4	24.7679	14.5736	0.1960	47.6652
P5	22.4869	14.2535	0.4993	45.9066
P6	24.5430	10.6403	0.4191	44.7883
P8	26.1151	14.3931	0.1699	49.5469
D1	6.5820	0.0795	0.0000	8.6446
D2	7.7148	0.3569	0.0000	10.1929
D3	6.9617	0.1944	0.0000	9.8322
D4	13.5910	0.5247	0.0000	20.5756
D5	18.3306	1.2516	0.0000	27.8545
D6	11.8656	0.6364	0.0000	17.2087
D7	31.8755	3.7288	0.0000	43.5598
D9	8.6739	0.9959	0.0000	13.4223
M1	21.6948	2.3791	0.0239	28.3090
M2	19.3937	0.4363	0.0314	26.0716
M3	288.8629	6.7459	0.0138	301.9086
M5	94.1799	8.2485	0.1768	112.9633
M6	26.0481	2.9014	0.2458	39.1696
M7	32.6834	7.9102	0.1908	50.4313
M8	28.4145	3.1787	0.0739	41.6876
M9	24.7122	8.0327	0.1289	45.7328
M11	25.2287	8.0595	0.1307	45.6014
M12	28.7412	7.7475	0.1466	45.8962

## APPENDIX-B

**Proceeding and Conferences:**

- 1) Manussada Ratanasak, Vudhichai Parasuk. “Mechanistic Studies for Roles of Di-n-Butyl 2-Cyclopentyl Malonate Donor with Ziegler-Natta Catalyst in Propylene Polymerization” and “Computer-Aided Design New Electron Donors in Ziegler–Natta Polypropylene Catalyst by QSPR model” Nanoscience and Nanomedicine Workshop. MSE, ERI@N, NITHM, IGS and CU, September 11-12, 2014, Nanyang Technological University, Singapore. (2 Posters Presentation)
- 2) Manussada Ratanasak, Vudhichai Parasuk. “DFT Study on the Roles of Malonate Donors in Propylene Polymerization using Heterogeneous Ziegler-Natta Catalyst” The 2014 IUPAC World Polymer Congress (MACRO 2014), July 6-11, 2014, Chiang Mai International Convention and Exhibition Centre, Chiang Mai, Thailand. (Poster Presentation)
- 3) Manussada Ratanasak, Vudhichai Parasuk. “Role of malonate donor on the insertion barrier and stereoselectivity of Ziegler-Natta catalyzed propylene polymerization” The Seventh Tokyo Conference on Advanced Catalytic Science and Technology (TOCAT7), June 1-6, 2014, Kyoto TERRSA, Kyoto, Japan. (Poster Presentation)
- 4) Manussada Ratanasak, Orphan Saengsawang, Thanyada Rungrotmongkol, Supot Hannongbua, Vudhichai Parasuk. “Design of New Electron Donors for Ziegler-Natta Catalyzed Propylene Polymerization by QSPR Model”, The 2013 International Workshop on Frontiers of Theoretical and Computational Physics and Chemistry (WFTCPC 2013), December, 9-12, 2013, The Tide Resort, Bangsaen Beach, Chon buri, Thailand. (Poster Presentation)

5) Manussada Ratanasak, Oraphan Saengsawang, Thanyada Rungrotmongkol, Supot Hannongbua, Vudhichai Parasuk. “Design of New Electron Donors for Ziegler-Natta Catalyzed Propylene Polymerization by QSPR Model”, 6th Asian Pacific Conference of Theoretical and Computational Chemistry (APCTCC-6), July,10-13, 2013, Hilton Hotel in Gyeongju, Korea. (Poster Presentation)

6) Manussada Ratanasak, Oraphan Saengsawang, Thanyada Rungrotmongkol, Vudhichai Parasuk, Supot Hannongbua. “QSPR study on Electron Donors for Ziegler-Natta Catalyzed Propylene Polymerization”, Pure and Applied Chemistry International Conference 2013 (PACCON 2013), January, 23-25, 2013, The Tide Resort, Bangsaen Beach, Chon buri, Thailand. (Poster Presentation)





**Award:**

Poster Presentation Awards (2nd Prize). “DFT Study on the Roles of Malonate Donors in Propylene Polymerization using Heterogeneous Ziegler-Natta Catalyst” The 2014 IUPAC World Polymer Congress (MACRO 2014), July, 6-11, 2014, Chiang Mai International Convention and Exhibition Centre, Chiang Mai, Thailand.

**Publications:**

- 1) Ratanasak M., Parasuk V. Roles of malonate donor on activity and stereoselectivity of Ziegler–Natta catalyzed propylene polymerization. *Journal of Organometallic Chemistry*, 2015, 775, 6-11. (IF2014 = 2.302)
- 2) Ratanasak M., Rungrotmongkol T., Saengsawang O., Hannongbua S., Parasuk V. Towards the design of new electron donors for Ziegler–Natta catalyzed propylene polymerization using QSPR modeling. *Polymer*, 2015, 56, 340-345. (IF2014 = 3.766).

## VITA

Miss Manussada Ratanasak

Born: June 5th, 1979 in Ranong, Thailand

Education: 1991-1996 Primary and Secondary School Rat Borikanukroh, Ratchaburi.

1997-2000 Bachelor of General Science, Chemistry major,  
Department of Science, Faculty of Liberal Arts & Science,  
Kasetsart University, Nakornprathom. (GPA: 3.12/4.00)

2001-2003 Master of Science, Physical Chemistry major,  
Department of Chemistry, Faculty of Science,  
Chulalongkorn University, Bangkok. (GPA: 3.18/4.00)

2011-2015 Ph.D. program in Nanoscience and Technology,  
Graduate School, Chulalongkorn University, Bangkok. (GPA: 3.88/4.00)

Work experience:

September 2009 - September 2010 Science Teacher at Assumption  
College Thonburi

November 2006 - July 2009 Personal Support Technician for Accelrys  
Software at Thai Equipment Research Co.,Ltd.

August 2004 - December 2005 Research Assistant at Computational  
Chemistry Unit Cell, Chulalongkorn University

